University of New Mexico
UNM Digital Repository

Earth and Planetary Sciences ETDs | Electronic Theses and Dissertations

7-10-2013

The discovery of baddeleyite (ZrO2) and chrome spinel in the basal Rooiberg Group of the 2.057 Ga Bushveld Complex, South Africa: Implications for the impact and igneous scenarios for the petrogenesis of the Rooiberg Group.

Eric Tegtmeier

Follow this and additional works at: https://digitalrepository.unm.edu/eps_etds

Recommended Citation
Tegtmeier, Eric. "The discovery of baddeleyite (ZrO2) and chrome spinel in the basal Rooiberg Group of the 2.057 Ga Bushveld Complex, South Africa: Implications for the impact and igneous scenarios for the petrogenesis of the Rooiberg Group.." (2013). https://digitalrepository.unm.edu/eps_etds/88

This Thesis is brought to you for free and open access by the Electronic Theses and Dissertations at UNM Digital Repository. It has been accepted for inclusion in Earth and Planetary Sciences ETDs by an authorized administrator of UNM Digital Repository. For more information, please contact disc@unm.edu.

Eric Tegtmeier
Candidate

Earth and Planetary Sciences
Department

This thesis is approved, and it is acceptable in quality and form for publication:

Approved by the Thesis Committee:

Wolfgang Elston, Chairperson

Adrian Brearley

Horton Newsom

Rhian Jones

The discovery of baddeleyite (ZrO_2) and chrome spinel in the basal Rooiberg Group of the 2.057 Ga Bushveld Complex, South Africa: Implications for the impact and igneous scenarios for the petrogenesis of the Rooiberg Group.

By

Eric Tegtmeier

B.S., Earth and Planetary Sciences, University of New Mexico, 2008

THESIS

Submitted in Partial Fulfillment of the

Requirements for the Degree of

Master of Science

Earth and Planetary Sciences

The University of New Mexico

Albuquerque, New Mexico

May, 2013

The discovery of baddeleyite (ZrO_2) and chrome spinel in the basal Rooiberg Group of the 2.057 Ga Bushveld Complex, South Africa: Implications for the impact and igneous scenarios for the petrogenesis of the Rooiberg Group.

By

Eric Tegtmeier

B.S., Earth and Planetary Sciences, University of New Mexico, 2008

M.S., Earth and Planetary Sciences, University of New Mexico, 2013

Abstract

The ~75 wt % SiO_2 Basal Rhyolite is one of seven chemically distinct units of the Dullstroom Formation, the oldest of four formations that comprise the 4-6 km thick siliceous Rooiberg Group of the 2.057 Ga Bushveld Complex, South Africa. The discovery of composite zircon-baddeleyite grains and chromite in the Basal Rhyolite demands a reassessment of proposed scenarios for its petrogenesis. These scenarios include: 1) crustal melting caused by, and differentiation of, intrusive ultramafic magmas of the 9 km thick Rustenberg Layered Suite and 2) crustal melting initiated by an impact of one or more bolides. Although evidence for shock metamorphism, key to verifying an impact origin, has not been found, it has been proposed that unique quench textures in the Basal Rhyolite formed during quenching from impact-induced superheat (T > 1686° C). The presence of coexisting zircon ($ZrSiO_4$) and baddeleyite (ZrO_2) has been documented in several impact structures as a result of the reversible reaction: $ZrSiO_4 \leftrightarrow ZrO_2 + SiO_2$ at ~1686°C. Therefore, the presence of zircon and baddeleyite in the Basal Rhyolite provides a test for an impact origin of the Basal Rhyolite. Electron Microprobe and Transmission Electron Microscope studies highlight several characteristics of the

baddeleyite that are inconsistent with their formation by impact processes. The size, shape, chemistry and configuration of chromites in the Basal Rhyolite also suggest that they once existed in the interstices to olivine or pyroxene in a mafic cumulate prior to entrainment. Since no cumulates are known to exist underneath the Bushveld Complex, the parent lithology of the chromite and baddeleyite is likely a mafic magma associated with the Rustenberg Layered Suite. Chemical similarities between chromites from this study and chromites of a baddeleyite-bearing chill sequence to the Bushveld Complex provide the grounds for future comparative studies of these minerals. At this point, endogenous processes more readily explain the presence and characteristics of composite zircon-baddeleyite grains and chromite. Their presence in the Basal Rhyolite suggests that a dynamic magmatic setting existed during the early stages of Rooiberg Group extrusion.

TABLE OF CONTENTS

LIST OF FIGURES

LIST OF TABLES

CHAPTER 1: INTRODUCTION

The ~2.06 Ga Rooiberg Group of the Bushveld Complex, South Africa, is the world's largest occurrence of predominantly siliceous *meltrock* associated with a unique Large Igneous Province (LIP). The term *meltrock* is used as a non-genetic term to describe the Rooiberg Group, usually interpreted as rhyolite, which is significantly different from a typical rhyolite in terms of texture and mineralogy. The Rooiberg Group was divided into the Dullstroom, Damwal, Kwaggasnek, and Schrikkloof formations by Schweitzer et al. (1995). Among the differences in trace mineralogy between portions of the Rooiberg Group and typical rhyolites, are baddeleyite and chrome spinel, which occur locally in the basal 200 m of the Dullstroom Formation, termed Basal Rhyolite by Schweitzer et al. (1995). These minerals are not known from conventional siliceous melts, but were discovered in the course of this study.

The Bushveld Complex is best known for massive ultramafic and mafic sills that comprise the Rustenberg Layered Suite (RLS), but it also hosts "a bewildering array of granites, granophyres, and felsites" (Wager and Brown, 1967), where "granites" refers to the Lebowa Granite Suite, and the now outdated term "felsite" refers to the Rooiberg Group. The Rooiberg Group forms the roof to the Bushveld Complex into which sills of the RLS and Lebowa Granite intruded sequentially even as the Rooiberg roof was being deposited (Hatton and Schweitzer, 1995). Hence, it can be inferred that the Bushveld Complex was an open system during most of its formation. The lithologies associated with the Bushveld Complex are among the most voluminous of their type in the geological record (Hatton and Schweitzer, 1995). However, despite over 100 years of study, their origin, as well as the origin of the Bushveld Complex as a whole remains

contentious. A major reason for this is the fact that the internal structure of the Bushveld Complex is largely concealed by late stage Lebowa Granite Suite.

According to the leading hypothesis, the Rooiberg Group is a conventional volcanic succession produced by a combination of assimilation and differentiation. In the past decade, increasing attention has been given to the siliceous portions of LIPs, in attempts to determine which process is dominant in producing large volumes of rhyolitic melt (Pankhurst et al., 2010; Bryan and Ernst, 2008; Bryan et al., 2002; Sheth, 2007; Miller and Harris, 2007; Ewart et al., 1998b; Ernst and Bell, 2010). In the mantle plume model for LIP formation, a mantle plume interacts with the crust and, through fractional crystallization and assimilation, a bimodal assemblage of mafic and felsic magmas are produced. Since intermediate magmas either exist in very small volumes, or have not been found at all in many LIPs, some workers have concluded that fractionation along an unbroken liquid line of descent cannot be the dominant mechanism responsible for producing siliceous melts. However, recent work has shown that large changes in silica concentration can occur over small temperature ranges, meaning that the volume of intermediate melts produced along an unbroken line of liquid descent may be small and possibly obscured by the plumbing of most LIPs. This reduces the need to find large volumes of intermediate magma in the fractionation scenario. In addition, geochemical and isotopic studies have demonstrated petrogenetic links between basaltic and rhyolitic compositions that are spatially and temporally related in several LIPs. (Ayalew and Gibson, 2009; Buchanan et al., 2002; Ewart et al., 2004a; Garland et al., 1995; Peate et al., 1992; Pankhurst, 2011).

When the mantle plume model for the Bushveld Complex was first proposed by Hatton (1995), it was suggested that the oldest Rooiberg Group magmas were comprised of a mixture of crustal and mantle melts, and with increasing time, they became comprised entirely of crustal melts. Since then, geochemical and isotopic studies have highlighted inconsistencies with the idea that the upper Rooiberg Group is comprised of crustal melts. Instead, these studies have shown that the Rooiberg Group shares similarities to the mantle-derived RLS, the 8-9 km-thick mafic intrusive sequence of the Bushveld Complex (Buchanan et al., 2002; Buchanan et al., 2004; Buchanan et al., 2006).

The mantle plume model for the origin of the Bushveld Complex is favored by many workers due to its ability to explain the enormous volume of melt produced by the Bushveld event (~ 1,000,000 km^3), but the nature of the tectonic setting into which the plume was emplaced remains highly controversial (Kinnaird, 2005). Objections to the plume model cite the absence of radial dike swarms associated with the Bushveld Complex, which are normally present in LIPs, as well as the absence of evidence for lithospheric extension, which some suggest is unavoidable when large volumes of melt are created (Elkins-Tanton, 2005). Additionally, the discovery of a 3 Ga inclusion in a diamond that erupted from a post-Bushveld kimberlite superimposed on the western Bushveld Complex suggests that the mantle must have been stable at depths of at least 140 km during Bushveld formation. This is because the presence of a mantle plume originating at the core-mantle boundary would have disrupted the stability field of the diamond and its inclusions (Susan Webb, personal communication 2008). Recent investigations into the structure of the Bushveld Complex by Clarke et al. (2009) have lead to the suggestion that parental Bushveld magmas were produced in a back-arc

setting associated with tectonism of the Limpopo and Magondi orogenies. However, this model fails to explain the high O^{18} values of the RLS. Recent work by Olsson et al. (2011) on a ~2.6 Ga dike swarm that appears to converge on a central locus within the eastern portion of the Bushveld Complex has led to a new model for the onset of Bushveld magmatism. In Olsson's model, the head of a mantle plume impacted the lower crust at 2.66-2.7 Ga producing the dike swarms, minor surficial volcanism, and a crystalline body at depth. It is hypothesized that this mafic body became increasingly dense as a result of eclogite-facies metamorphism and eventually sank into the mantle. The authors suggest that Bushveld magmatism was initiated when the sinking metamorphosed body passed through the upper mantle causing delamination decompressional melting of the mantle.

In contrast to the endogenic models, Rhodes (1975) and Elston (2008) proposed that the formation of the Bushveld Complex was initiated by one or more simultaneous impacts by large bolides. The proposed textural evidence for impact pertinent to this study is present within the Basal Rhyolite. Although French (1990) found no evidence for shock metamorphism required to verify impact (French and Koeberl, 2010), the impact scenario focuses on unique quench textures present in the Basal Rhyolite. These textures have been hypothesized to have formed as a result of rapid quenching from temperatures well above the realm of terrestrial siliceous igneous processes (Rhodes, 1975; Elston, 2008).

Detailed petrographic and geochemical studies of the Basal Rhyolite have not been carried out by previous workers. Most studies of the Rooiberg Group have focused on bulk chemistry, isotope, and trace element analyses of the most abundant rock types in

the lower and upper Rooiberg Group. The current study tests the impact hypothesis by investigating unique characteristics of the Basal Rhyolite, including its exotic quench textures, lack of optically resolvable or extractable zircon ($ZrSiO_4$), and its bulk Cr concentration of 170-920 ppm, well above what is expected in a typical rhyolite. The average Zr concentration in the Basal Rhyolite is ~228 ppm (Schweitzer et al., 1995) which is hardly a significant difference compared to what is expected in a rhyolite (217 ppm) (NAVDAT, 2013), although zircon grains are usually small in felsic volcanic rocks (<100 µm) and can sometimes be difficult, but not impossible to find by optical microscopy (Hanchar and Watson, 2003).

In this study, an electron microprobe was used to locate previously undetected Zr-bearing phases in multiple outcrops of the Basal Rhyolite. The Zr is present in composite zircon-baddeleyite grains <20 µm in size, as well as irregularly shaped zircon grains < 15 µm long. This study has also found chrome spinel, a Cr-bearing oxide which forms a solid solution between the Fe and Al-bearing end members magnetite and hercynite. The chrome spinels are euhedral and range from 20-220 µm in size with compositions that range from Cr-magnetite to Mg-bearing chromite. The presence of both baddeleyite and chrome spinel is unexpected in a siliceous melt. Baddeleyite was previously known only in silica-undersaturated, and alkalic igneous rocks, and chromite in rocks that contain high proportions of ferromagnesian silicates. In the case of baddeleyite, however, there is a single exception noted in the literature: the presence of a 100 µm euhedral baddeleyite crystal documented in a late stage Yellowstone rhyolite (Bindeman and Valley, 2001).

This goal of this study is to utilize the composition, morphology, and spatial characteristics of the composite zircon-baddeleyite grains and chromite, as well as their

lateral extent in three outcrops of the Basal Rhyolite, to propose and discuss the igneous and impact processes that could potentially account for the unusual and unexpected occurrence. Intrinsic characteristics of the processes proposed for the impact and igneous scenarios, such as the energy or temperatures associated with each, need to be compatible with both the characteristics of the two unexpected minerals and other characteristics of the Basal Rhyolite as a whole. Since the baddeleyite and chromite occur in a quenched siliceous melt, it is also assessed how their residence in such a melt may have affected their chemical composition. In this study, all the constraints listed above are kept in mind as the likelihood of each scenario is assessed. After thoughtfully weighing all current data, the igneous scenario is preferred, although potential avenues of future work are proposed that may help differentiate between the impact and igneous scenarios further.

CHAPTER 2: GEOLOGIC SETTING

The Bushveld Complex occurs within a ~400 km four-lobed basin, superimposed on the 2.65-2.05 Ga Transvaal Supergroup, a basin-fill sequence up to 15 km-thick, comprised predominantly of quartz arenites, dolomites, and shale with minor volcanic flows (Fig. 1) (Kinnaird, 2005). The predominantly siliceous Rooiberg Group has an unconformable contact with the ≤ 5 km Pretoria Group, the youngest group of the Transvaal Supergroup.

THE ROOIBERG GROUP

At present, the Rooiberg Group is preserved over an area of 50,000 km^2 (Schweitzer et al., 1995) within the Bushveld basins. It may have extended beyond these basins (Twist and French, 1983), but to date, no evidence for this has been found. The maximum thickness of the Rooiberg Group was between 5 and 6 km (Hatton and Schweitzer, 1995). The only known section in which all four formations are exposed is near Loskop Dam where a ~3.5 km of section is preserved (Fig. 1), but the base has been destroyed by melting and metamorphism by intrusions of the Rustenberg Layered Suite below (von Gruenewaldt, 1972).

THE RUSTENBERG LAYERED SUITE

Ultramafic and mafic cumulates of the RLS have been subdivided into five distinct zones based on chemistry and the occurrence of distinct cumulate horizons. In ascending order these zones are: 1) Marginal; 2) Lower; 3) Critical; 4) Main; and 5) Upper. Where not covered by younger sediments, the RLS crops out in discontinuous

crescent shaped bodies that help define the eastern, western, and northern lobes of the main Bushveld basin. A fourth basin is largely covered in the south. All units of the RLS are tilted towards the center of each basin, and when present, the Rooiberg Group assumes the same tilt. Individual cumulate layers are traceable over distances of at least 70 km in the eastern and western lobes. This has led many workers to suggest that layered units of the RLS in each lobe are connected at depth, however recent gravity models suggest this is likely not the case (Kinnaird, 2005). The RLS intruded as sills mainly along an unconformable contact between the Rooiberg Group and the upper Pretoria Group, although in some areas, the basal Rooiberg Group occurs beneath the floor of the RLS or as felsic screens within RLS sills (Hatton et al., 1995).

THE RASHOOP GRANOPHYRE AND THE LEBOWA GRANITE SUITE

Intrusions of the RLS led to re-melting and recrystallization of portions of the Rooiberg Group and Transvaal Supergroup which produced the Rashoop Granophyre (Kinnaird, 2005). Some units of the Rashoop Granophyre are also thought to represent Rooiberg Group melts that did not reach the surface, cooling slowly at depth (Kinnaird, 2005). Late stage granites of the Lebowa Granite Suite intruded as horizontal sheets, mostly wedged between the RLS and parts of the Kwaggasnek Formation of the Rooiberg Group. Emplacement of these granites uplifted the overlying Rooiberg Group and Rashoop Granophyre and depressed the RLS beneath (Kinnaird, 2005). Intrusion of the Lebowa Granite Suite shows evidence of being synchronous with the uppermost Rooiberg Group, implying that the deposition of the Rooiberg Group spanned the entire duration of the Bushveld event (Hatton and Schweitzer, 1995).

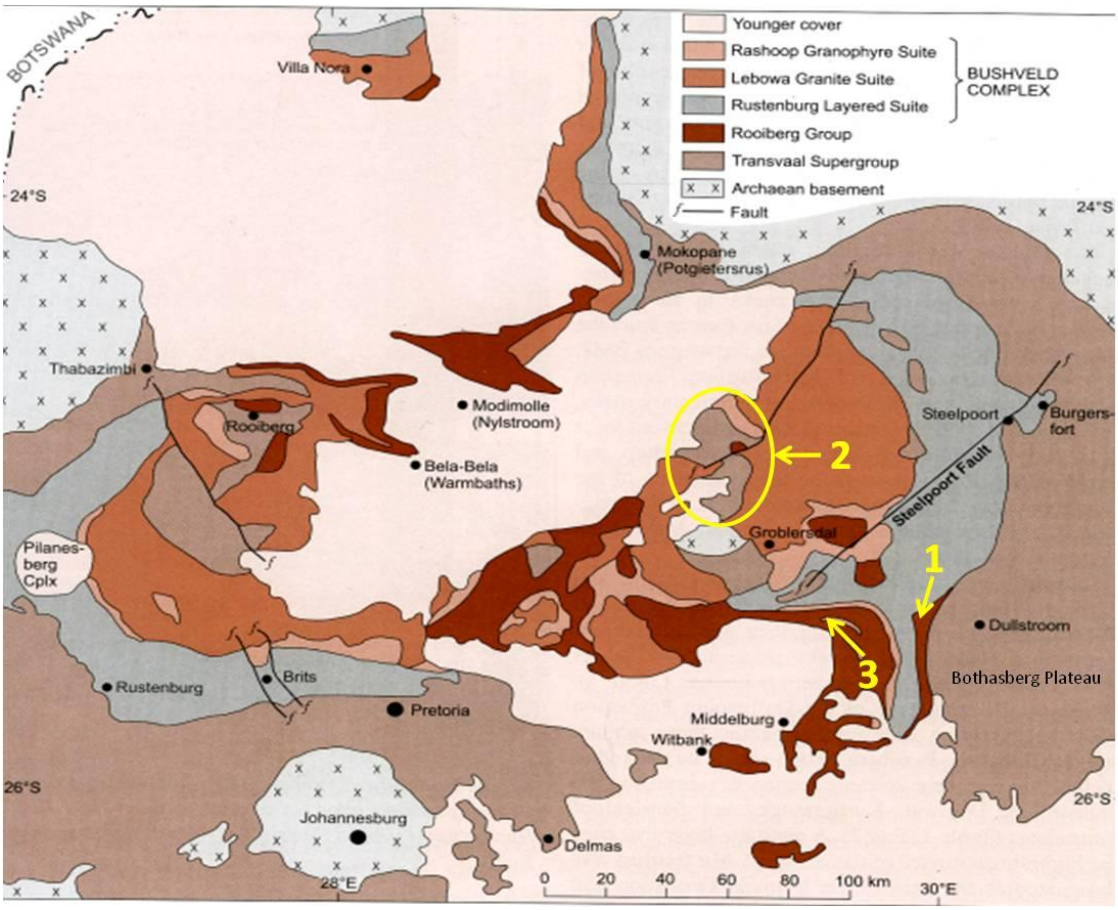

Figure 1. Simplified geological map of the Bushveld Complex. Locations pertinent to this study are: 1) Type Dullstroom Formation 2) Stavoren and Marble Hall Inliers, 3) Loskop Dam. Modified from Buchanan et al. (2002).

COMPOSITIONS OF THE ROOIBERG GROUP

The Dullstroom Formation has the highest chemical variability of all four Rooiberg Formations. This study adopts the terminology of Schweitzer et al. (1995) which defines 6 distinct compositions: 1) low-Ti basaltic andesite; 2) the 75 wt % SiO_2 Basal Rhyolite; 3) high-Ti basalt; 4) high-Mg felsite; 5) low-Mg felsite; and 6) high Fe-Ti-P andesite (Schweitzer et al., 1995). The top of the Dullstroom Formation is marked by the last flow of the high-Mg felsites. The Damwal Formation is comprised of dacites

and rhyolites. A compositional break separates the Damwal and Kwaggasnek Formations, with the Kwaggasnek being comprised mainly of rhyolites and intercalated sedimentary horizons. Another chemical break, along with a possible hiatus in deposition, exists between the Kwaggasnek and Schrikkloof Formations. The Schrikkloof Formation is characterized by flow-banded rhyolites and many other rock types that resemble conventional volcanic rocks along with discrete sedimentary interbeds. Outcrops of the Dullstroom and Damwal Formations are restricted to the eastern Bushveld Complex, while the Kwaggasnek and Schrikkloof Formations are found in the southeastern and western Bushveld Complex.

KEY OUTCROPS OF THE ROOIBERG GROUP

The type-Dullstroom Formation in the Messchunfontein section

The type-Dullstroom section occurs in three paleo-channels, one of which is named the Messchunfontein section (Fig. 1). The Basal Rhyolite occurring in the Messchunfontein section is one of three occurrences of the Basal Rhyolite analyzed in this study. In the type-Dullstroom Formation, the low-Ti basaltic andesite, Basal Rhyolite, high-Mg felsite, and high-Ti basalts occur below the floor of the RLS (Fig. 1). With the exception of the high-Mg felsite, these units are not present above the RLS. The High Fe-Ti-P andesite is the only mafic composition of the Dullstroom Formation occurring above the RLS, and is chemically distinct from the mafic compositions that occur below the floor of the RLS. All units of the Dullstroom Formation in the Messchunfontein section, including the Basal Rhyolite, are hydrothermally altered (Schweitzer and Hatton, 1995).

The paired Stavoren and Marble Hall Inliers

In the Stavoren Inlier, hydrothermally altered low-Ti basaltic andesite and the Basal Rhyolite overlie slightly folded and hydrothermally altered sedimentary rocks of the upper Pretoria Group (hereafter referred to as the Makekaan Subgroup), in a ~10 x 15 km outcrop, commonly referred to in the literature as a "fragment" (Fig. 1). The Stavoren Inlier is situated on the NW side of a SW-NE trending structure that according to field mapping by Hartzer (1995) and Walraven (1970) formed prior to the Bushveld Complex but also records displacement during and after wards. On the SE side of this structure, another fragment, the Marble Hall Inlier, contains highly deformed sediments of the lower part of the Pretoria Group. No Rooiberg rocks are present in the Marble Hall Inlier.

The Basal Rhyolite forms a small range of ridges and hills confined to the southeastern margin of the Stavoren Inlier which rise nearly 100 m above the surrounding plains comprised of the Mackekaan Subgroup. The low-Ti basaltic andesite occurs locally in a single paleo drainage near the base of a hill, making it difficult to know the full extent of its volume beneath the Basal Rhyolite. An unusual characteristic shared by the Stavoren and Marble Hall inliers is that neither one contains outcrops of the Magaliesberg Formation, a quartzite that forms prominent, weathering-resistant ridges outside of the Bushveld Complex. In the stratigraphy of the Pretoria Group, the Magaliesberg Formation falls directly in the interval between the youngest metasediments preserved in the Marble Hall Inlier and the oldest sediments that occur in the Stavoren Inlier. A simplified geologic map of the Marble Hall inlier and the southern margin of the Stavoren Inlier can be found in figure 2.

Loskop Dam

Near Loskop Dam the lower Dullstroom Formation, including the Basal Rhyolite, has re-melted due to the intrusion of the RLS. According to von Gruenewaldt (1972) the melt rose through a zone of contact metamorphism to form a 2,000 – 2,500 m sill of red rock, identified as granophyre. This study analyses a portion of the granophyre that is presumed to represent remelted Basal Rhyolite. Despite areas where the lower Rooiberg Group has been recrystallized, the remaining Rooiberg Group is preserved in a 3.5 km thick section that preserves the upper Dullstroom Formation, Damwal, Kwaggasnek, and Schrikkloof Formations. The Damwal Formation comprises low-Mg felsite and high-energy sedimentary interbeds (Eriksson et al., 1994). Unlike the sedimentary units interbedded in the Damwal Formation, sedimentary interbeds in the Schrikkloof Formation are almost entirely comprised of locally derived Rooiberg Group rocks.

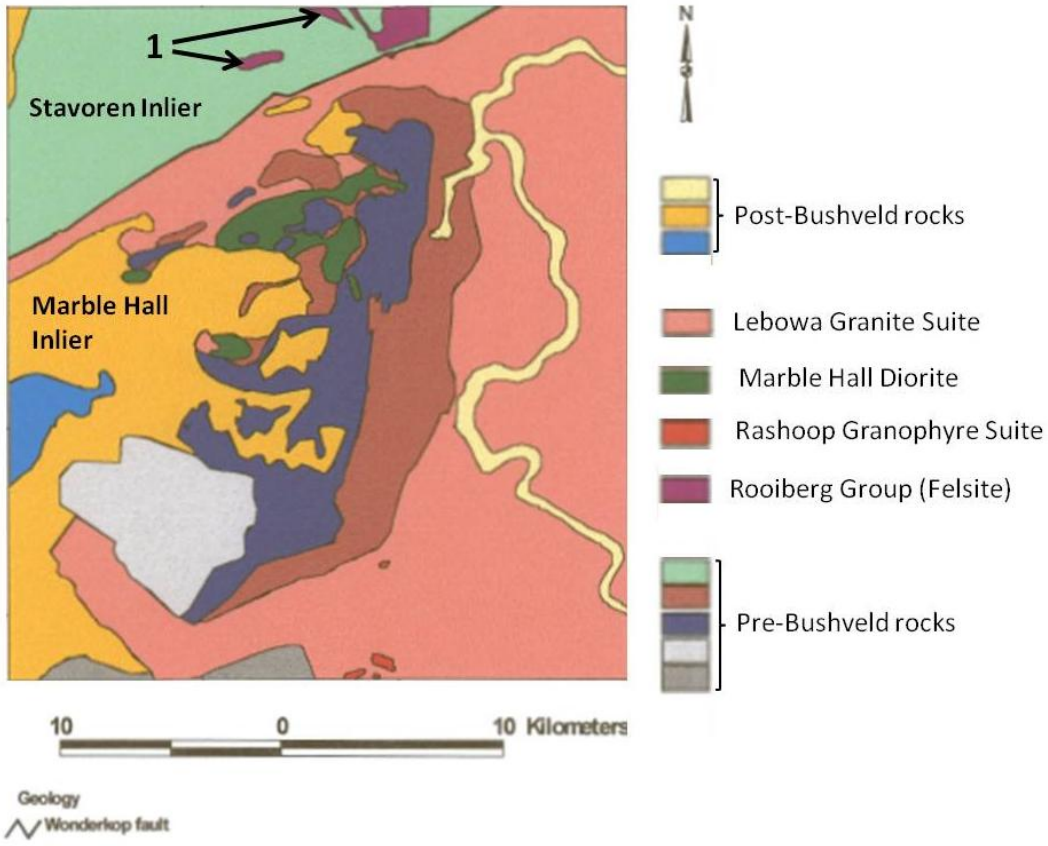

Figure 2. Simplified geologic map of the Stavoren and Marble Hall inliers.1: Outcrops of Basal Rhyolite surrounded by Pretoria Group sediments of the Mackekaan Formation. Modified after Babayeju 1999.

CHAPTER 3: BACKGROUND AND PREVIOUS WORK

GEOCHEMICAL AND ISOTOPIC STUDIES OF THE ROOIBERG GROUP

Prior work consists mainly of magmatic-petrogenetic models in which different authors have attempted to derive the origin of the Rooiberg Group. When the mantle plume model for the Bushveld Complex was first proposed by Hatton (1995), it was suggested that the Damwal, Kwaggasnek, and Schrikkloof Formations of the Rooiberg Group were composed of partially melted lower crust. This model considered the Dullstroom Formation to be a mixture of crustal melt with an early RLS magma. Alternatively, Maier et al. (2000) proposed that all of the Rooiberg Group formed by mixing between a mafic magma and melted lower crust. In this model, the increase in silica content with height is the result of smaller volumes of mafic magma being included in the mixtures.

More recent geochemical and isotopic studies have proposed alternatives to deriving most of the upper Rooiberg Group from crustal melts. For example, Buchanan et al. (1999, 2002) proposed that the low-Mg felsites of the Damwal and Kwaggasnek Formations are petrogenetically related to the low-Ti basalts and basaltic andesites of the Dullstroom Formation. In later studies it was also shown by Buchanan et al. (2004, 2006) that with increasing stratigraphic height and SiO_2 content, the concentration of incompatible trace elements (including the Rare Earth Elements (REEs)) and the magnitude of the negative Eu anomaly increases. These chemical trends provide additional evidence that the siliceous melts of the Damwal Kwaggasnek and Schrickloof Formations originated by fractional crystallization of a magma of similar origin to the low-Ti basalts of the Dullstroom Formation. The low-Ti basalts of the Dullstroom

Formation were in turn related by Buchanan et al. (2004) to the RLS by similarities in their Rb/Sr and Nd/Sm isotopic ratios. These similarities are thought to provide evidence that the Rooiberg Group and RLS were ultimately derived by differentiation of the same, or chemically similar, source (Buchanan et al., 2004). Buchanan et al. (2002) proposed that the source of the Rooiberg Group consisted of two or more shallow magma chambers where mafic magmas of the RLS (or a similar source), underwent crustal assimilation and extensive differentiation to form magmas of the Rooiberg Group. The Basal Rhyolite, however, represents a highly silicic melt near the base of the Dullstroom Formation that has not yet been included in these types of geochemical studies. Therefore, an interpretation of its origin as a crustal melt, a differentiate, or a mixture of both, remains unresolved by the igneous models at this time.

Since most siliceous rocks of the Rooiberg Group have an average SiO_2/Al_2O_3 ratio of 5.83, a K_2O/Na_2O ratio of 2.068, (Twist, 1985) and are associated with late stage A-type Lebowa granites, Pankhurst et al. (2011) proposed that the Rooiberg Group represents a key example of the geochemical model of Turner and Rushmer (2009) on a massive scale. These models calculated that efficient crystal fractionation of mafic mantle sources provided a better fit to observed compositions of low-Ti rhyolites and A-type granites, found in most LIPs, than does production of these rock types by melting of crustal sources. Their study also concluded that rhyolites with a high SiO_2/Al_2O_3 ratio (between 5 and 7) and a high K_2O/Na_2O ratio (between 1.5 and 2) are diagnostic of compositions produced by efficient crystal fractionation of a mafic mantle source. Low ratios of SiO_2/Al_2O_3 (~4) and K_2O/Na_2O (<1.5) are characteristic of tectonic settings associated with lithospheric extension or back-arc basins.

Vantongeren et al. (2010) showed that the Damwal, Kwaggasnek or Schrikkloof Formations can be modeled as a differentiate of the Main zone of the RLS. As evidence they provided a geochemical model where the average bulk composition of each Rooiberg formation, in amounts equivalent to their estimated extruded volume, was added to the present day bulk composition of the Main Zone. Vantongeren et al. (2010) showed that the resulting composition of each mixture can produce pyroxene compositions documented in the Main Zone, but could not have crystallized from a melt having a bulk composition of the Main Zone today. Vantongeren et al. (2010) concluded that the RLS could have been a hypabysal intrusion in which Rooiberg and RLS magmas formed a stratified magma chamber. However, Buchanan et al. (2004) noted that since the high-Ti basalts of the Dullstroom Formation are enriched in incompatible trace elements, they likely resided in a different chamber and formed from a chemically-distinct source.

DIFFERENCES BETWEEN THE IMPACT AND IGNEOUS PLUME SCNEARIOS

A mantle plume can be applied to both the impact and igneous scenarios for the formation of RLS magmas. However, the origin of the plume in each interpretation varies considerably. Hydrocode calculations by Jones et al. (2001) have modeled that impact-induced decompression melting of the mantle is possible, and named the type of plume produced an I-type plume, or impact plume. Ivanov and Melosh (2003) concede that such an event, though improbable, is possible after the late heavy bombardment, but only in impact events that result in a final crater with a diameter of 400-500 km. The origin of the mantle plume in the igneous model is not constrained, but most workers suggest that it

originated in the deep mantle. Whether formed by decompression-induced melting of the mantle by impact, or melting of the mantle by a traditional mantle plume, magmas of the RLS are likely to be responsible for producing the Rashoop Granophyre and Lebowa Granite by crustal melting.

IMPACT INTERPRETATION OF THE ROOIBERG GROUP

The impact scenario proposes that the Basal Rhyolite present in the Stavoren Inlier represents an impact melt in the form of a high energy, high temperature (>1686 °C) debris flow, while the Basal Rhyolite in the Type-Dullstroom Formation represents a cooler distal facies (Elston, 2007). The progressive increase in silica content observed throughout the Rooiberg Group is suggested to represents evolution of a central meltpool, which overflowed repeatedly as it differentiated, equilibrated with the crust, and was invaded by Lebowa granite. Almost all exposures of the Rooiberg Group are interpreted as repeated overflows of the central meltpool. Elston (2007) interpreted the sedimentary intercalations in the Damwal Formation as deposits associated with tsunami-like influxes of water which triggered overflows of the evolving central meltpool (Caress and Elston, 1997). The origin of the Rooiberg Group from an overflowing central meltpool allows the impact scenario to account for the absence of eruptive centers for the Rooiberg Group, as noted by Twist and French (1983) and Eriksson et al. (1995).

IMPACT INTERPRETATION OF THE STAVOREN AND MARBLE HALL INLIERS

The juxtaposition of relatively undeformed upper Pretoria Group sedimentary rocks in the Stavoren Inlier against highly deformed lower Pretoria Group sedimentary rocks found in the Marble Hall Inlier, with the intervening Magaliesberg quartzite absent, can be attributed to the crater modification stage of multi-ring impact craters as modeled by Collins et al. (2002) (Wolf Elston, personal communication). In this scenario, the highly deformed, pre-Magaliesberg Formation sediments of the Marble Hall Inlier represent intensely heated and plastically deformed strata of an unstable central uplift which collapsed outwards. The relatively undeformed Mackekaan Subgroup of the Stavoren Inlier, on the other hand, represents strata that collapsed inward from the crater wall during crater modification and now rests adjacent to the Marble Hall Inlier. In this scenario, the Basal Rhyolite represents a superheated impact melt (T >1686 °C) which entrained the "missing" Magaliesberg Formation in a high-energy debris flow.

IGNEOUS INTERPRETAION OF THE ROOIBERG GROUP

The absence of eruptive centers has led many proponents of the igneous models to favor the extrusion of the Rooiberg Group along multiple fissures (Vantongeren et al., 2010; Lenhardt and Eriksson, 2012) but to date none have been found. Lenhardt and Eriksson (2011) cite an increase in the frequency and thickness of sedimentary intercalations with increasing stratigraphic height in the Rooiberg Group as evidence that extrusions were closely spaced during early Rooiberg deposition (i.e., during formation of the Dullstroom Formation), with larger hiatuses in eruption occurring during deposition of the Kwaggasnek and Schrikkloof Formations. The source of the Rooiberg

Group magmas is thought to be one or more shallow magma chambers as suggested by Vantongeren et al. (2010), and Buchanan et al. (2002).

IGNEOUS INTERPRETATION OF THE STAVOREN AND MARBLE HALL INLIERS

The Stavoren Inlier has been interpreted as a roof pendant in the Lebowa Granite while the Marble Hall Inlier has been interpreted as a floor-attached dome of pre-Bushveld sediments immersed in granite. Deformation of Pretoria Group sediments in the Marble Hall inlier has been mapped as a NW-striking anticline that was refolded along a NE striking anticlinal fold (Walraven, 1970). Mapping by Walraven (1970) considered the strike-slip fault separating the Stavoren and Marble Hall inliers to be an extension of the Wonderkop Fault (Fig. 2) Outside the Bushveld Complex, the Wonderkop fault trends NE-SW and enters the Eastern Lobe near its NE edge where it becomes obscured by granite of the Lebowa Granite Suite. If the trend of the Wonderkop Fault as it enters the eastern lobe is traced, it is in alignment with the trend of a major fault between the Stavoren and Marble Hall inliers on that fault's NE end. A ~45° difference in the orientation of the Wonderkop Fault outside the Bushveld Complex with the central segment of the fault immediately between the two inliers has been attributed to a change in fault orientation due to a restraining bend existing between the two inliers. Hartzer (2000) attributed wrench faulting in the restraining bend to the formation of a positive flower structure and a series of duplex structures during tectonism along the Wonderkop fault which occurred at some point after the Bushveld Complex formed.

Gravity and high-density airborne magnetic data (Babayeju, 1999) highlighted another major N-S trending fault, lacking a surface expression, which defines the eastern

edge of the Marble Hall Inlier. A magnetic high in the center of the Marble Hall fragment has been interpreted as a magnetic plug of high-density crystalline material at unknown depth (Babayeju, 1999). Deformation associated with interference folding and some faulting in the area is thought by Walraven (1970) to have pre-dated intrusion of the RLS. The Inlier itself is interpreted by Babayeju (1999) as pre-deformed Transvaal Supergroup emplaced as a horst after intrusion of the RLS. Density data is interpreted by Babayeju (1999) to indicate the presence a sill of RLS underneath the Stavoren Inlier. However, it is unknown at what depth, or how thick, the proposed RLS sill may be.

CHAPTER 4: SAMPLES

SAMPLE LOCALITIES

This study analyzed four thin sections of Basal Rhyolite from the Stavoren Inlier, one thin section of remelted Basal Rhyolite near Loskop Dam identified as granophyre by von Gruenewaldt (1972), and one thin section of the Basal Rhyolite from the Messchunfontein section. The Basal Rhyolite from these three localities represents both the small population of the only preserved critical basal zones of the Rooiberg Group as well as areas where the basal zone was remelted by the RLS. An understanding of these samples is important because they represent some of the earliest rocks formed by the Bushveld event. Most of the work in this study has focused on samples from the Stavoren Inlier because of time constraints.

STAVOREN INLIER

The Basal Rhyolite can be interpreted as a progression from a rock in which incompletely melted sediments of the underlying Mackekaan Subgroup are the major component, to almost complete melt at the top that has entrained partially melted and recrystallized quartz grains. The succession as a whole is entirely different from what is expected in conventional volcanic rocks (Wolf Elston, personal communication 2012).

Two textures of the Basal Rhyolite in the Stavoren Inlier

The Basal Rhyolite was sampled from outcrops located in drainages and hills found near the southern margin of the Stavoren Inlier. Among the unique quench textures are a pseudospherulitic texture and a deformed acicular texture. Pseudospherulites are roughly spherical bodies ($\leq$ 1.5cm) that lack the radial internal texture of true spherulites.

Samples of Basal Rhyolite with the deformed acicular texture represent a stratigraphically higher portion of the Basal Rhyolite than samples with the pseudospherulitic texture.

Pseudospherulitic texture

Samples W95-35, W91-102, and 95-34 exhibit the pseudospherulitic texture. This study has divided the overall texture of the rock into two distinct regions: pseudospherulitic aggregates and the matrix between them. The pseudospherulitic aggregates range in size from 1-15 mm. When small (1-4 mm), they are shaped like snowflakes and when large (8-15 mm), they resemble irregularly-shaped spheres with shallow embayments by the matrix. W95-35 is comprised chiefly of large pseudospherulitic aggregates while W91-102 and 95-34 contain smaller pseudospherulitic aggregates.

Quartz in samples with the pseudospherulitic texture There are four morphologies of quartz in samples with pseudospherulitic texture, some of which can be found in both the matrix and the aggregates (Fig. 3).

Morphology 1: This morphology consists of sheaves of thin elongate quartz needles (5-20 µm wide, 50-500 µm long), that radiate outward from a common center. These sheaves are commonly found at the interface between the pseudospherulitic aggregate and the matrix. Near the end of the sheaths, the needles are occasionally flared outward giving them a plumose appearance. Small, randomly oriented needles are also very common in the inner regions of the pseudospherulitic aggregates.

Morphology 2: This morphology consists of randomly oriented quartz needles (40-250 µm wide, 0.2-1.5 mm long) that commonly have swallow tail terminations. The larger needles tend to be segmented and are far less numerous than morphology 1 in pseudospherulitic rocks

Morphology 3: This morphology consists of subrounded to subangular quartz grains that range in size from 50 x 150 µm to 200 x 300 µm. They are found in both the matrix and internally to the pseudospherulitic aggregates. They appear partially melted around their rims.

Morphology 4: This morphology is best described as clusters of tabular quartz grains 150 x 350 µm in size that occur in random orientations. These clusters are generally found near the interface between the pseudospherulitic aggregate and the matrix.

Feldspars in rocks with the pseudospherulitic texture: Two types of feldspar, albite and K-feldspar, occur intermixed with the quartz morphologies. Albite occurs adjacent to most of the quartz needles as small, irregularly shaped, occasionally elongate crystals. K-feldspar occurs in small patches within the pseudospherulitic aggregates but also forms a continuous rim which exhibits true spherulitic texture around every pseudospherulitic aggregate. When viewed under cross polarized light, the aggregates as a whole appear to break down to a mosaic comprised of numerous irregularly shaped patches. Each patch has its own extinction angle from those adjacent to it. Some of the longer quartz needles cross through multiple patches. Segments of these needles go extinct in accordance with the extinction angle of the patch they are cutting across.

Minerals in the matrix: The matrix has quartz morphologies 2, 3, and 4. Minerals surrounding these quartz morphologies consist predominantly of albite and spherulitic K-feldspar. Most quartz needles are completely rimmed by albite though some are also partially rimmed by K-feldspar. The quartz grains of morphology 3 are more numerous and are slightly larger in the matrix, reaching sizes up to 0.5 mm. They also exhibit evidence for incipient melting along their margins in the form of a cloudy reaction rim. Minor and accessory minerals present include rutile, biotite, monazite, chlorite, epidote, calcite, barite, magnetite, ilmenite, and chrome spinel

Deformed Acicular Texture

The deformed acicular texture is illustrated in figure 4. Samples with this texture are characterized by numerous quartz needles ranging in size from 30 x 300 µm to 100 µm x 1.5 mm. Similar to quartz needles found in samples W95-35 and W91-102, the quartz needles are segmented and commonly exhibit well-defined swallow tail terminations which can reach up to 100 µm in length. However, they differ from quartz needles from W95-35 and W91-102 in that they are far more numerous, and are occasionally bent where they appear to have interacted with the tips of other needles or aggregates of quartz grains. The orientations of the smaller needles are generally random, whereas the larger needles appear to be oriented by flow. Round quartz grains 150-200 µm in diameter are often found between the needles. Large subrounded quartz grains (0.5-1 x 1 mm) are rare in this texture with up to three occurring in each the two thin sections observed. Along their margins, these quartz grains appear to be decomposing into thin, tabular shaped grains similar to the type 4 quartz in the pseudospherulitic aggregates. The groundmass between the laths and quartz grains is composed mainly of

altered K-feldspar, sericite, and secondary Fe-Mg minerals. There is no plagioclase within this lithology. Large irregular patches of calcite are also present between the quartz laths, along with small apatite crystals. Monazite is very common in irregularly shaped grains ranging in size from 10-20 µm. Other minor minerals present are rutile, barite, small clusters of chrome spinel, and very small (< 30 µm) magnetite grains.

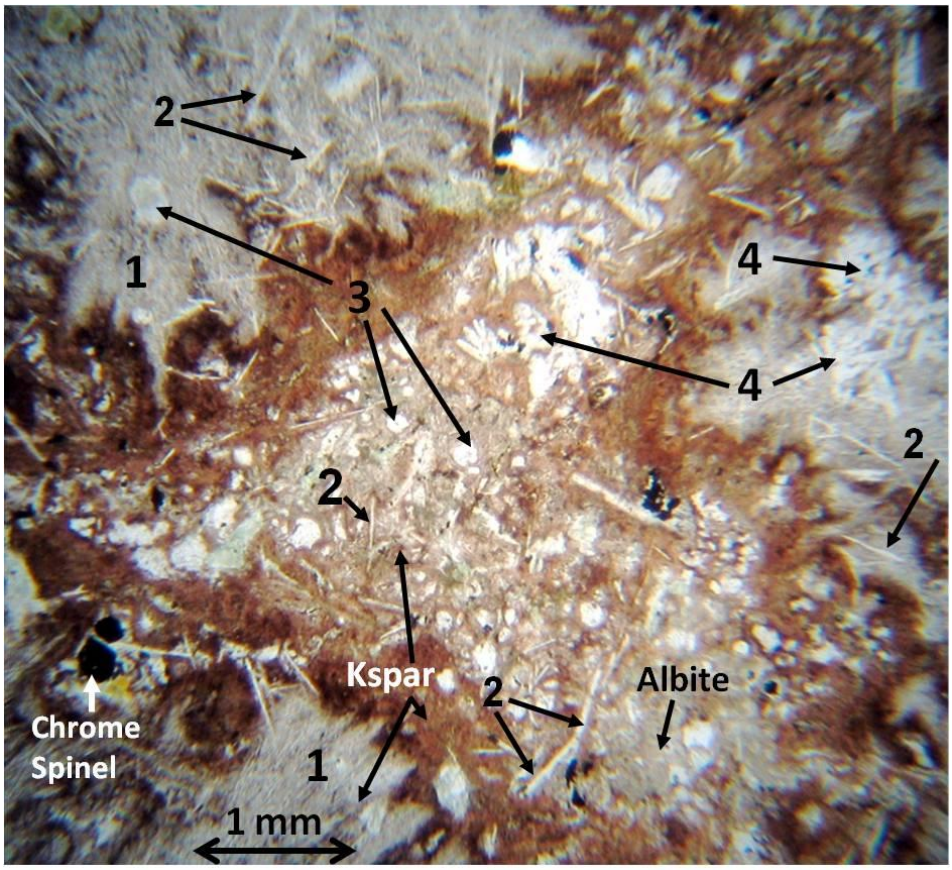

Figure 3. Photomicrograph of the pseudospherulitic texture of the Basal Rhyolite found in sample W91-102. Four morphologies of quartz, two feldspars, and chrome spinels are highlighted. Plane polarized light (PPL).

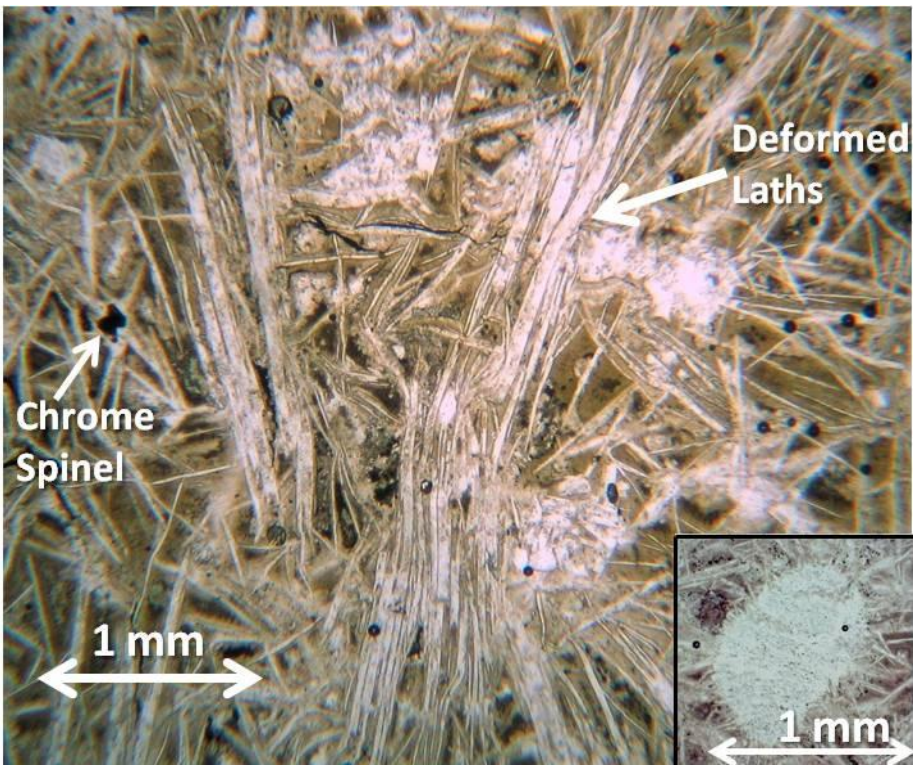

Figure 4. Photomicrograph of the deformed acicular texture found in sample W03-07. Bright minerals are all quartz. Brown patches in between grains are altered K-feldspar. Inset image in bottom right is an example of a large quartz inclusion that appears to be decaying into thin, tabular shaped crystals. (PPL).

The remelted and recrystallized Basal Rhyolite near Loskop Dam

A massive red rock at the base of the Loskop Dam section, described by Twist (1985), was interpreted by von Gruenewaldt (1972) as a sill of granophyre composed of remelted lower Dullstroom Formation. Patches of micrographic texture, typical of granophyre, only make up a small part of this rock (Fig. 5). Possibly residual quench textures occur in rounded, isolated patches throughout the sample, and may contain morphologies of quartz similar to type 1 quartz needles from samples of the Stavoren Inlier with pseudospherulitic texture. The patches of micrographic texture usually occur around large phenocrysts of sodic plagioclase, angular quartz grains, and patches of residual quenched material. Sphene is present in small amounts and is usually found near

ilmenite grains with well-developed exsolution lamellae. Some ilmenite grains exhibit magnetite overgrowths. Apatite, chlorite, and calcite are also present in the groundmass in minor amounts

Basal Rhyolite of the Messchunfontein section

The basal Rhyolite in the Messchunfontein section (Fig. 6) contains quartz needles similar in size to those of type 2 and 4 in the pseudospherulitic texture of the Stavoren Inlier, but are less common. Rather than being rimmed by albite or orthoclase like the needles in the pseudospherulitic aggregates, the needles are suspended in a matrix of Ca-Na plagioclase, alkali feldspar, and amphibole. Rare, sub-rounded quartz grains, 1.5-2 mm in diameter, are present in the matrix and exhibit a reaction into thin, tabular, quartz grains along their margins. Isolated patches of type 4 morphologies and large magnetite grains, ~600 µm long, are also present.

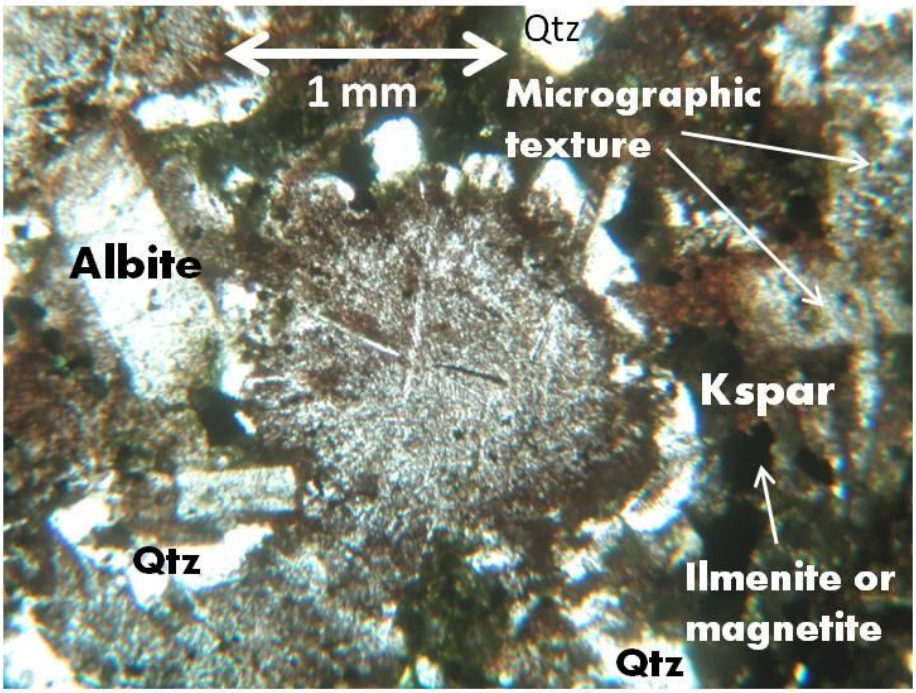

Figure 5. Photomicrograph of sample W03-61 highlighting the texture of the Basal Rhyolite that has been partially remelted and recrystallized as granophyre at Loskop Dam. Center: quench textures similar to quartz types 1 and 2 of the pseudospherulitic aggregates. Brown material is alkali feldspar. (PPL)

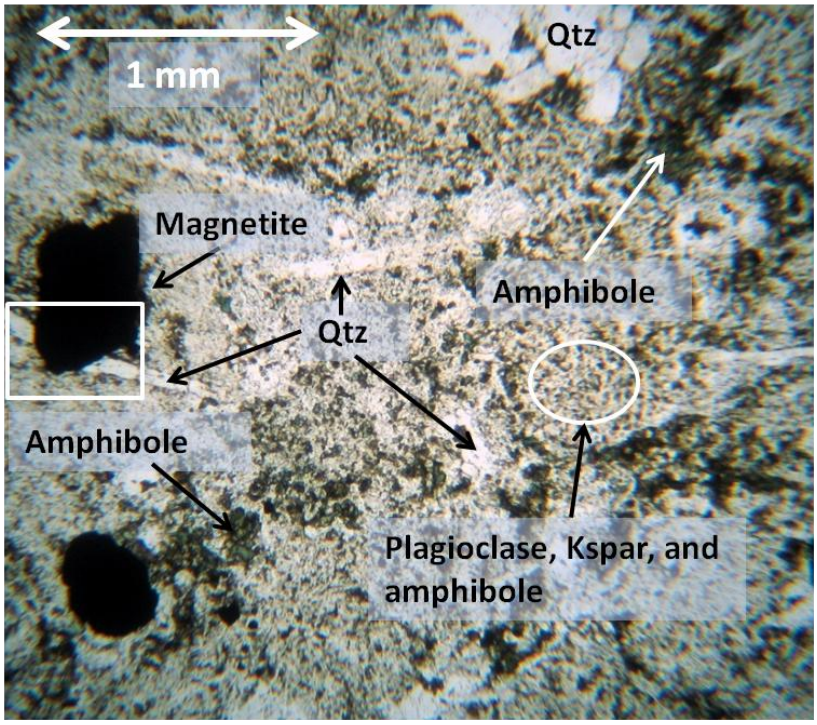

Figure 6. Photomicrograph of sample W08-11which highlights the texture of the Basal Rhyolite in the Messchunfontein section. Quartz occurs as needles similar to morphology 2 and patches similar to morphology 4 of the Stavoren Inlier. Abundant amphibole, Ca-Na plagioclase, and K-feldspar are present as a fine matrix (white oval). A large magnetite grain appears to have deflected a quartz needle into the subsurface of the thin section (white square). (PPL).

CHAPTER 5: METHODS

XRF

Twenty grams of each sample were crushed by ceramic mortar and pestle and were ground into a fine powder with a Spex Shatterbox. The powder samples were then pressed into pellets and analyzed using a Rigaku ZSX Primus II wavelength dispersive X-ray fluorescence (XRF) spectrometer at the University of New Mexico. Loss on ignition (LOI) corrections were carried out to account for volatile species.

ELECTRON MICROPROBE

Quantitative analysis and compositional mapping were carried out using a JEOL 8200 Superprobe electron microprobe (EMP), operating at an accelerating voltage of 15 kV and beam current of 10 nA. This instrument is equipped with five wavelength–dispersive X-ray spectrometers (WDS) and an UTW Noran energy dispersive (EDS) detector. Quantitative elemental maps for Zr were obtained from several regions using a focused beam. Analyses of baddeleyite and zircon were performed by focused beam analysis for sixteen elements (Si, Y, Al, Nd, Ca, Hf, Zr, Sm, Ti, Pb, Fe, La, Th, Yb, Ce and U). Peak counting times varied from 20 seconds for the major elements (Si, Al and Zr), 30 seconds for Hf and Ca, and 40 seconds all other elements. Elemental calibration was performed using CM Taylor Company Microprobe Standards as follows: Ca on diopside; Al, Si and Fe on almandine, U on UO_2 monazite, Sm on $SmPO_4$, Ti on rutile, Zr and Hf on ZrO_2, Y on YAG monazite, Pb on pyrochlore monazite, Ce and La on REE glass #3 (Drake and Weill, 1972), Nd on $NdPO_4$, Yb on $YbPO_4$, and Th on ThO_2 monazite. Analyses of chrome spinel were performed by focused beam analysis for

fourteen elements (Cr, Al, Fe, Mg, Zn, Mn, Ti, Si, Ca, Na, V, Co, P, and K). Peak counting times varied from 20 seconds for the major elements (Cr, Fe, Si,) and 30 seconds for all other elements. Elemental calibration was performed using CM Taylor Company Microprobe Standards as follows: Cr on chromite, Mn on spessartine, V on V metal, Co on Co metal, Fe and Ti on ilmenite, Si, Ca, and Mg on diopside, Zn on sphalerite, Al and K on orthoclase, P on apatite, and Na on albite. Sodium and K were always analyzed first in the sequence to minimize volatile loss. A ZAF correction procedure was applied to all the data. Additional functions in the JEOL 8200 software allowing for empirical corrections of the possible elemental peak overlaps between Co and Fe, V and Ti, and Mn and Cr were used. All analyses had their Fe^{3+} concentrations estimated by assuming stoichiometric criteria according to the method of Droop (1987). Backscattered electron (BSE) images were collected using the Electron Microprobe and the FIB-SEM.

FIB-SEM (FOCUSED ION BEAM – SECONDARY ELECTRON MICROSCOPE)

TEM samples were prepared using the focused ion beam (FIB) technique, using a FEI Quanta 3D FEGSEM/FIB instrument. A platinum protective layer (2 microns thick and 2 microns wide) was deposited in a strip across the area of interest prior to FIB sample preparation to minimize ion beam damage. FIB milling was carried out using a Ga ion beam with an accelerating voltage of 30 kV and beam currents ranging from 7 nA during the earliest stages of milling, progressively decreasing to 7 pA as the thickness decreased. The final stage of milling to obtain a sample thickness of <100 nm was performed using a 5kV beam and a beam current of 70 pA to minimize surface

amorphization of the sample. The samples were removed from the thin section by the in situ lift out technique using an Omniprobe 200 micromanipulator and were transferred to a Cu TEM half grid. Final ion milling to electron transparency was carried out with the samples attached to the TEM grid.

TEM (TRANSMISSION ELECTRON MICROSCOPY)

A JEOL 2010 high resolution transmission electron microscope (HRTEM) and JEOL 2010F FASTEM field emission gun scanning transmission electron microscope (STEM/TEM) at the University of New Mexico were used to analyze the TEM sections. Both instruments were operated a voltage of 200 kV. A variety of TEM techniques were used to characterize the samples including: Bright Field TEM imaging, Dark Field STEM imaging, High Resolution Transmission Electron Microscopy (HRTEM), Selected Area Electron Diffraction and Energy Dispersive X-ray Microanalysis.

CHAPTER 6: XRF, ZIRCON, AND BADDELEYITE

XRF ANALYSES

XRF data for the bulk rocks from this study and Schweitzer (1998) are given in table 1. There are significant differences in the composition of the Basal Rhyolite from individual samples of Basal Rhyolite from the Stavoren Inlier. For example, the rocks with pseudospherulitic texture (W91-102 and W95-35) have significantly higher Cr_2O_3 and Na_2O than the rock with deformed acicular texture (W03-07). Sample W95-35 has more than double the Zr of sample W91-102 (405 and 185 respectively). The Basal Rhyolite at Loskop Dam has a ~6 wt % less SiO_2, ~1.4 wt % less MgO, 140 to 804 ppm less Cr, and ~5% more Fe_2O_3 than the Basal Rhyolite from the Stavoren Inlier. The Basal Rhyolite at the Messchunfontein Section is similar to that of the Stavoren Inlier with the exception of having slightly lower Cr content (~129 ppm), and higher MgO and CaO contents. Notable is the absence of U in all bulk samples analyzed.

ZIRCON ($ZRSIO_4$) AND BADDELEYITE (ZrO_2)

Stavoren Inlier

Zirconium-bearing phases were thoroughly documented in samples W95-35 and W91-102 from the Stavoren Inlier, while those in W03-07 and 95-34 were not. Zirconium X-ray maps for samples W95-35 and W91-102 are shown in figure 7.

W95-35

Zirconium X-ray maps indicate that Zr is widely distributed in very small blebs (<10 μm^2) throughout the sample (Fig. 7A). Investigations of these blebs by Backscattered Electron (BSE) imaging led to the discovery of two populations of Zr-

bearing phases: **1)** <10 µm composite grains consisting of zircon and baddeleyite and **2)** <10 µm irregular shaped zircon grains (Fig. 8). The composite zircon-baddeleyite grains occur in the interstices of quartz and feldspar. Some zircon-baddeleyite composite grains appear to retain vestiges of a tabular crystal form viewed from the side or end on (Fig. 8A, 8D, 8E) which is the typical crystal form of baddeleyite in mafic lithologies (Heaman and LeCheminant, 1993). Some zircon grains occur without baddeleyite and exhibit irregular morphologies that are not consistent with zircons typically found in a rhyolite (Fig. 8F). Normally zircon is present in rhyolites as euhedral, zoned grains which range in size from 20-60 µms. Similar to the zircon-baddeleyite composite grains, irregular shaped zircon crystals are located in the pseudospherulitic aggregates as well as the matrix.

W91-102

The Zr X-ray map for W91-102 (Fig. 7B) shows that, like W95-35, Zr is widely distributed into small blebs. However, in W91-102 tiny areas of very low Zr concentration are much more common and small areas of high Zr concentration are slightly less common. Each pixel indicative of higher Zr detection levels (50-72) are anhedral zircon grains ranging in size 4-10 µm (Fig. 9A, 9B, 9C); each Zr detection level of ~13 led to the discovery of very small (0.5-1.5 µm) anhedral zircon grains (Fig. 9D). Baddeleyite was not found in 91-102 despite a thorough search. Similar to W95-35, the zircons are usually found along grain boundaries between quartz and feldspar, however some of the smaller grains in the groundmass were often completely enclosed by feldspar or quartz.

Oxide	BRLD	MS	PT-SI	PT-SI	DAT-SI	Schweitzer SI	Schweitzer MS
Sample #	W03-61	W08-11	W91-102	W95-35	W03-07		
SiO_2	69.48	70.23	76.34	76.61	74.67	75.24	70.22
TiO_2	0.62	0.42	0.27	0.27	0.23	0.26	0.4
Al_2O_3	12.46	13.61	11.17	11.91	11.55	10.52	12.56
Fe_2O_3	8.25	5.87	2.94	3.11	2.60	3.10	4.69
MnO	0.20	0.13	0.07	0.10	0.08	0.09	0.11
MgO	0.65	3.67	2.05	2.47	1.64	1.68	2.72
CaO	2.10	4.35	0.67	1.20	0.88	0.94	4.24
Na_2O	3.01	2.06	2.79	1.59	0.00	1.26	1.72
K_2O	4.13	3.32	4.00	4.61	3.63	4.69	3.25
P_2O_5	0.14	0.10	0.08	0.08	0.07	0.19	0.09
LOI					3.49	2.12	N/A
Total (%)	101.03	103.76	100.39	101.95	98.85	100.00	100
Nb (ppm)	16	6	7	6	9	5	6
Zr (ppm)	311	129	185	405	255	231	194
Y (ppm)	49	13	16	16	28	20	21
Sr (ppm)	92	164	83	75	33	111	222
Rb (ppm)	142	91	104	144	233	193	110
Zn (ppm)	252	52	112	97	87	135	55
Cu (ppm)	46	7	6	7	6	1	1
Ni (ppm)	9	45	28	27	26	16	36
Cr (ppm)	23	129	837	759	173	507	139
V (ppm)	10	92	42	43	33	39	80
Ba (ppm)	881	782	1300	1681	630	1432	885
Sc (ppm)	12	15	7	7	6	5	14
Ga (ppm)	N/A	N/A	N/A	N/A	N/A	9	12
Hf (ppm)	54	9	13	19	36	1	0
U (ppm)	0	0	0	0	0	0	0
Th (ppm)	N/A	N/A	N/A	N/A	N/A	15	14
Pb (ppm)	54.10	9	13	19	36	6	7
# Samples	1	1	1	1	1	7	4

Table 1: Bulk rock XRF data from this study and Schweitzer (1998). BRLD = Basal Rhyolite remelted and recrystallized as granophyre near Loskop Dam, MS = Messchunfontein, PT-SI = Pseudospherulitic Texture of the Stavoren Inlier, DAT-SI = Deformed Acicular Texture of the Stavoren Inlier. XRF data from Schweitzer (1998) comes from two localities, the Stavoren Inlier (SI) and the Messchunfontein section (MS).

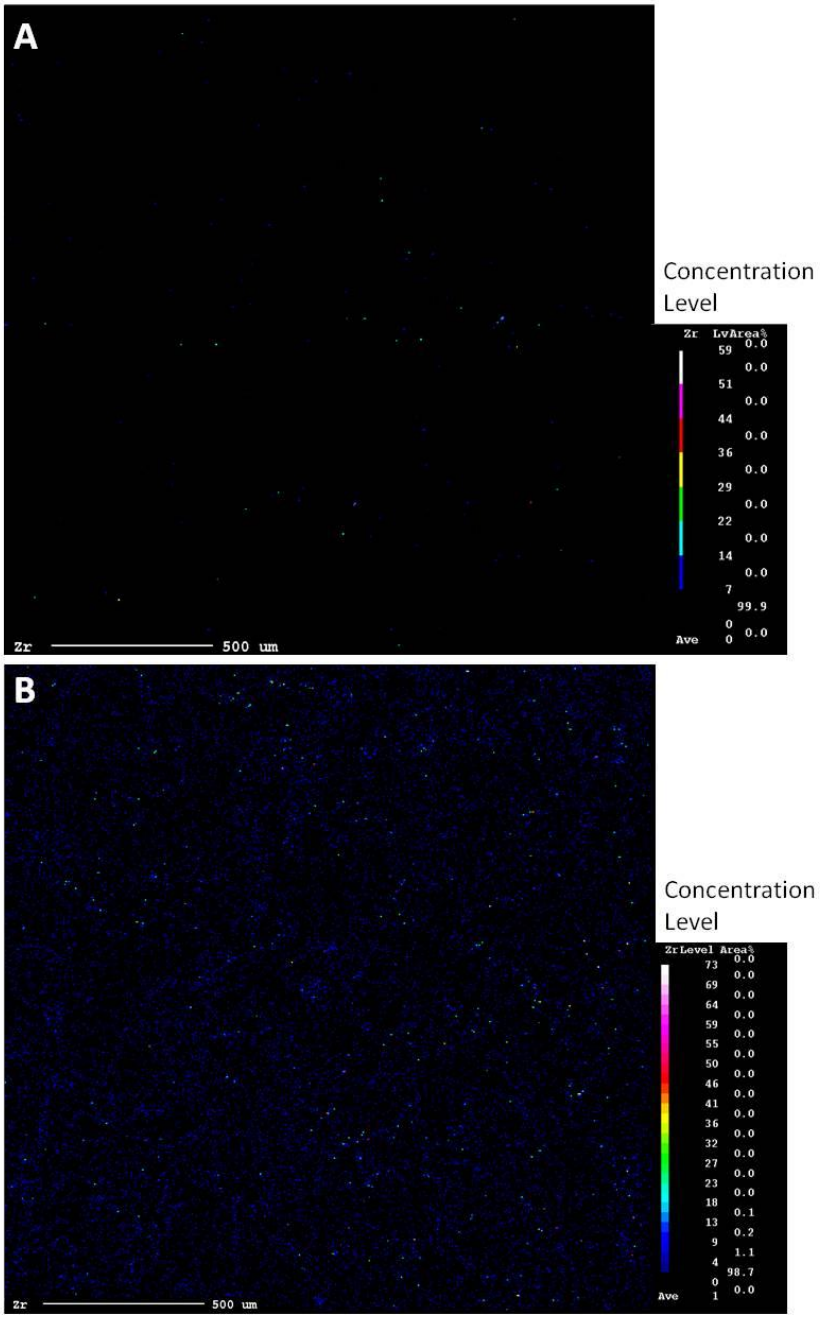

Figure 7. 2.5 x 2.5 mm Zr X-ray maps of samples W95-35 and W91-102. **A)** W95-35, pixels representing Zr concentration levels of 14 and higher represent a Zr-bearing phase. **B)** Zr X-ray map of W91-102: Light blue, web-like pattern of very low Zr concentration is due to background. All individual pixels or clusters of 2-3 pixels with concentration level of 13 and higher (scale on right) represent a Zr-bearing phase.

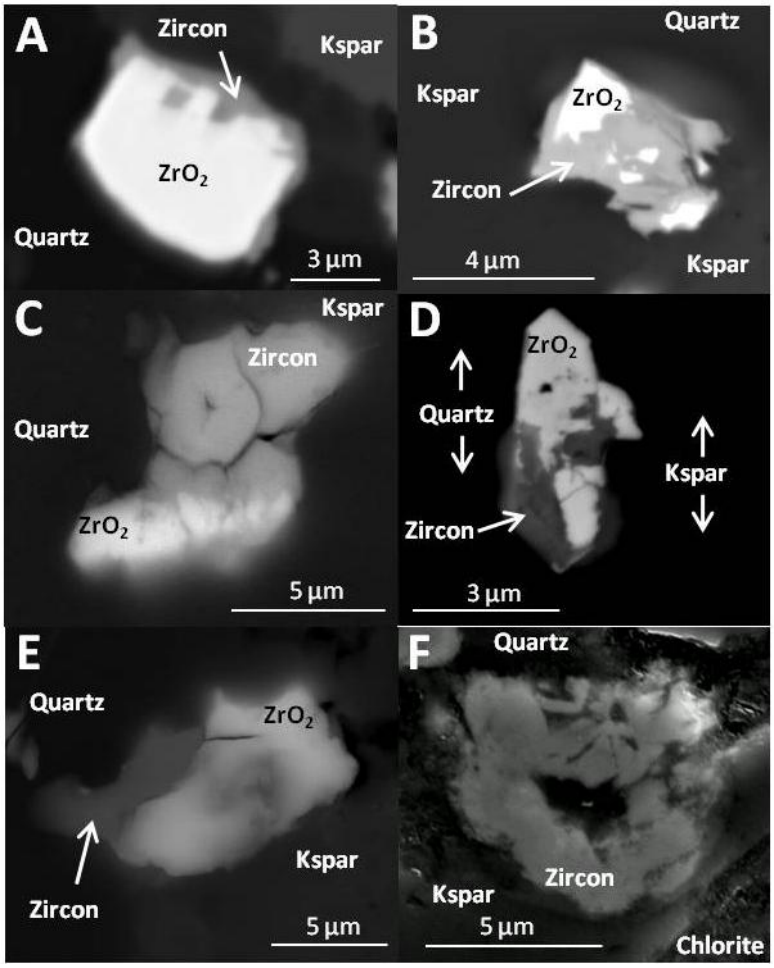

Figure 8. Backscattered electron images of composite zircon-baddeleyite grains and irregularly shaped zircon in W95-35. A-E All composite grains are between quartz and feldspar. All baddeleyites have zircon rims of variable thickness. Baddeleyite grains in A and E have the smallest amount of zircon in the observable portion of the grain compared to B and C which have more zircon than baddeleyite. Grain F consists entirely of zircon; tabular grains most prominent the upper part of the grain.

W03-07 and 95-34

Zirconium X-ray maps were not produced for these samples. One zircon grain has been found in W03-07 after a significant amount of searching in BSE mode at high magnification. An image of this grain is found in figure 10A. An in-depth search for Zr-bearing phases from 95-34 has not yet been carried out, and is beyond the scope of this study.

Messchunfontein Section

Time allowed only a very brief EDS survey of W08-11 which located only one zircon grain and no baddeleyite (Fig. 10B). The zircon is similar in size to those found in the Stavoren Inlier and also exists along a grain boundary between quartz and K-feldspar. It differs from most zircon grains of the Stavoren Inlier in that it seems to exhibit what could be considered a subhedral morphology.

Recrystallized Basal Rhyolite Near Loskop Dam

A high magnification EDS investigation led to the discovery of composite zircon-baddeleyite grains in sample W03-61. Many, but not all of the composite zircon-baddeleyite grains, are larger ($\leq$ 20 x 12 μm) than those found in the Basal Rhyolite from the Stavoren Inlier (Fig. 11). As opposed to baddeleyite in the Stavoren Inlier, the baddeleyite grains near Loskop Dam usually exhibit well-defined crystal forms, some of them as twinned crystals parallel to each other or at acute angles. Within isolated composite grains of zircon-baddeleyite, individual baddeleyite crystals are separated by thin veneers of zircon. Figure 11A shows twinned baddeleyite crystals completely enclosed in quartz with a thin veneer of zircon between the quartz and baddeleyite. Some zircon exhibits sizes and shapes similar to those of tabular baddeleyite crystals (Fig. 11E).

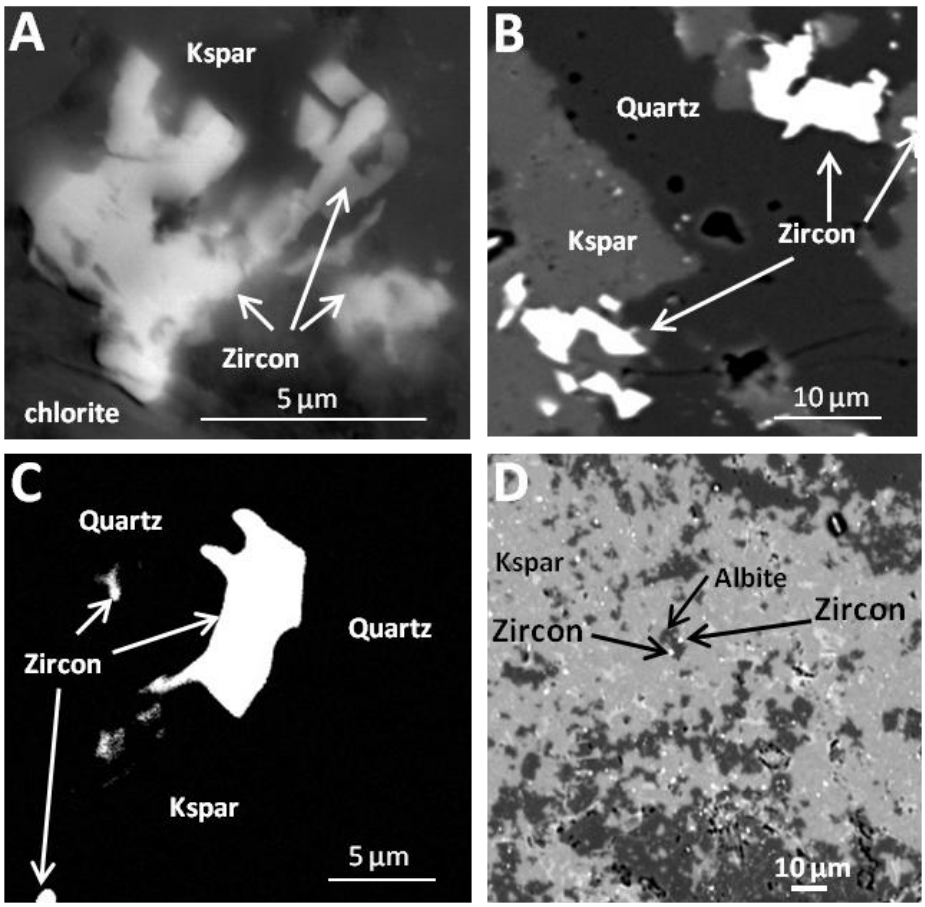

Figure 9. Backscattered electron images of zircon grains from sample W91-102. Image A was taken by FEGSEM; B-C by EMP. **A-C)** Irregular shaped zircon in clusters of grains of various sizes. Large grains have tabular shaped offshoots. **D)** Two 1x1 µm zircon grains on either side of a small patch of albite in a matrix dominated by K-feldspar. Most of the bright inclusions are magnetite and rutile, though some others may be zircon.

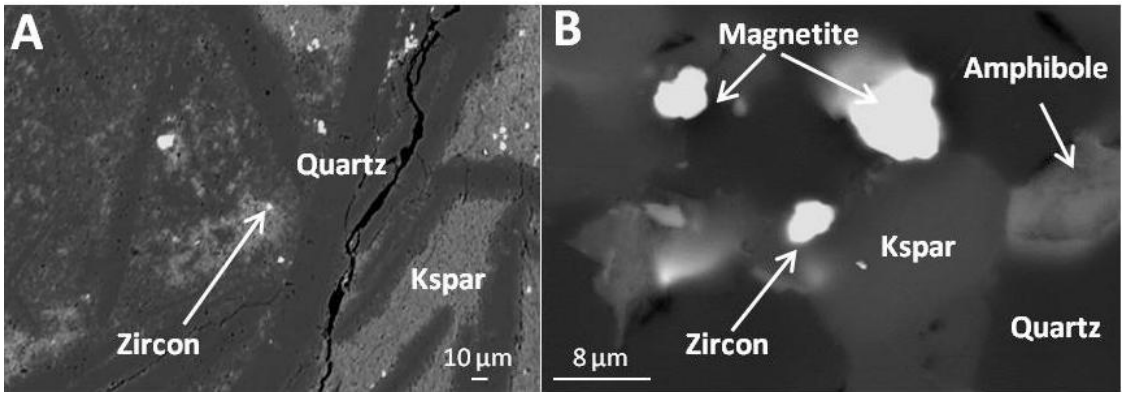

Figure 10. Zircon grains from W03-07 and W08-11 **A)** The only zircon grain found in a thorough search of W03-07 (deformed acicular texture) of the Stavoren Inlier. Other bright patches turned out to be monazite, magnetite, and apatite. **B)** The only zircon grain found in a brief search of the Basal Rhyolite of the Messchunfontein section (W08-11). Both zircons occur in grain boundaries between quartz and feldspar and are < 10 µm long.

WDS ANALYSES OF ZIRCON AND BADDELEYITE

To avoid analytical overlap between zircon, baddeleyite, and matrix, tiny grains from W95-35, W91-102 and W03-61, were analyzed by WDS with a focused beam and low beam current. Despite these efforts, it remained difficult to obtain analyses without significant overlap of a nearby phase, particularly in samples W95-35 and W9-102. As a result, there are only two acceptable analyses of baddeleyite and nine analyses of zircon from these two samples. In sample W03-61, however, phase overlap was not a problem for baddeleyite because their grain size was large enough. Only two zircon crystals in W03-61 were large enough to contain the entire beam. Table 2 shows the average compositional analyses of zircon and baddeleyite from both localities. In figure 12 the concentration of HfO_2, TiO_2, and FeO of the baddeleyites from this study are plotted on a ternary diagram superimposed over a similar diagram from Heaman and LeCheminant (1993). They plot in the area of overlap between the fields of lunar basalts, diabase dikes, and gabbros, but mostly in the diabase dike field. No analyses plot in the kimberlite field.

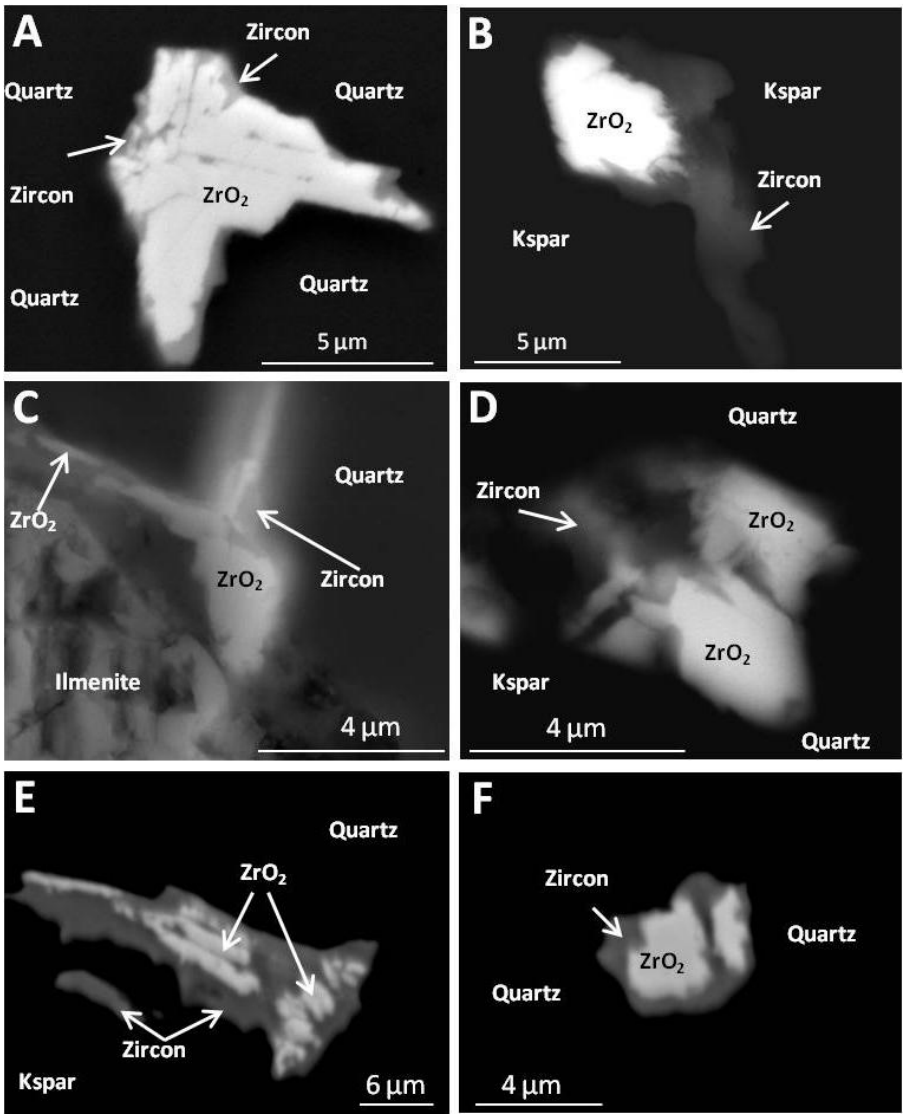

Figure 11. Backscattered electron images of composite zircon-baddeleyite in the Basal Rhyolite near Loskop Dam (W03-61). **A)** A group of twinned tabular baddeleyite crystals completely surrounded by quartz. Zircon forms thin rims between baddeleyite and quartz and individual baddeleyite grains. **B)** A patch of baddeleyite with a long tail of zircon. A ragged reaction front separates baddeleyite and zircon. **C)** Twinned baddeleyite grains variably replaced by zircon on the edge of an ilmenite grain. **D)** End-on view of a tabular composite zircon-baddeleyite grain. **E)** Aggregate of tabular baddeleyite grains of various sizes exhibiting thick zircon rims. **F)** Zircon-baddeleyite composite grain which may represent a tabular multiphase grain viewed end on.

TEM ANALYSES

To determine the crystal structure, crystallographic orientation, microstructure, and assess the 3-dimensional relationship between zircon and baddeleyite, FIB-TEM sections were prepared from the composite zircon-baddeleyite grains shown in images C and D of figure 8 (Fig. 14A,14B respectively). High resolution TEM images and electron diffraction patterns, both useful in characterizing the degree of crystallinity of a phase, show that the zircon is partially metamict (Figs. 13, 14). Dark field images and electron diffraction patterns of the zircon and baddeleyite are shown in figure 14. The dark field images show zircon embaying irregularly shaped patches of baddeleyite, while the electron diffraction patterns indicate baddeleyite patches are monoclinic and vary in orientation by only a few degrees.

Oxides	Baddeleyite (Stavoren Inlier)	Baddeleyite (Loskop Dam)	Zircon (Stavoren Inlier)	Zircon (Loskop Dam)
SiO_2	5.98	0.62	32.31	31.36
$Y2O_3$	0.06	0.23	2.31	3.61
$Al2O_3$	0.04	0.07	3.04	2.19
Nd_2O_3	0.02	0.04	0.41	0.15
CaO	0.06	0.07	1.82	2.10
HfO_2	1.67	1.63	0.00	0.00
ZrO_2	88.82	94.56	44.34	49.27
Sm_2O_3	0.02	0.02	0.08	0.00
TiO_2	1.79	1.02	1.34	0.07
PbO	0.07	0.11	0.13	0.02
FeO	0.43	0.83	1.92	1.25
La_2O_3	0.01	0.01	0.04	0.05
ThO2	0.05	0.03	0.98	0.28
Yb_2O_3	0.05	0.15	0.30	0.49
Ce_2O_3	0.03	0.04	0.62	0.28
UO_2	0.18	0.21	0.37	0.53
Total	99.27	99.65	90.01	91.66
# Analyses	2	18	8	2

Table 2. Average compositions of zircon and baddeleyite from this study. The presence of 6% SiO_2 in baddeleyites from the Stavoren Inlier is due to beam overlap with quartz.

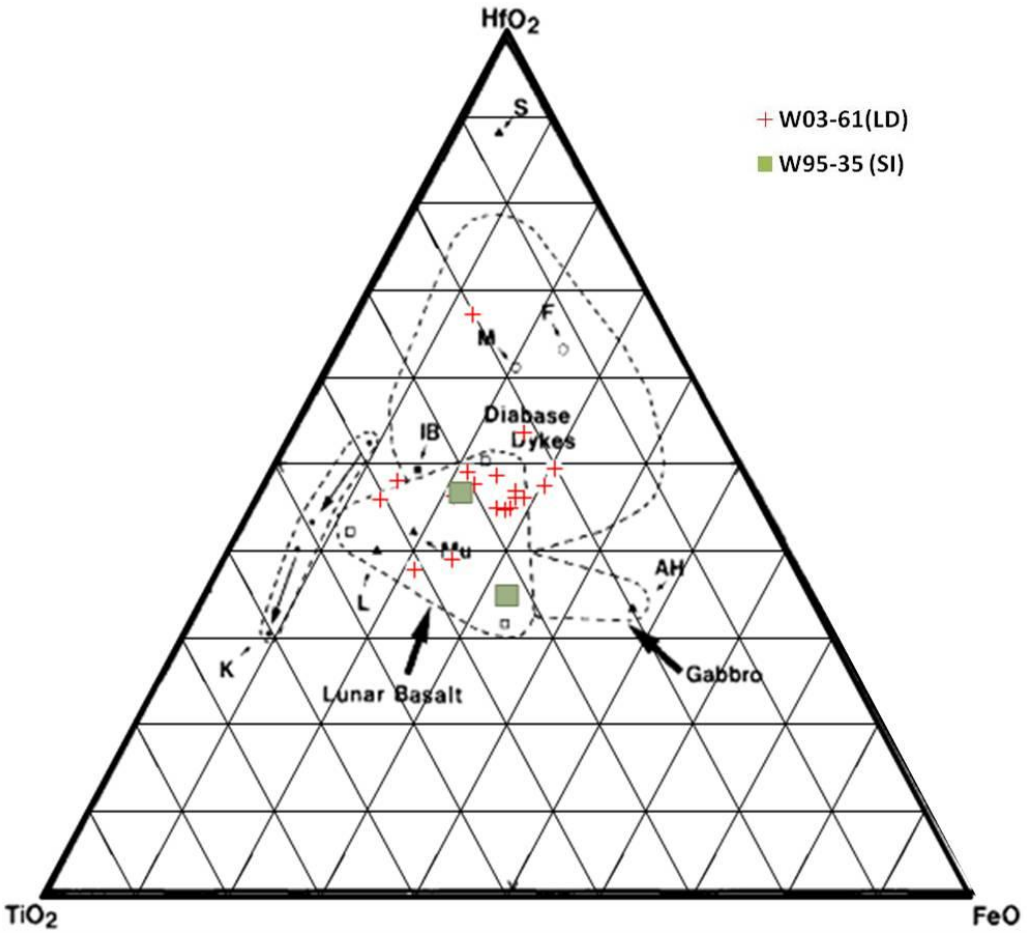

Figure 12. HfO_2-TiO_2-FeO ternary plot of baddeleyites from this study (green squares and red crosses) superimposed over a similar plot from gabbros, diabase dikes, kimberlites, and lunar basalts (after Heaman and LeCheminant 1993). LD = Loskop Dam, SI = Stavoren Inlier. Plots are based on weight % oxides. Baddeleyites from this study fall within the overlapping regions of diabase dykes, gabbro, and lunar Basalts.

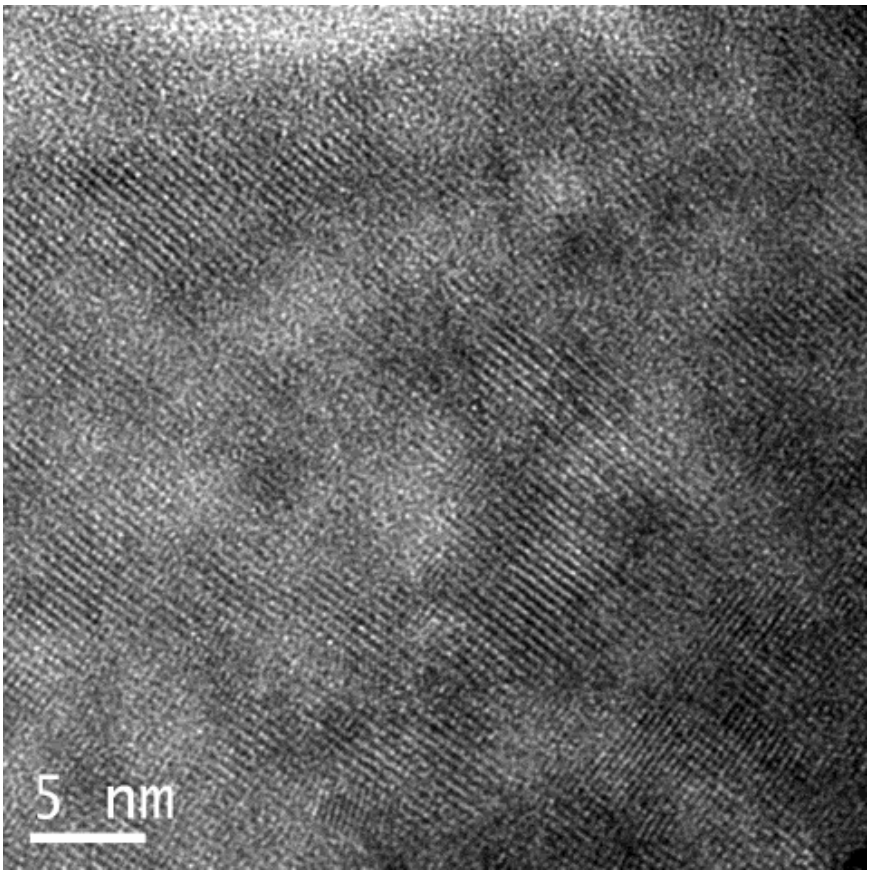

Figure 13. HRTEM image of zircon highlighting its partially metamict condition. The lighter regions are comprised of $ZrSiO_4$ that shows no structure (i.e. lattice fringes) and are clearly indicative of metamict regions.

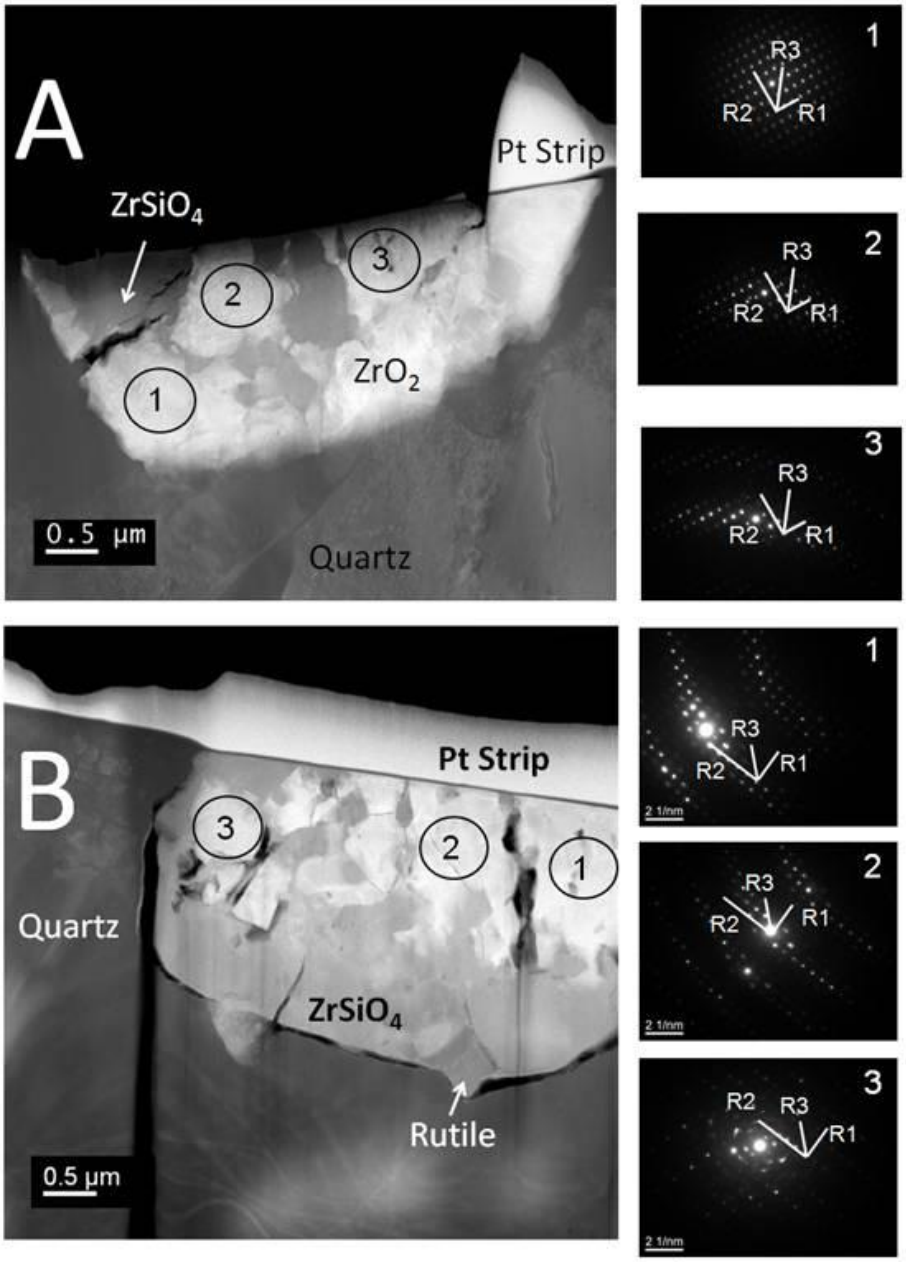

Figure 14. Dark field Z-contrast STEM images and electron diffraction patterns from FIB prepared composite zircon-baddeleyite grains from W95-35. Image A and B both show embayment of baddeleyite by zircon. This texture suggests the baddeleyite patches were part of a single crystal, partially replaced by zircon. Circled numbers in A and B indicate locations on individual baddeleyite patches where electron diffraction patterns were obtained. The corresponding electron diffraction patterns are shown on the right. All patches of baddeleyite within a single composite grain have similar crystallographic orientations (R1, R2 and R3), within 1-2 degrees. This confirms that they are indeed remnants of a larger crystal. The blurred background in the third diffraction pattern of grain B is due to overlap with metamict zircon.

CHAPTER 7: DICUSSION OF ZIRCON AND BADDELEYITE

EVIDENCE FOR BADDELEYITE AS A PRIMARY PHASE

The textural relationship between zircon and baddeleyite highlighted in STEM bright and dark field images from sample W95-35 and in high resolution BSE and SEI images from W03-61 (Figs. 11 and 14) suggests that zircon partially replaced elongate, tabular shaped baddeleyite crystals. This is confirmed by the electron diffraction patterns of baddeleyite in two composite zircon-baddeleyite grains. In these electron diffraction patterns, the isolated patches of baddeleyite within each composite zircon-baddeleyite grain have similar orientations (Fig. 14, images on right). A common morphology of baddeleyite crystals, similar to those that are best preserved in the Basal Rhyolite in the Stavoren Inlier and those in the Basal Rhyolite near Loskop Dam, but larger, can be found in figure 15. Zircons with a tabular shape similar to that of baddeleyite crystals in W03-61 (Fig. 11E) and to a lesser extent in W95-35 (Fig. 7F), may suggest that some zircon is pseudomorphous after baddeleyite. In addition to zircon formed by replacement of baddeleyite as the Basal Rhyolite cooled, zircon may have also crystallized directly out of the melt, close to or isolated from baddeleyite. This proposed population of primary zircon is represented by tail-like offshoots of zircon emanating from partially replaced baddeleyite grains in W03-61, as well as the anhedral zircon grains present in sample W91-102 and W95-35.

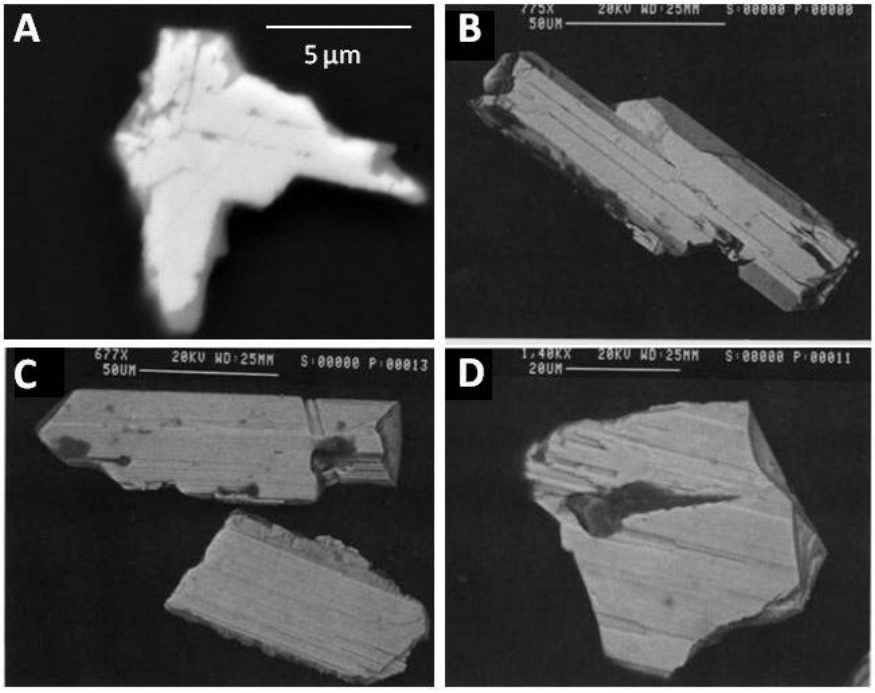

Figure 15. Baddeleyite from the Loskop Dam locality, compared with baddeleyite from gabbros and diabase dikes (Heaman and LeCheminant 1993). **A)** BSE image of twinned, euhedral baddeleyite from this study. **B)** BSE image of composite twinned baddeleyite crystal from the Fortress gabbro sill, Mackenzie swarm, Northwest Territories, Canada. **C)** BSE image of two euhedral baddeleyite grains from the Mystery Lake diabase, Mackenzie swarm, Manitoba, Canada. **D)** BSE image of a broken baddeleyite crystal from the Thule sill, Mackenzie swarm, Ellesmere Island, Northwest Territories, Canada.

ABSENCE OF DETECTABLE Hf IN ZIRCON

Perhaps the most remarkable feature common to all of the zircons in this study is their complete lack of HfO_2, which is ubiquitous in zircon throughout the geologic record. Zr and Hf are both quadravalent over a wide range of redox conditions and their ionic radii (0.84 Å and 0.83 Å, respectively) are similar (Shannon, 1976).

EVIDENCE ZIRCON WAS HYDROTHERMALLY ALTERED FROM A METAMICT STATE

Pure zircon has a stoichiometric composition of 67.5 wt % ZrO_2 and 32.8 wt % SiO_2 (Hoskin and Schaltegger, 2003). Zircon is stable during hydrothermal alteration,

unless it is in a metamict state. There are three characteristics of the zircons in this study which suggests they have been hydrothermally altered and confirms they are metamict (Figs. 13, 14).

1. Zircons have ~45 wt % ZrO_2 (Table 2), which is 22% less than pure zircon. Depletion in Zr is indicative of hydrothermal alteration (Geisler et al., 2003).

2. Enrichments in Y_2O_3, FeO, Al_2O_3, and CaO (Table 2), which normally fall beneath the detection limit of WDS analyses (Hoskin and Schaltegger, 2003).

3. Low totals of all zircon analyses, which suggest the presence of a hydrous phase (Geisler et al., 2003).

DIFFERENCES IN U, Th, AND Hf CONCENTRATION BETWEEN ZIRCON AND BADDELEYITE

The U and Th concentrations of the zircons studied are significantly higher than those in baddeleyites. Therefore, sources of U and Th, other than the baddeleyite being replaced, must have been available for incorporation into zircon as the Basal Rhyolite cooled. The most likely source of additional U and Th is the surrounding melt.

The absence of Hf in zircon, a characteristic of all zircons analyzed in this study, despite being separated by 60 km, has never been reported in metamorphic, hydrothermal, or hydrothermally altered zircon. Hafnium concentrations in primary igneous zircon have been shown to decrease with increasing temperature (Hoskin and Schaltegger, 2003), but never to the point where Hf is completely absent.

TiO_2 CONCENTRATION OF BADDELEYITE FROM THE STAVOREN INLIER AND LOSKOP DAM

According to Heaman and LeCheminant (1993) the TiO_2 concentration of baddeleyite increases with increasing temperature of crystallization. The average TiO_2 concentration of baddeleyites from the Basal Rhyolite near Loskop Dam is 1.02 wt %, while the average TiO_2 concentration of baddeleyite in the Stavoren Inlier is 1.79 wt % (2 analyses). The fact that baddeleyites in the Stavoren Inlier are more TiO_2 rich than zircons from the same locality (Table 2) suggests that phase overlap with zircon is not responsible for the higher concentration of TiO_2 in baddeleyite in the Stavoren Inlier than baddeleyites from the Basal Rhyolite near Loskop Dam.

CHAPTER 8: CHROME SPINEL

NOMENCLATURE

Chromite is a member of the spinel group, with the general formula $(Fe^{2+}, Mg)_8(Fe^{3+}, Cr, Al)_{16}O_{32}$. The nomenclature for chrome spinel is based on the ratio of the trivalent cations, Cr^{3+} and Fe^{3+}. If Fe^{3+} is more concentrated than Cr, the mineral is referred to as Cr-magnetite. The substitution of Zn or Mn for Mg in a chromite is indicative of metasomatism or metamorphism. In these cases, the terms zincochromite and Mn-enriched chromite are used, respectively.

STAVOREN INLIER

XRF data from this study and from Schweitzer (1998) show that the Basal Rhyolite of the Stavoren Inlier has Cr concentrations that range between 173 and 900 ppm (Table 1). This is abnormally high for a conventional rhyolite, which normally contains 10-13 ppm Cr (NAVDAT, 2013). This study has determined that Cr in the Stavoren Inlier is located in Cr-bearing phases varying in size, composition, and texture. It also appears that differences in Cr concentration of the bulk rock correlate with the texture of the rock. Samples with pseudospherulitic textures, W95-35 and W91-102, contain 760-837 ppm Cr, while the deformed acicular texture (W03-07) contains 170 ppm Cr. The Cr-bearing phases range in size from 30-230 µm and commonly occur in small clusters of 3-8 grains, uncommonly as isolated sub-rounded crystals 100-150 µm in size, and in arcuate chains up to 2.5 mm in length which are comprised of up to fifty 20-150 µm euhedral crystals.

The Cr-bearing phases from samples W95-35, W91-102 and 95-34 have been divided into 5 compositional types based on their Cr_2O_3, MgO, and SiO_2 contents. Several compositional types may be present in a single grain, due to zoning. Types 1 and 3 have been further sub-divided into subgroups based on sufficient chemical variation in SiO_2, MgO, ZnO and MnO. Chromium-bearing phases from sample WO3-07 have only been analyzed using EDS, so their compositions are not included in table 3.

Oxides	Type 1a	Type 1b	Type 1c	Type 2	Type 3a	Type 3b	Type 4	Type 5	Silicate inclusions
Cr_2O_3	26.44	25.98	37.76	7.63	20.01	20.19	15.02	29.89	2.69
Fe_2O_3	24.71	30.78	24.69	57.95	N/A	N/A	48.12	N/A	N/A
FeO	13.10	24.25	21.02	31.11	25.59	25.23	28.72	25.24	13.34
Al_2O_3	11.25	9.91	9.57	0.82	10.96	9.66	3.13	6.01	21.41
MgO	0.02	0.15	8.14	0.00	1.19	2.77	0.01	0.26	2.69
SiO_2	2.22	0.06	0.05	0.19	13.37	19.38	0.11	4.38	40.74
TiO_2	0.58	0.73	0.42	1.09	3.40	2.30	1.09	1.22	0.42
ZnO	17.78	1.05	0.22	0.84	4.22	4.21	2.21	6.84	0.00
MnO	4.08	8.82	0.74	0.66	1.69	1.71	2.03	3.51	0.00
K_2O	0.00	0.00	0.00	0.00	0.69	0.65	0.00	0.11	8.35
V_2O_3	0.09	0.04	0.01	0.10	0.23	0.18	0.10	0.17	0.71
CoO	0.03	0.04	0.06	0.04	0.02	0.02	0.03	0.03	0.01
CaO	0.06	0.01	0.01	0.01	0.25	0.58	0.01	0.38	0.00
Na_2O	0.00	0.00	0.00	0.00	0.24	0.21	0.00	0.32	0.00
Total	100.39	101.80	102.68	100.44	81.86	87.10	100.58	78.36	89.71
# Analyses	20	12	15	16	13	14	8	28	2

Table 3. Compositions of the 5 types of Cr-bearing phases present in Stavoren Inlier. FeO vs Fe_2O_3 has been calculated for types 1, 2, and 4 by stoichiometery using the method of Droop (1987). Despite the inclusion of all the elements present in initial EDS analyses, the WDS analyses of types 3 and 5 resulted in low totals. Calculations are based on 24 cations and 32 oxygens.

Type 1

Type 1 is characterized as chrome spinels, which have so far only been found in sample 95-34. They have been divided into three subgroups: 1a. zincochromite, $(Fe^{2+}, Mg, Zn, Mn, Si)_{8.37}$ $(Fe^{3+}, Cr, Al, Ti)_{15.11}$ O_{32}, 1b. Mn-rich chrome spinel, (Fe^{2+}, Mg, Mn,

$Zn)_{8.11}$ $(Fe^{3+}, Cr, Al)_{15.66}$ O_{32} and 1c. Mg-bearing chromite, $(Fe^{2+}, Mg)_{7.87}$ $(Cr, Fe^{3+}, Al)_{15.81}$ O_{32} (Table 3).

Figure 16 shows the zonal relationship between the three subgroups in the largest type 1 grain studied. All three are present in the largest grains (> 75 µm) that are in or near, a 2.5 mm long arcuate chain of chrome spinel (Figs. 16 A, B). In the smaller grains (<75 µm), the place is taken by the Mn-rich zone. To highlight how the compositions behave along a traverse from left to right along the width of a type 1 chrome spinel, a 33-point traverse using WDS analyses was created (Fig. 17).

Spatial behavior of the type 1 chrome spinel composition

For the ease of description, types 1a, 1b, and 1c are hereafter referred to as the zincochromite patches, the high-Mn zone, and the high-Mg core respectively.

In the high-Mg core, the concentrations of Fe_2O3, Al_2O_3, and FeO increase slightly and Cr_2O_3 and MgO decrease slightly near the diffuse boundary with the high-Mn zone. Outward in the high-Mn zone, MnO, Fe_2O_3, Al_2O_3, and FeO increase, as MgO and Cr_2O_3 decrease. In the zincochromite patches, ZnO and MnO concentrations are relatively stable while Fe_2O_3 increases and Al_2O_3 and FeO decrease.

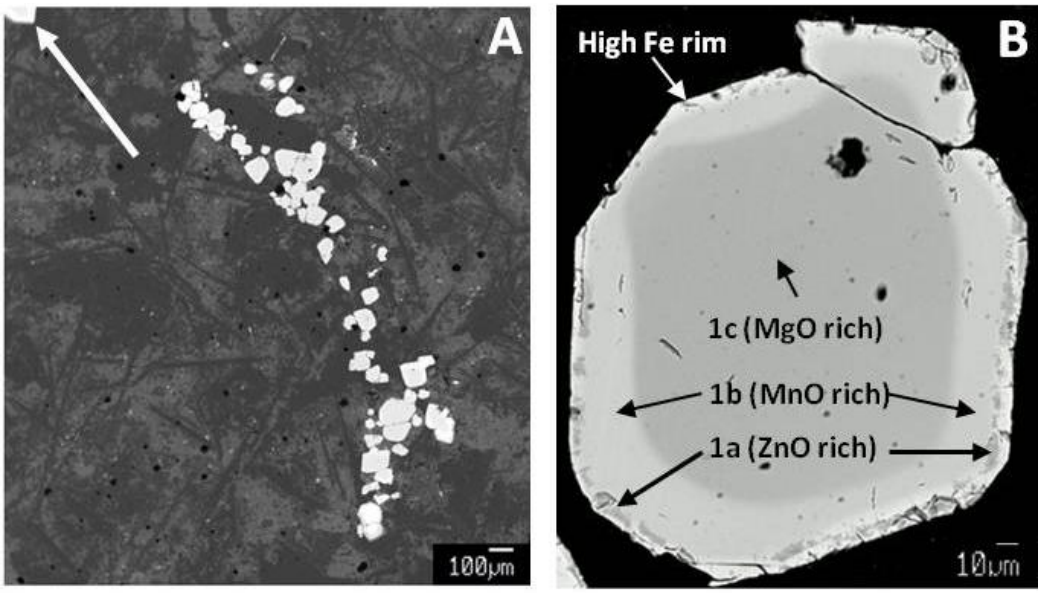

Figure 16. Backscattered electron images of type 1 chrome spinel in sample 95-34. **A)** BSE image of a ~2.5 mm long arc of over 50 type 1 chrome spinels. Grains range in size from 20-230 µm, with the smallest grains (<75µm) containing only types 1a and 1b and grains > 75 µm containing cores of type 1c. The chain is surrounded by a mixture of quartz patches (dark gray), 0.5-1 mm quartz needles with random orientations, and patches of interstitial K-feldspar and albite (light and medium gray, respectively). The location of the grain shown in image B is just off this image next to the chromite grain indicated by a white arrow. **B)** BSE image of a large type 1 grain. The entire grain is discontinuously rimmed by a thin veneer of a high Fe chrome spinel that is likely Cr-magnetite. Type 1a (zincochromite) occurs as isolated patches within a discrete zone near the margins of the grain and is mostly enclosed by type 1b (Mn-rich) composition. Type 1b encloses type 1c (Mg-rich) with a diffuse boundary separating the two. The shape of the 1c core preserves a remnant euhedral morphology that is also adopted by the outermost margin of the entire grain.

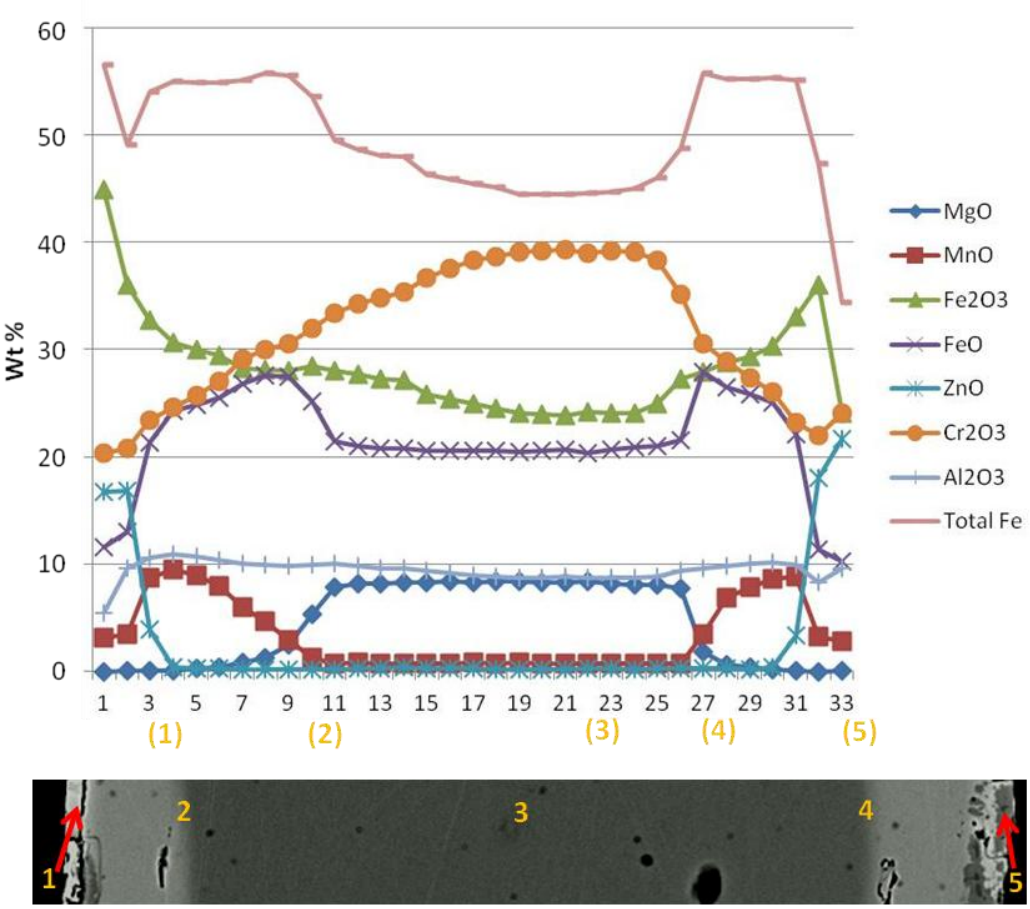

Figure 17. Compositional variation of type 1 chrome spinel along a left to right traverse. **Top)** plot of the 33 analyses showing the relationship between ZnO, MnO, and MgO content as well as Al_2O_3, Cr_2O_3, FeO, Fe_2O_3, and total Fe. **Bottom)** A backscattered electron image showing the portion of the type 1 grain traversed. Transitional points of traverse are indicated by orange numbers.

Types 2 and 3

Type 2 occurs in sample W91-102 as euhedral rims surrounding subrounded cores of type 3a and 3b (Fig. 18). In the cores, micron-scale intergrowths of an unknown volatile phase (little black dots in Figs. 18A, 18B), cause low totals in WDS analyses of 3a and 3b (Table 3). As a result, types 3a and 3b are not incompatible with spinel stoichiometery. Very small, bright inclusions in the type 3 cores contain elevated Fe (Fig. 18C).

High Fe^{3+} and low Cr classify type 2 as Cr-magnetite, $(Fe^{2+}, Mg)_{8.27}$ $(Fe^{3+}, Cr, Al)_{15.38,}$ $O_{32.}$ Microlites with elevated Ti are also present as (<0.5 µm x 4 µm) gray laths in type 2 Cr-magnetite (Fig. 18C). They are oriented in two directions, ~60° apart, and are interpreted as exsolution lamellae. Silicate inclusions in type 2 Cr-magnetite (Fig. 18B, 18C), occur as larger dark blebs which conform to the polygonal outline of the entire grain. There is an exception to the relationship of type 2 rimming type 3 compositions. This is evident in figure 18D, where type 3 appears to be rimming type 2.

Types 4 and 5

Types 4 and 5 occur in samples W91-102 and W95-35. They are similar to types 2 and 3 in that one (type 4) is consistent with a Cr-magnetite and the other, (type 5), does not fit to spinel stoichiometery due to tiny intergrowths of a volatile-bearing phase. A wide variety of spatial relationships has been documented between these two types (Fig. 19). The spatial relationships have been divided into 3 groups: 1) 5-80 µm thick type 4 rims partially surrounding type 5 cores (Fig. 19A, 19B), 2) exsolved grains of type 4 composition within a type 5 host (Fig. 19C, 19D) and 3) grains comprised solely of type 5 composition (Fig. 19E). Type 4 compositions that form rims around type 5 cores (Fig. 19A, 19B) vary slightly in composition from those that occur as exsolved microlaths in type 5 cores (Fig. 19C, 19D). Due to the small size of the type 4 microlaths within type 5 cores, obtaining analyses with minimal overlap proved difficult. However, by focusing on areas where the microlaths existed in densely packed regions, two reasonably acceptable analyses were made. These analyses show a marked decrease in TiO_2 content from 1.5 wt % in the rims, to 0.05 wt % in the exsolved type 4 compositions. The effects of phase overlap can be ruled out since the type 5 composition only contains 0.2-0.4 wt % TiO_2.

SiO_2 is slightly elevated (0.5 wt %) in the type 4 microlaths whereas the type 4 rims contain <0.05 wt %. Like the type 4 rims, the overall composition of the exsolved type 4 microlaths, is consistent with Cr-magnetite.

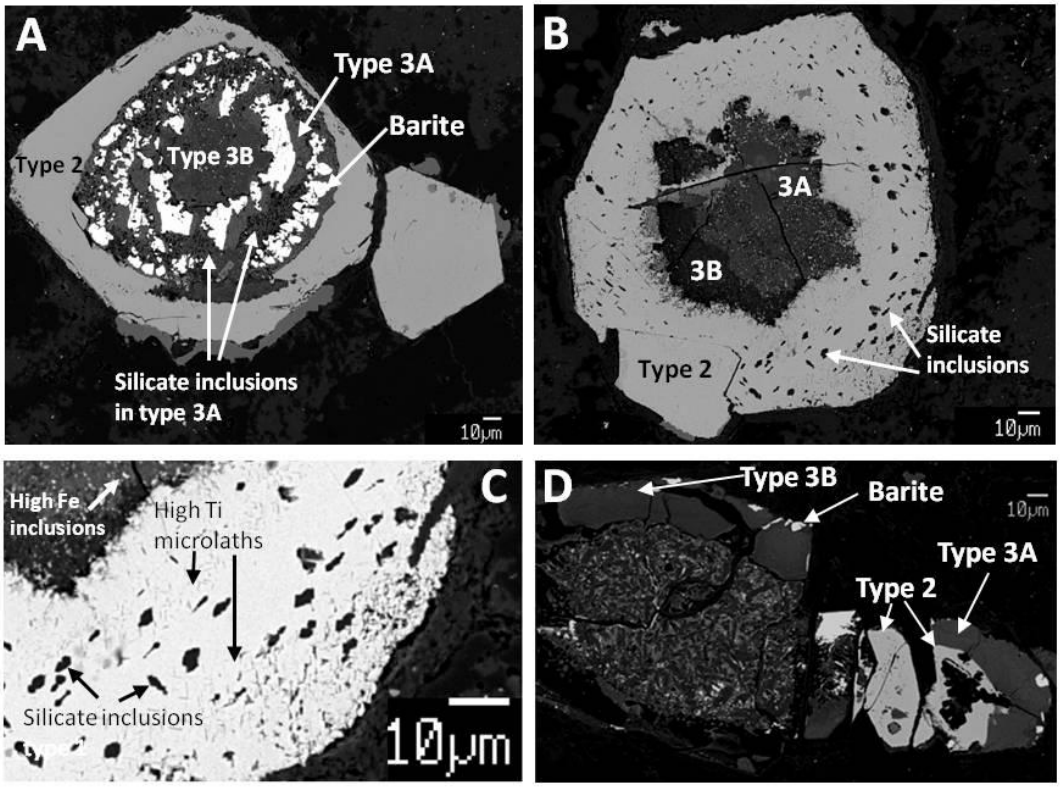

Figure 18. Backscattered electron images highlighting the spatial relationship between chrome spinel types 2 and 3. **A)** Euhedral type 2 rim surrounding a type 3 core with barite occurring in concentric bands. Black dots in type 3 represent an unknown silicate phase. **B)** Euhedral type 2 rim around a core comprised of type 3 compositions. Silicate inclusions are abundant in the rim. The core does not contain barite and differences in the type 3 compositions are well pronounced. **C)** High magnification image of the bottom right corner of the grain shown in image B. Two bands of high-Ti microlaths in the type 2 rim are highlighted as are high Fe inclusions in the type 3 core. **D)** Chrome spinels in W95-35 where type 3 compositions rim type 2 composition (bottom right). The composition of the "wormy" texture in the core of the grain on the left has not been thoroughly analyzed.

Chrome spinels in W03-07

Chrome spinels are not as common in sample W03-07 as they are in samples W91-102, W95-35, and 95-34. This is expected considering the lower bulk Cr concentration of the sample (173 ppm). The chrome spinels occur in clusters of 2-3 grains are embayed with Cr-muscovite (Fig. 20). The chrome spinels lack MgO cores and Cr-magnetite rims but have homogenous Cr_2O_3, ZnO, and MnO concentrations throughout.

SPINELS AT LOSKOP DAM

Chrome spinels are not present in the remelted Basal Rhyolite near Loskop Dam, which only has 23 ppm Cr. Instead, the compositions of spinels in this locality are ilmenite and magnetite.

SPINELS IN THE BASAL RHYOLITE OF THE MESSCHUNFONTEIN SECTION

The basal rhyolite occurring in the Messchunfontein section has a Cr concentration ranging from 90-300 ppm. This is significantly lower than the Basal Rhyolite in the Stavoren Inlier, but still well above the normal concentration in a typical rhyolite. In general, the spinels are far more numerous but smaller than they are in the Stavoren Inlier. The investigation of spinel populations in this locality is limited to a few EDS analyses which showed that most spinels are magnetite with a small proportion of spinels with 3-5 wt % Cr_2O_3 and 95-97 wt % total Fe.

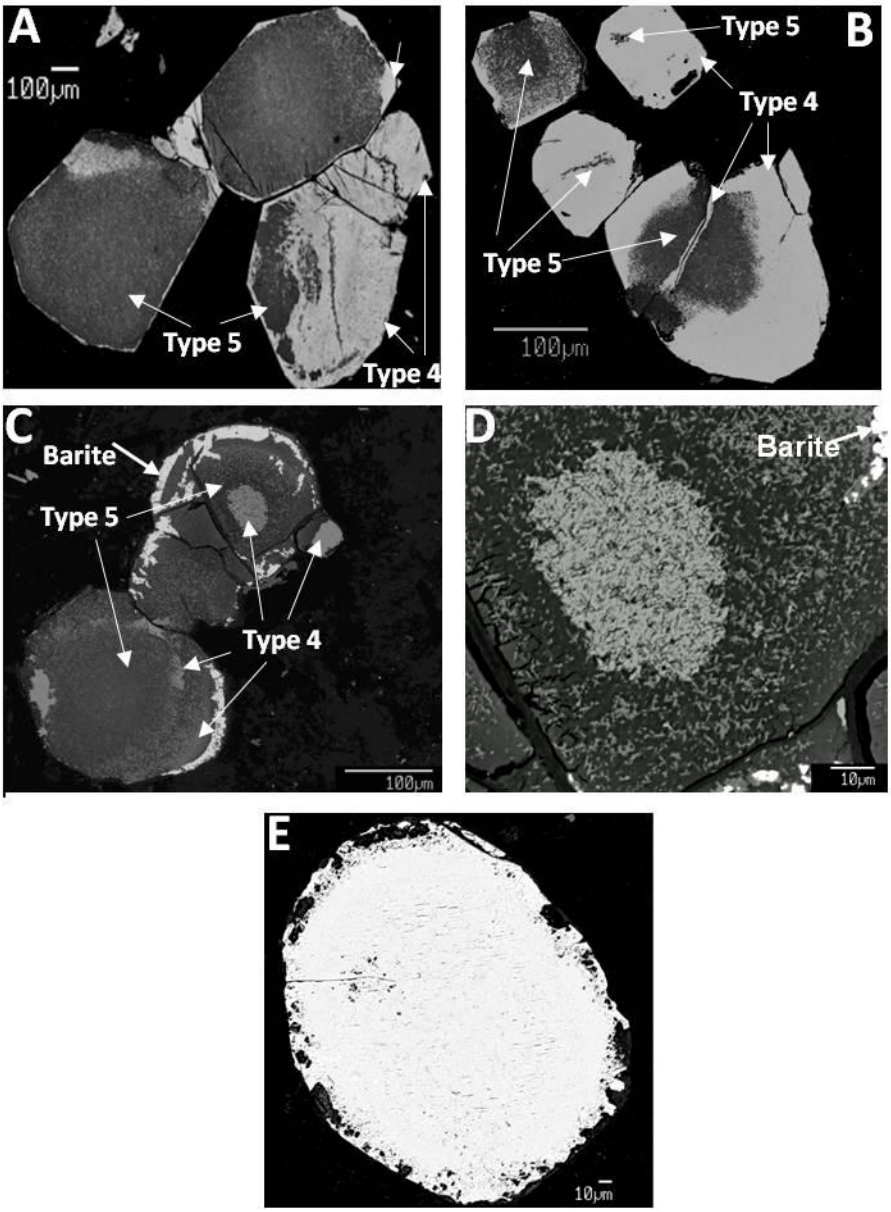

Figure 19. Backscattered electron images showing the textures associated with type 4 and 5 chrome spinel. **A)** A cluster of three euhedral grains in W91-102. Grains on the left and top center have a discontinuous, 5-10 µm thick, type 4 rim and areas where type 4 compositions are found immersed in the type 5 core. The type 4 composition immersed in type 5 has an exsolved appearance. Grain on right has a nearly continuous rim that penetrates far into the type 5 core. An irregular boundary exists between the two phases. **B)** An irregular boundary between types 4 and 5 is highlighted in the bottom right and upper left grains. Small patches of type 5 composition are found in the two grains that are predominantly type 4 composition. A thin veneer of type 4 is present along a fracture running through the bottom right grain. **C)** Cluster of 3 sub-rounded grains exhibiting exsolution lamellae of type 4 composition within a type 5 host. Note the absence of a type 4 rim and discrete bands containing a higher density of exsolution in the bottom left grain. Very bright phase near rounded margins of grain is barite. **D)** Close up of type 4 chromite exsolving out of a type 5 host. **E)** A sub-rounded type 4 grain in W95-35 with multiple silicate inclusions, exsolution lamellae of a high-Ti phase, and a corroded outer margin rimmed by Cr-bearing muscovite.

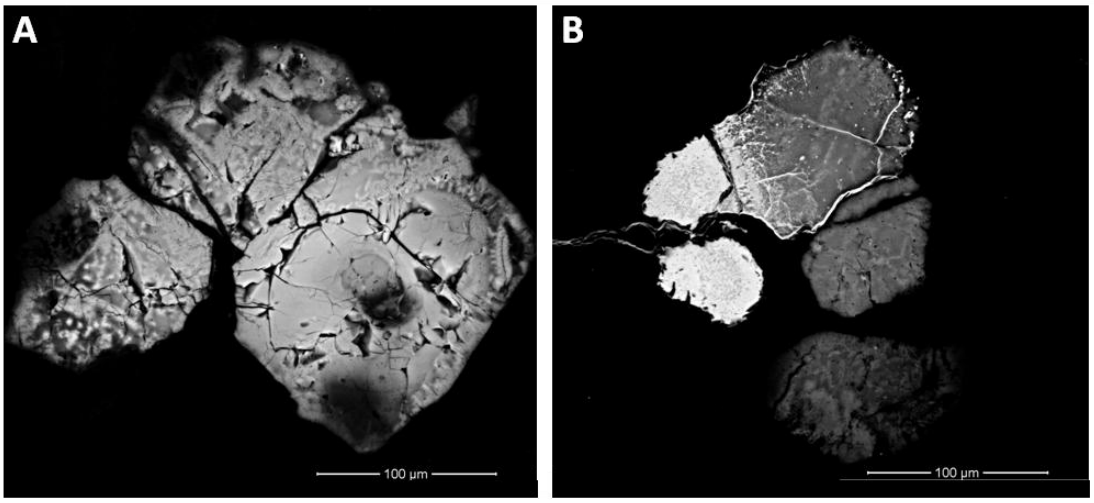

Figure 20. Chrome spinel in W03-07. Images taken in BSE mode by field emission gun SEM. WDS analyses were not carried out on these grains so their chemistry is not well documented. It is known that they lack Mg and are enriched in ZnO and MnO. **A)** Dark fractures within and in between grains are filled with Cr-muscovite. **B)** A MnO vein (left, bright) significantly enriches portions of chrome spinel in Mn.

COMPARISON OF STUDIED CHROME SPINELS WITH SPINELS FROM VARIOUS IGNEOUS ENVIRONMENTS

Broad, but well-defined chemical trends exist between chrome spinels from various magmatic environments (Roeder, 1994; Stowe, 1994, Barnes and Roeder, 2001). In most studies of chrome spinel, compositions are plotted on the Cr-Al-Fe^{3+} triangular plot representing the edge of the spinel prism, as well as the longitudinal spinel prism plots Cr/(Cr+Al) and Fe^{3+}/(Fe^{3+}+Al+Cr) vs Fe^{2+}/(Mg+Fe^{2+}), and TiO_2 vs Fe^{3+}/(Fe^{3+}+Al+Cr). A global spinel database compiled by Barnes and Roeder (2001) contains these chemical plots for 21,000 chrome spinel analyses. The plots highlight how variations in chrome spinel composition can vary based on parent melt composition, degree of fractionation, subsolidous re-equilibration with ferromagnesian silicates, metamorphism, and metasomatism. The plots also show the differences in chemistry found in chrome spinels from the following magmatic provinces/environments: mantle xenoliths, ophiolites, continental layered intrusions, alkali and lamprophyric rocks,

tholeiitic basalts, Alaskan zoned ultramafic complexes, basalts, and lithologies altered by metasomatism and metamorphism. Several well-defined trends, the Fe-Ti trend, the Cr-Al trend, the Rum trend, and the kimberlite trend, are marked on these plots with more than one trend being present in some environments. In order to compare chrome spinels of this study to chrome spinels from generalized igneous environments, their compositions have been superimposed on the Cr-Al-Fe^{3+} triangular plot, the plots Cr/(Cr+Al) and Fe^{3+}/(Fe^{3+}+Al+Cr) vs Fe^{2+}/(Mg+Fe^{2+}), and the plot of TiO_2 vs Fe^{3+}/(Fe^{3+}+Al+Cr) from Barnes and Roeder (2001) (Fig. 21).The Cr-bearing, type 3 and type 5 compositions, could not have their Fe^{3+} and Fe^{2+} recalculated because they do not fit a spinel stoichiometery, and are not used in the plots.

Chemical plots of types 1, 2, and 4 superimposed on plots of the entire global spinel database

In the Cr-Al-Fe^{3+} triangular plot, type 2 chrome spinels are located close to the Fe-Cr join near the Fe apex. Type 4 compositions occur slightly to the right of the Fe-Cr join and further away from the Fe apex than type 2 compositions. The zincochromite patches and high-Mn zones of type 1 chrome spinels contain more Cr and Al than types 2 and 4 placing them relatively close to Fe-Ti trend. However the zincochromite patches and high-Mn zones plot far from the Fe-Ti trend in the plots of Cr/(Cr+Al) and Fe^{3+}/(Fe^{3+}+Cr+Al) vs Fe^{2+}/(Fe^{2+}+Mg) because they lack Mg entirely.

Composition of the high-Mg cores

Similar to the zincochromite patches and high-Mn zones, the high Mg cores also plot very close to the Fe-Ti trend in the triangular plot Cr-Al-Fe^{3+}. However, unlike the zincochromite patches and high-Mn zones, the high-Mg cores also fall very close to the

Fe-Ti trend in the plots of Cr/Cr+Al and Fe^{3+}/Fe^{3+}+Cr+Al vs. $Fe^{2+}/(Fe^{2+}$+Mg) due to having appreciable Mg. In the plot of TiO_2 vs $Fe^{3+}/(Fe^{3+}$+Al+Cr) the high-Mg cores plot far below the Fe-Ti trend due to their low TiO_2 concentration.

Precautions to be kept in mind when comparing chrome spinels from this study to those from generalized igneous environments

It is well documented that chrome spinels in mafic lithologies are susceptible to post-crystallization compositional changes through subsolidus requilibration with ferromagnesian silicates, metasomatism, and metamorphism (Cameron, 1975; Hatton and von Gruenewaldt, 1985; Barnes, 2000; Liipo et al., 1995; Wylie et al., 1987; Roeder, 1984; Weiser et al., 1997; Barnes and Roeder, 2001). These processes make it difficult and, in many cases, impossible to determine the original liquidus composition of chromite. This can hinder attempts to correlate separated chromite populations (Yudovskya and Kinnaird, 2010). For chromites in this study, another potential obstacle in determining their parent lithology is the fact that they reside in a siliceous melt, a magma type in which chrome spinel has never been documented previously. Since many of the phase relations found in this study have not been documented before, detailed knowledge of the effects of subsolidus requilibration of chromite with minerals such as Na-rich plagioclase, orthoclase, and quartz is not available. This is in contrast to studies focused on lithologies where chrome spinels are typically present as a minor or major phase, and are proximal to ferromagnesian silicates such as olivine and pyroxene with which they crystallized (Irvine, 1965;

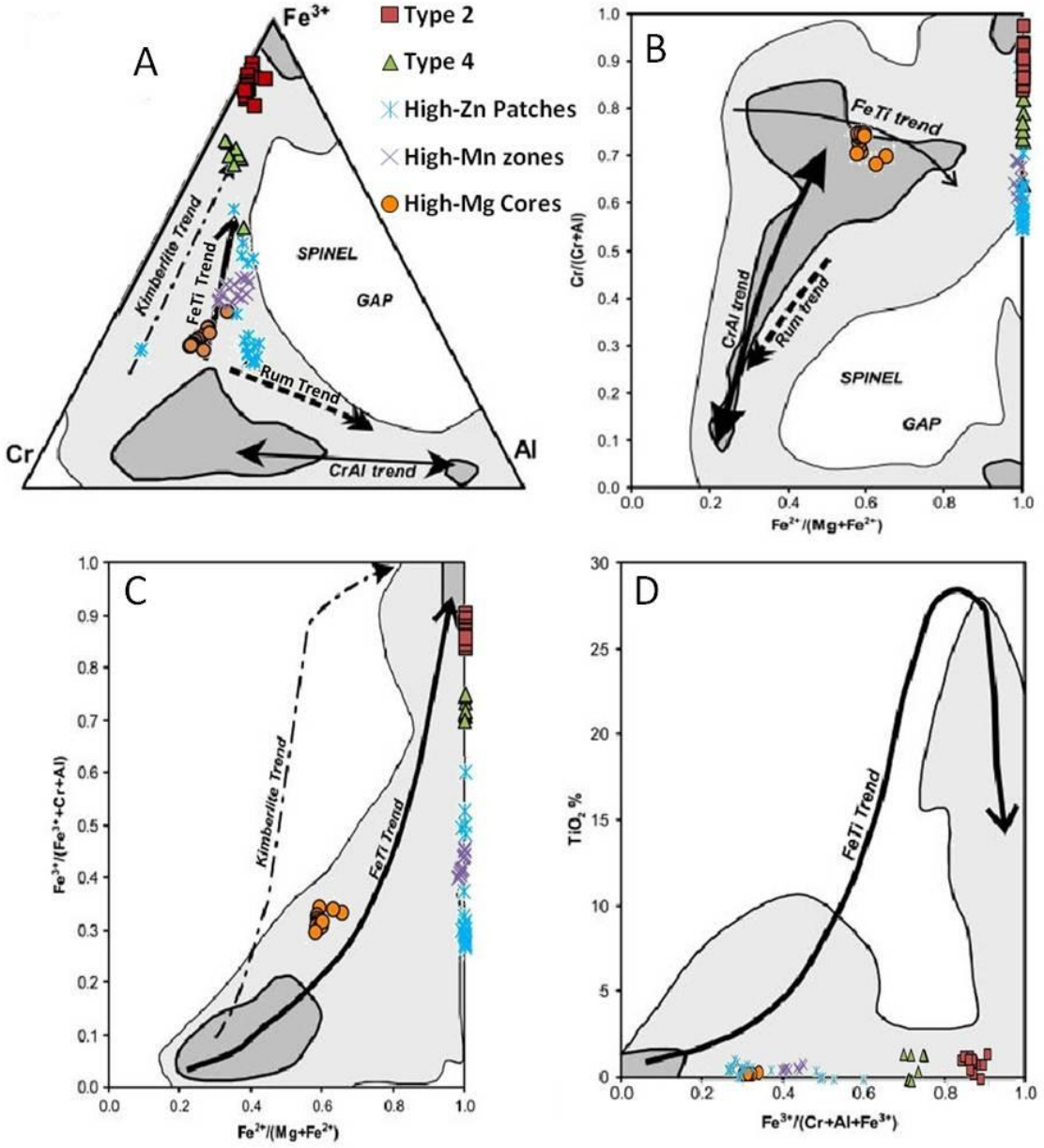

Figure 21. Compositions of chrome spinels from this study superimposed over spinel compositions from the global spinel database compiled by Barnes and Roeder (2001). Shaded regions represent the most densely packed data points of the global database (dark gray 50%, light gray 90%). **A)** Triangular plot Cr-Al-Fe^{3+} **B)** Cr/(Cr+Al) vs Fe^{2+}/(Mg+Fe^{2+}) **C)** Fe^{3+}/(Fe^{3+}+Cr+Al) vs Fe^{2+}/(Mg+Fe^{2+}), **D)** TiO_2 vs Fe^{3+}/(Fe^{3+}+Al+Cr). Direction of arrows indicates more evolved compositions, except for the Cr-Al trend highlighted in image A, which does not necessarily signify increasing degrees of evolution.

Cameron, 1977; Roeder, 1994; Naldrett et al., 2010; Yudovskya and Kinnaird, 2010).

The limited sample size of this study imposes another limitation: only chromites from 3

stratigraphically unconstrained samples have been analyzed in detail so far. This is in contrast to the typical sampling treatment of mafic lithologies where variation in chromite compositions due to fractional crystallization, injection of fresh magma, and subsolidus re-equilibration with ferromagnesian minerals are observed over known distances within and between layered units (Hulbert and von Gruenewaldt, 1985). In these settings, chemical trends due to fractionation can be observed both spatially, and in the context of parental magma type(s) (Cameron, 1977; Barnes, 2000; Naldrett et al., 2010; Yudovskaya and Kinnaird, 2010). These are constraints that are not available in this study because the exact parent melt of the chromite grains has not been established.

CHAPTER 9: DISCUSSION OF CHROME SPINEL

COMPOSITION

The compositions of the Cr-bearing phases documented in this study are complex. Schweitzer and Hatton (1995) suggested that two hydrothermal events affected the Dullstroom Formation including the Basal Rhyolite: 1) hydrothermal alteration related to intrusion of RLS sills, and 2) hydrothermal alteration associated with deposition of the Damwal Formation. Therefore, the chrome spinels need to be categorized in terms of the extent of alteration they have experienced. There is a distinct possibility that other alteration events also affected the Basal Rhyolite, but to date, only the study of Schweitzer et al. (1995) has addressed this problem. A thorough assessment of all the secondary alteration events that affected the Basal Rhyolite is beyond the scope of this study. The possibility that the chrome spinels were entrained from a mafic lithology also raises the question of whether or not immersion in the siliceous Basal Rhyolite, while it was molten, affected their composition.

The main goal of this discussion is to tentatively determine what, if any, relatively or completely unaltered chrome spinels are present in the Basal Rhyolite. If such a population is found, their compositions will be compared to chrome spinel bearing environments documented in the database of Barnes and Roeder (2001), to try and determine what their most likely source environment is. If a likely source is narrowed down, important constraints will be placed on how the impact and igneous scenarios can describe their occurrence in the Basal Rhyolite.

THE FE-TI TREND

The Fe-Ti trend represents the tendency of mafic magmas to increase in Fe^{3+} and Ti concentration as well as their $Mg^{2+}/Mg^{2+}+Fe^{2+}$ ratio (hereafter referred to as Mg #) during prolonged fractional crystallization. This is due to Mg being preferentially incorporated into early-crystallizing olivine and pyroxene in contrast to Fe^{3+} and Ti, which are incompatible in early crystallizing phases (Irvine, 1967; Stowe, 1994; Roeder, 1994; Barnes and Roeder, 2001). These changes in melt composition can be tracked through the composition of chromites as they crystallize from the constantly evolving melt, assuming there are no injections of fresh magma to the system (Hatton and Von Gruenewaldt, 1985). Another process that increases Fe^{3+}, Ti, and the Mg# of chromite is the exchange of Mg and Fe^{2+} between chromite and surrounding Fe-Mg silicates (usually olivine) or trapped fractionating liquids (Barnes and Roeder, 2001; Kamenetsky et al., 2001; Roeder, 1994; Stowe, 1994; Hulbert and von Gruenewaldt, 1985).

CRITERIA FOR CHROMITE TO REPRESENT A PRIMARY IGNEOUS COMPOSITION

In a study of chromite from komatiites, Barnes (1998) defined a chromite as retaining a primary composition if it had $Fe^{2+}/Mg+Fe^{2+} > 0.15$, lacked extensive replacement by Cr-magnetite, and did not show significant enrichment in Mn and Zn, both commonly regarded as a strong sign of secondary alteration (Barnes, 1998; Liipo et al., 1995; Wylie et al., 1987). Although these criteria were used in a study of chromites whose parental magma type is well-established, the main purpose for their implementation was to eliminate the effects of secondary processes that can affect chromites regardless of their magmatic provenance which makes these criteria applicable

to the chromites from this study. The type 1 high-Mg cores have a $Mg/Mg+Fe^{2+}$ value between 0.38 and 0.42, lack significant replacement by Cr-magnetite, and contain ~0.67 wt % MnO which is only 0.15 wt % higher than an arbitrary filter line used by (Barnes, 1998; Stephen Barnes, personal communication). Therefore, the high-Mg cores are considered to be the most primitive igneous composition found in this study, but whether or not they represent a primary igneous composition that preserves the effects of igneous growth zoning or subsolidous re-equilibration needs further evaluation. This is due to the possibility that the composition of the high-Mg cores was affected by interaction with the Basal Rhyolite which in itself represents a complicated problem.

Since chemical reactions between chrome spinel and silica oversaturated melts or minerals commonly found in silica oversaturated melts have not been studied, a way to approximate the extent of alteration, if it exists, is by utilizing the size, morphology, and configuration of the chrome spinels to determine the most likely ultramafic or mafic environment in which they crystallized. Then, by comparing the compositions of chromite from that environment to the high-Mg cores of this study, a first order approximation can be made regarding how much their composition may have changed from the compositions that are expected.

SIGNIFICANCE OF CHROMITE AS EUHEDRAL, 20-230 μM CRYSTALS IN CLUSTERS AND ARCUATE CHAINS

Most chrome spinels from this study are euhedral, 30-230 mm in size, and occur in discrete clusters of several grains or arcuate chains up to 2 mm in length. The only igneous environment that produces chromites with these characteristics is a stratiform intrusion. In these types of intrusions, chromites exhibit euhedral and subhedral

morphologies, are on average 200 µm in size, and occur in isolated clusters and chains interstitial to ferromagnesian silicates (Duke, 1983). These similarities suggest that at some point, the chrome spinels from this study existed interstitially to ferromagnesian silicates such as olivine or pyroxene. As a visual comparison, chrome spinels from this study are compared to a cluster of chromites in intrusive komatiite magma from the Eastern Goldfields Superterrane of the Yilgran Craton of Western Australia, as well as chromites from the lower zone of the Bushveld Complex in the northern limb (Fig. 22).

CHEMICAL PLOTS OF CHROME SPINELS FROM THIS STUDY SUPERIMPOSED OVER PLOTS OF CHROMITES FROM CONTINTENTAL MAFIC INTRUSIONS

To determine if the compositions of the most primitive chromite of this study and those from continental mafic intrusions (which contain stratiform intrusions), are similar, the chemical plots of types 1, 2, and 4 are superimposed on chemical plots for continental mafic intrusions by Barnes and Roeder (2001) in figures 23 and 24. Chromites from continental mafic intrusions have been subdivided into three populations: 1) chromites occurring in chromitites (layers containing 50-90% chromite), 2) chromites that occur in cumulates of Fe-Mg silicates, and 3) chromites in subvolcanic intrusions and flood basalt provinces. The high-Mg cores show strong similarities to all of these environments; with the closest matches being with chromites from cumulates comprised predominantly of Fe-Mg silicates and chromitites. Given the configuration of chromite grains in arcuate chains and clusters, the configuration in which they normally occur in Fe-Mg silicate cumulates, and impure (silicate bearing) chromitites, these types of environments seems to be the best match. These similarities also suggest that because the high-Mg cores do

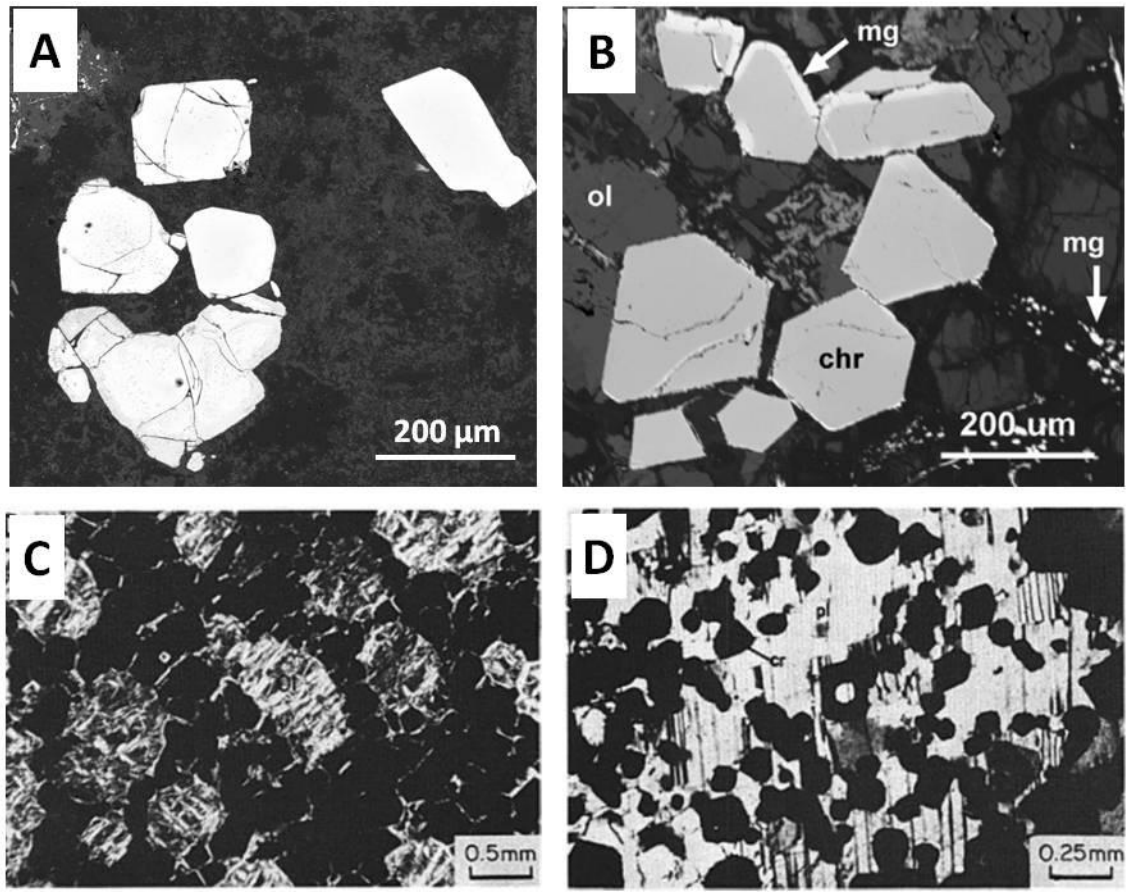

Figure 22. A comparison of chrome spinels from this study to those occurring in an Australian komatiite and those found in the lower zone of the Bushveld Complex. **A)** A cluster of type 4 Cr-magnetite in W91-102 that lacks type 5 cores. **B)** A cluster of chromite grains in a komatiite from the Eastern Goldfields Superterrane (EGS) of the Yilgarn Craton, Western Australia. Modified after Locmelis et al. (2011). **C)** Chain-textured chromite (black) surrounding cumulous olivine grains in a chromite rich cumulate of the lower zone of the Bushveld Complex. Modified after Hulbert and von Gruenewaldt, (1985), PPL **D)** clusters of chromite in the Lower Zone. Modified after Hulbert and von Gruenewaldt, (1985), PPL.

not have significant differences in chemistry compared to chromites of similar sizes, morphology, and configurations within continental mafic intrusions, the compositions of the high-Mg cores were likely not affected significantly by reaction with the Basal Rhyolite. Because the RLS represents the largest continental mafic intrusion in the geologic record, and is temporally and spatially related to the Basal Rhyolite, these chemical similarities warrant further exploration between the chrome spinels and this study and portions of the Bushveld Complex.

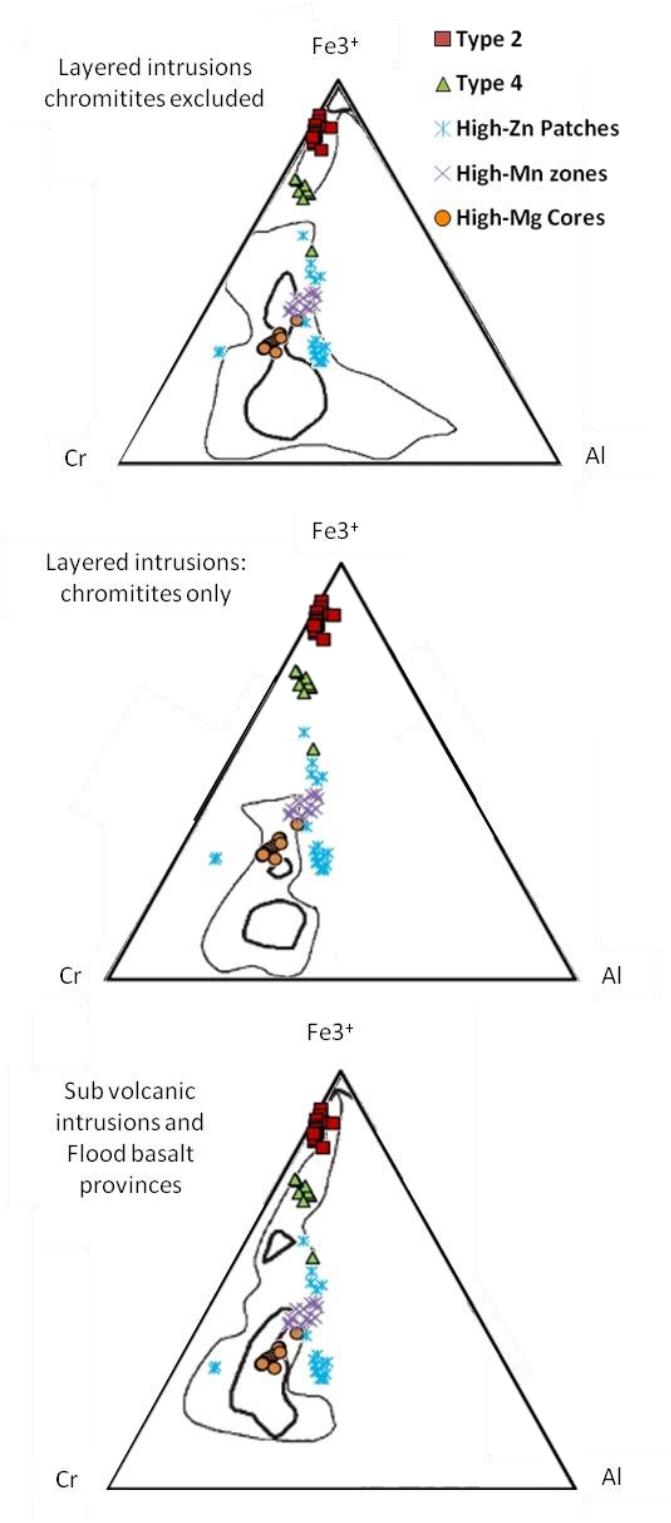

Figure 23. Compositional plots of types 1, 2, and 4 from this study superimposed over triangular plots for chromites from continental mafic intrusions. Chromites from continental mafic intrusions are divided into three types: chromitites excluded, chromitites only, and subvolcanic intrusions + flood basalt provinces. Area enclosed by light lines represent 90% of the data and regions enclosed by heavy lines represent 50% of the data. Modified after Barnes and Roeder (2001).

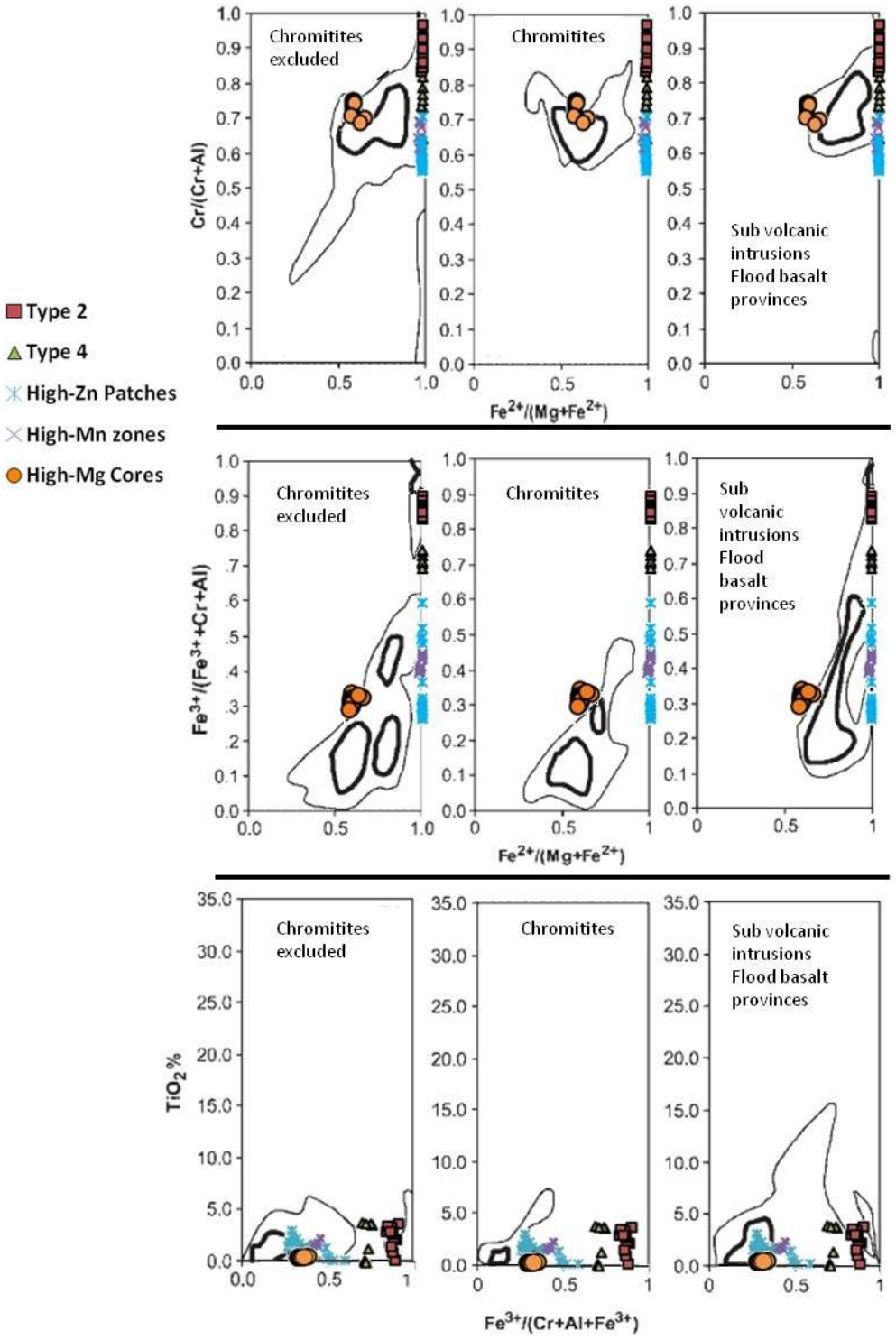

Figure 24. Types 1. 2 and 4 superimposed over compositional plots of chromite from continental mafic intrusions. Areas enclosed by light lines represent 90% of the data and regions enclosed by heavy lines represent 50% of the data. The high-Mg cores show the most similarity to chromites from cumulates and chromites from chromitite layers. Modified after Barnes and Roeder (2001).

ARE THE LOW TiO_2 CONTENTS OF THE HIGH-MG CORES A POTENTIAL INDICATOR OF THEIR PARENT MELT COMPOSITION?

The plot of TiO_2 vs $Fe^{3+}/(Fe^{3+}+Al+Cr)$ (Fig. 21) indicates that the TiO_2 concentration of the high-Mg cores are lower than expected for a chromite that contains 24-25% Fe_2O_3 and plots along Fe-Ti trend in the graphs Cr/Cr+Al vs $Fe^{2+}/Mg+Fe^{2+}$ and $Fe^{3+}/Fe^{3+}+Cr+Al$ vs $Fe^{2+}/Mg+Fe^{2+}$. This raises the question of why Fe_2O_3 is enriched in the high-Mg cores while TiO_2 is not. Since TiO_2 concentrations are not enriched by subsolidous requilibration with Fe-Mg silicates, a possible explanation is that Ti was not partitioned into the chromite during crystallization. This brings to attention a compositional similarity between the high-Mg cores and chrome spinels from Alaskan Zoned Ultramafic Complexes (AZUCs), a unique population of chrome spinels given their own treatment in the database of Barnes and Roeder (2001) (Fig. 25). Chromites from AZUCs plot along the Fe-Ti trend but have abnormally low TiO_2 concentrations. It has been proposed that the low TiO_2 concentrations of the chromites in AZUCs, despite their high Fe^{3+} concentration, is due to the presence of amphibole as a liquidous phase as chromite crystallizes. Amphibole is not typically found in chromite bearing lithologies, and it is thought when amphibole is present, Ti preferentially partitions into amphibole over chromite during crystallization. The abnormally low concentration of Ti in chromites from this study may be more useful in linking chromites from this study to a parent body than the Mg#, especially since low Ti in a high Fe^{3+} chromite is rare.

Since the chemical plots of Barnes and Roeder (2001) only portray the ratios between the divalent and trivalent cations, the bulk compositions of chrome spinels from AZUCs were extracted from the global database, averaged based on lithology, and compared to the high-Mg cores of this study (Table 4). When the compositions are

compared, obvious similarities in wt % Fe_2O_3, FeO, Cr_2O_3, Al_2O_3, and MgO are highlighted, especially between chromites from chromitite layers found in AZUCs. Given these similarities, it may be possible that the high-Mg cores were initially low in Ti and high in Fe^{3+} by virtue of crystallizing in an amphibole bearing liquid prior to becoming entrained in the Basal Rhyolite.

A RECENTLY DISCOVERED CHILL SEQUENCE TO THE BUSHVELD COMPLEX: A POSSIBLE SOURCE OF THE CHROME SPINELS

The possibility chromites are low in Ti because of competition for Ti with amphibole may be reasonable due to the recent discovery of a 1 km-thick chill sequence of parental melts of the Bushveld Complex in the northeastern portion of the eastern lobe of the Bushveld Complex (Wilson, 2012). Of particular significance is the fact that amphibole is ubiquitous in the chill sequence at ~5% modal abundance, and that most chromites within it have low TiO_2 and high Fe^{3+} concentration (Wilson et al., 2012). To date, Wilson (2012) has characterized the basal 33 m of this chill sequence and in doing so, has found three distinct populations of chromite: 1) chromites associated with pyroxene dunites (units 10 and 11), 2) chromites occurring in pyroxene and olivine cumulates (units 15 and 18 respectively) and 3) chomites associated with chilled and quenched zones (Wilson et al., 2012).

The presence of amphibole and the low TiO_2 concentration of the chromites in the chill sequence may point towards an environment where amphibole acted as a buffer for Ti during crystallization, similar to environments proposed for AZUCs. Since the 1 km thick chill sequence represents the oldest magmas associated with the RLS discovered to date, contains chromites with high Fe^{3+} and low TiO_2 which occur in clusters of euhedral

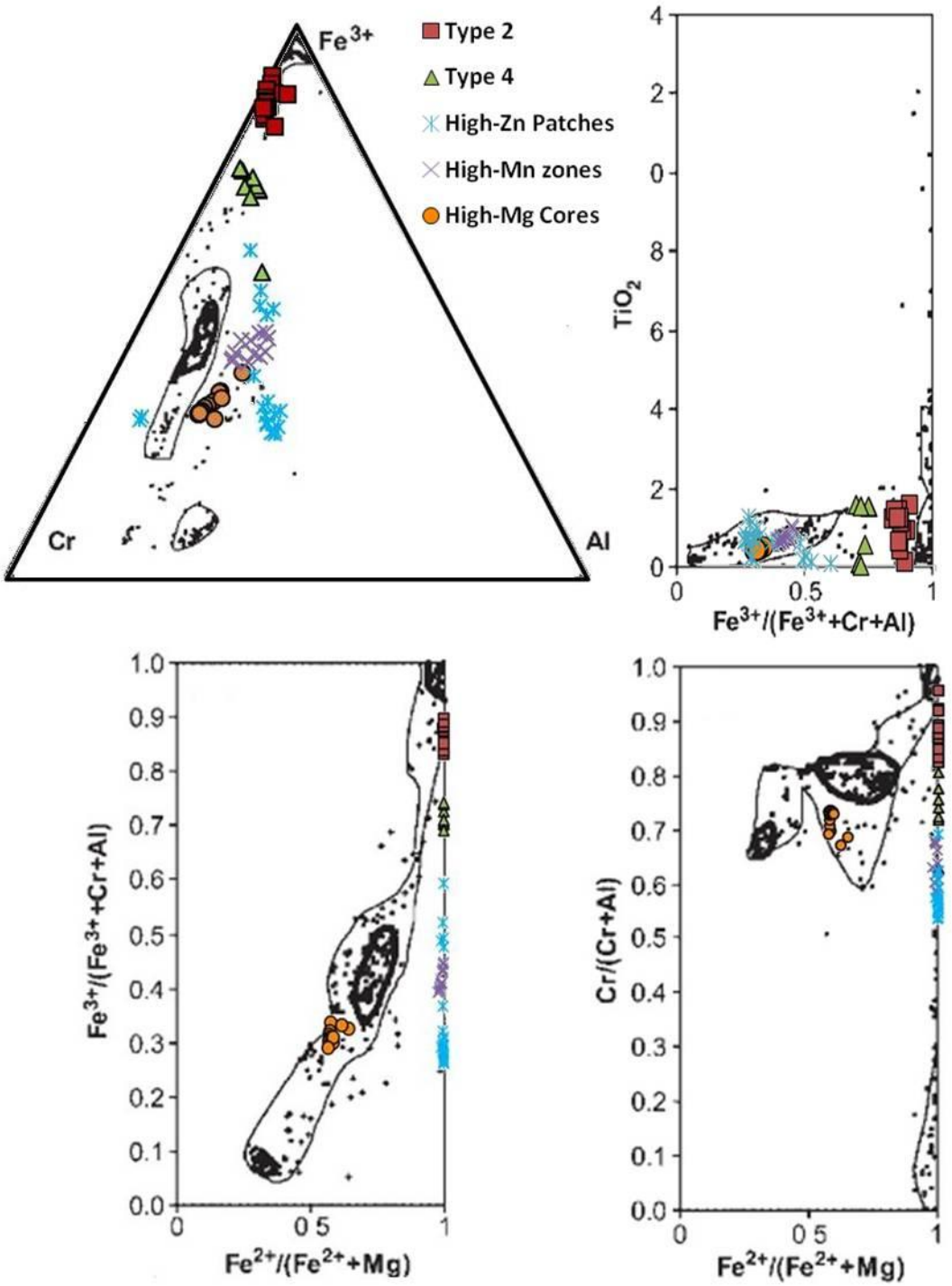

Figure 25. Plots of types 1 2 and 4 from this study superimposed over plots of Alaskan Zoned Ultramafic Complexes (AZUCs). Areas enclosed by light lines represent 90% of the data and areas enclosed by heavy lines represent 50% of the data. Modified after Barnes and Roeder (2001).

Oxide	Chromitite layers (AZUC)	High-Mg cores (this study)	Dunnite-Chromitite layers (AZUC)
SiO_2	0.24	0.05	0.26
TiO_2	0.61	0.42	0.82
V_2O_3	0.00	0.01	0.00
Al_2O_3	6.61	9.57	5.80
Cr_2O_3	41.16	37.76	33.51
Fe_2O_3	25.03	24.69	32.34
FeO	18.85	21.02	21.57
MnO	0.55	0.74	0.61
MgO	7.88	8.14	5.79
CaO	0.07	0.01	0.06
Na	0	0	0
K_2O	0	0	0
# analyses	100	15	29

Table 4. Chemistry of chromites from chromitite and unite-chromitite layers of Alaskan Zoned Ultramafic Complexes (AZUCs) vs the high-Mg cores of this study. All chrome spinels are high in Fe, low in Ti and have fairly similar Cr, Mg, and Ti contents.

grains within olivine/pyroxene cumulates, and also contains both zircon and baddeleyite (Allan Wilson, personal communication), some portion of it, or a source similar to it, is a great candidate for the source of chromite and baddeleyite found in the Basal Rhyolite. While the areal extent of the chill sequence remains unknown, it has been suggested by Wilson and Chunnett (2012) that the chill sequence may be widespread and may exist under the marginal zone in other areas.

The composition of chromites in olivine and pyroxene cumulates of the new chill sequence are also compared to the high-Mg cores of this study (Fig. 26). Chromites from the olivine/pyroxene cumulate of unit 18 show similarities in composition to the high-Mg cores of this study in the chemical plots $Mg/Mg+Fe^{2+}$ vs $Cr/(Cr+Al)$, Cr/Fe_{total} vs $Cr/(Cr+Al)$ and Cr cations vs Al cations. The graph of Cr/Fe_{total} vs Cr/Cr+Al tracks the evolution of the spinel with progressively lower Cr/Fe_{total} and Cr/Cr+Al values indicating more evolved compositions. The graph of Cr cations / Al cations is another way of tracking the evolution of chromites, with Cr becoming lower with increasing

fractionation and Al becoming higher (Wilson, 2012). The average composition of the high-Mg cores is compared to the three chromite compositions from unit 18, an olivine pyroxene cumulate in the new chill sequence (Table 5). These are the only published stoichiometric compositions of chromites occurring in cumulates of the chill sequence to date.

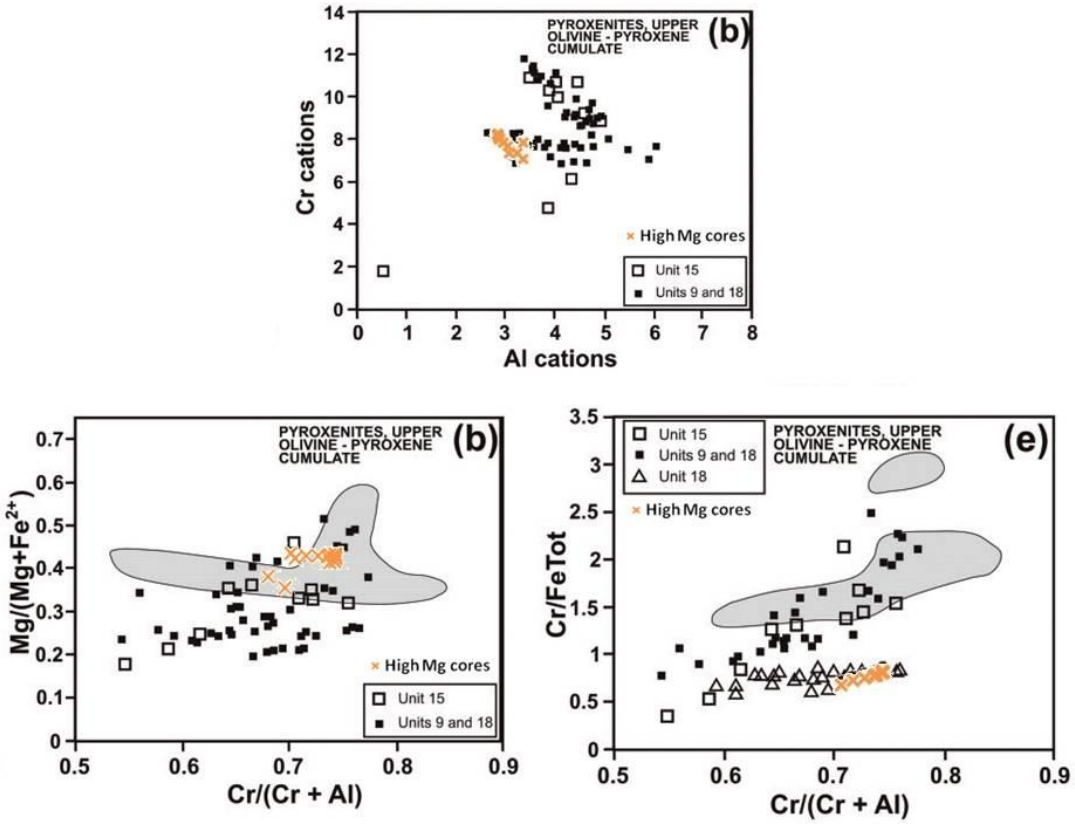

Figure 26. Comparing the compositions of the high-Mg cores to compositions of chrome spinels from the newly discovered chill sequence of the parental melts to the Bushveld Complex. Regions shaded in gray represent the range of chromite compositions from portions of the chill sequence that are dominated by spinifex textures.

oxide	High-Mg cores	Unit 18	Unit 18	Unit 18
Cr_2O_3	37.76	44.83	35.96	31.72
Fe_2O_3	24.69	9.13	18.93	27.23
FeO	21.02	21.48	25.43	26.65
Al_2O_3	9.57	15.18	10.34	9.30
MgO	8.14	8.27	6.03	4.02
SiO_2	0.05	0.01	0.01	0.02
TiO_2	0.42	0.33	2.07	0.20
ZnO	0.22	N/A	N/A	N/A
MnO	0.74	0.36	0.33	0.36
K_2O	0.00	N/A	N/A	N/A
V_2O_3	0.01	N/A	N/A	N/A
CoO	0.06	N/A	N/A	N/A
CaO	0.01	0.01	0.01	0.10
Na_2O	0.00	N/A	N/A	N/A
Total	102.68	99.60	99.10	99.51
# analyses	15	1	1	1

Table 5. Compositions of chromites from an olivine cumulate of the new chill sequence (unit 18) compared to the high-Mg cores of this study. Only 1 chromite in unit 18 has relatively high TiO_2

POSSIBLE SCENARIOS FOR THE BEHAVIOR OF THE DIVALENT AND TRIVALENT CATIONS IN THE HIGH-MG CORES

As highlighted in figure 17, MgO and FeO exhibit relatively stable concentrations throughout the high-Mg core, with MgO becoming slightly less concentrated and FeO becoming slightly more concentrated in the high-Mn zone. In contrast, Fe_2O_3 Cr_2O_3 and Al_2O_3 are only stable over a short distance near the center of the high-Mg core, and upon exiting this region, rise or fall in concentration by several wt %. If it is assumed that the high-Mg cores represent the cores of grains once interstitial to olivine, the stable FeO and MgO concentrations may represent thorough requilibration between the high-Mg core and olivine. The concentrations of Fe_2O_3, Cr_2O_3 and Al_2O_3 on the other hand, would not have requilibrated, due to the sluggish diffusion rates of Cr Al and Fe^{3+} in olivine (Kamenetsky et al., 2001). In this case, the rise in Fe^{3+} and Al, which corresponds to a decrease in Cr, may possibly represent primary igneous zoning.

ALTERATION IN TYPES 2-5

Chrome spinel types 2 and 4 are similar to the population of chrome spinels from metasomatized and metamorphic environments in the database of Barnes and Roeder (2001) (Fig .27). This population is characterized by enrichment in Fe^{3+} along with depletion in Cr and Al (Hulbert and von Gruenewaldt, 1985; Barnes, 1998; Barnes and Roeder, 2001). In contrast to type 1, which possibly retains a primary composition (high-Mg cores), types 2 and 4 (Cr-magnetite) and the Cr-bearing phases they enclose (types 3 and 5 respectively), are thoroughly altered by metasomatism. Evidence for this is the homogenization of Zn and Mn throughout the type 3 and 5 cores and the widespread occurrence of small inclusions of a hydrous silicate phase. Since many of the type 3 and 5 cores contain barite, never before documented in altered chrome spinel, it is suggested that the alteration event responsible for types 3 and 5 occurred prior to alteration which formed the type 2 and 4 rims. The alteration event responsible for forming types 3 and 5 is likely the same as that which formed barite completely isolated from chrome spinel in other parts of the sample. Because Schweitzer and Hatton (1995) associated an increase in Ba, Zn, and Mn amongst other mobile elements with hydrothermal alteration caused by intrusion of the RLS, it seems reasonable that the type 3 and 5 compositions as well as the zincochromite patches and high-Mn zone of type 1 chrome spinel formed during this same event. The type 2 and 4 rims may have then formed in a later hydrothermal event but since these thick Cr-magnetite rims are not present in type 1 compositions it would imply that this event did not affect all chromites equally.

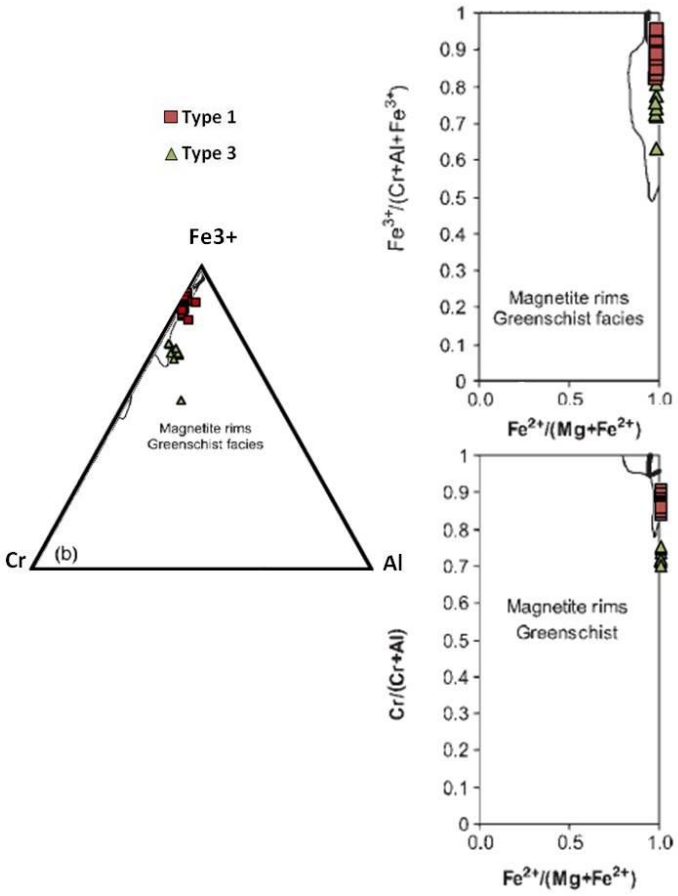

Figure 27. Plot of types 2 and 4 superimposed over magnetite rims and greenschist facies metamorphosed chrome spinels. Modified after Barnes and Roeder (2001).

CHAPTER 10: IMPACT VS. IGNEOUS SCENARIOS

SIGNIFICANCE OF BADDELEYITE AND CHROMITE

The discovery of baddeleyite and chrome spinel in the Basal Rhyolite reinforces the assertion of Elston (1994; 2008) that the Basal Rhyolite is not a typical rhyolite. The presence of these two minerals is important because not only is their existence in a siliceous melt completely unexpected, but they each provide important constraints on the impact and igneous scenarios in terms of how well process associated with each scenario can explain their observed characteristics. Some of the chrome spinels of this study are high in Mg, euhedral, and up to 230 µm in size, which require equilibrium conditions in a low energy mafic environment (Barnes, 1998). Because of this, both scenarios suggest that chromite is derived from an ultramafic or mafic contaminant, but offer different interpretations of the process by which contamination occurred. The issue is whether or not baddeleyite is also a contaminant (igneous scenario) or crystallized directly from a high temperature, siliceous impact melt.

THE IMPACT INTERPRETATION OF BADDELEYITE

The impact hypothesis asserts that baddeleyite crystallized directly from the Basal Rhyolite, which was initially comprised of completely melted sediments of the Transvaal Supergroup that reached temperatures in excess of 1686 ° C (Wolf Elston, personal communication). In this scenario, the Zr comprising baddeleyite was derived from Zr-bearing phases in the sediments that were completely melted in the initial impact melt, which then overflowed and picked up clasts of sedimentary rock present along the crater floor. In the binary phase diagram ZrO_2 - SiO_2, an invariant point exists at 1686 ° C

which represents the reversible reaction $ZrO_2+SiO_2 \leftrightarrow ZrSiO_4$ (Fig. 28). According to the impact hypothesis, the baddeleyite crystallized from the melt at temperatures above this invariant point and partially reacted to zircon at temperatures ≤ 1686 °C during cooling (Elston, personal communication). However, either due to rapid cooling rates or a thin veneer of zircon acting as a barrier between the remaining baddeleyite and the melt, the reaction did not always go to completion. The absence of baddeleyite altogether in sample W91-102 is suggested to be due to slower cooling rates which allowed the reaction to complete (Elston, personal communication). However, this does not account for the fact that Zr bearing phases are more numerous in this sample, or why they exhibit irregular textures. These characteristics of the zircon may indicate that a population of zircon crystallized out of the melt independently from baddeleyite during a period of rapid cooling at lower temperatures.

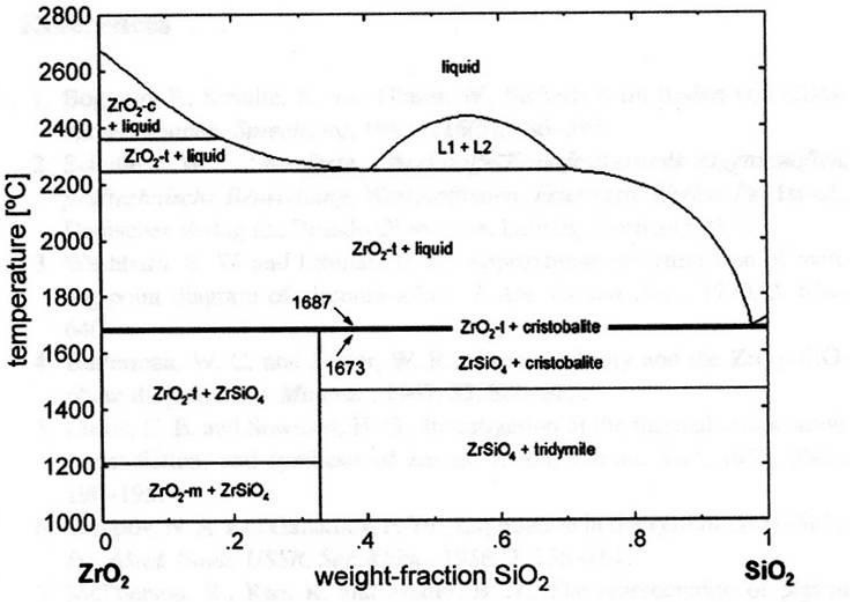

Figure 28. ZrO_2-SiO_2 phase diagram. Graph taken from Butterman and Foster (1967).

THE IMPACT INTERPRETATION OF CHROMITE

For reasons previously mentioned, the impact scenario interprets chromite as a contaminant from pre-Bushveld mafic lithologies (Elston, personal communication 2012). It is suggested that these grains were incorporated into the impact melt from an undiscovered mafic basement rock beneath the Bushveld Complex.

ADVANTAGES OF AN IGNEOUS INTERPRETATION OF BADDELEYITE AND CHROMITE

Baddeleyite

It has been shown experimentally in the system SiO_2 – ZrO_2 that ZrO_2 is stable above 1686 °C, but only when the mixture contains at least 2% ZrO_2 (Fig. 28). This is not the case with the rocks in this study, which contain ≤ 405 ppm Zr. Although binary phase diagrams do not accurately represent multicomponent systems, the igneous model assumes that zirconia would not crystallize in a rapidly cooling, silica oversaturated, multicomponent melt with such a low Zr concentration. Furthermore, the crystal form and chemistry of baddeleyite grains from the Basal Rhyolite are both consistent with baddeleyite from mafic igneous rocks (compare Figs. 8A 8D, 11A, 11C, 11E with Fig. 15B, 15C, 15D). Even if it could be said with confidence that ZrO_2 can crystallize in a siliceous melt at temperatures greater than 1686° C, it is judged to be unlikely that its Hf, Ti, and Fe concentration would plot in the overlapping fields of ZrO_2 from mafic environments (Fig. 12).

Chromite

The occurrence of undeformed, euhedral chromite in isolated clusters of 2-8 crystals, as well as arcuate chains containing up to 50 individual crystals, is judged as difficult to reconcile with rapid excavation of a mafic igneous rock from the depths of an impact crater. Chrome spinels with high Fe^{3+} and low Ti are uncommon in the geologic record, and require amphibole at the liquidus as chromite forms (Barnes and Roeder 2001). This uncommon condition has actually been discovered in the ultramafic rocks of a ~1 km chill sequence, recently discovered in a drill core, ~100 km east of the Stavoren Inlier (Wilson, 2012). It is argued here that, if a lithology with these characteristics already exists and was emplaced relatively close to the surface (~2 km deep), it is a more probable source of the chromites than a speculative deep source, that meets the same chemical requirements.

Compositions aside, another problem is the reconciliation of why entrained chromite would have endured the extremely high temperatures of the impact melt while entrained zircons completely melted and provided the Zr required for the impact melt to subsequently crystallize ZrO_2.

THE IGNEOUS SCNEARIO: POSSIBLE MECHANISMS RESPONSIBLE FOR THE PRESNCE BADDELEYITE AND CHROMITE

Two igneous mechanisms may be responsible for the presence of baddeleyite and chromite in the Basal Rhyolite: 1. magma mixing with coeval mafic magmas related to the RLS, or 2. assimilation of mafic minerals during its ascent through the crust.

Inheritance of baddeleyite and chromite by magma mixing

Relative age constraints, imposed by the presence of RLS sills emplaced above the basal Dullstroom Formation in the Messchunfontein section, rule out the critical zone, main zone, and upper zone of the RLS as potential candidates for mixing. Zones of the RLS which may pre-date the Basal Rhyolite are the Lower Zone, Marginal Zone, and parental magmas to the Bushveld Complex (Schweitzer et al., 1995). The hypothetical parental magmas are proposed in models for the RLS, but the recently discovered chill sequence may represent an actual example. The chill sequence is the only member of the RLS in which baddeleyite has been documented. In the mixing scenario, chromite and baddeleyite would likely be derived from a recently formed cumulate prior to the mixing.

An assessment of RLS magmas that may be coeval to the Basal Rhyolite

The recently discovered chill sequence to the Bushveld Complex: The chill sequence represents a very strong candidate for the source of chromite and baddeleyite due to the similarities of chromite compositions it contains and those found in this study, as well the fact that it contains baddeleyite.

The Marginal zone: The marginal zone is not always present at the base of the RLS. The most common composition of the marginal zone is norite that has been contaminated by underlying Transvaal Supergroup sediments (Kinnaird, 2005). Chromite has not been documented as an accessory phases in the marginal zone, suggesting it is not strong candidate for the source of chromite in the Basal Rhyolite.

The Lower zone: Scattered chromite occurs in the lower zone in an orthopyroxene/olivine cumulate which is situated above two uniform orthopyroxene

layers and a harzburgite layer (Kinnaird, 2005). A limited literature search associated with this study found no compositional data for the chromites from the Lower Zone.

The likelihood that baddeleyite and chromite are entrained from pre-Bushveld lithologies

If entrained from pre-Bushveld lithologies, the characteristics of chromite indicate that the source was likely a chromite-bearing olivine/pyroxene cumulate or a chromitite layer. Currently, there are no known mafic cumulates that predate the Bushveld, but some may occur at depth, obscured by the Bushveld Complex itself. The only locality where rocks older than the Transvaal Supergroup are found is in the Dennilton dome, a floor-attached dome consisting of basement rock which occurs south of the Stavoren and Marble Hall inliers. The lithologies present in the Dennilton dome, from oldest to youngest are: the Vaalfontein Suite (gneisses) with xenoliths of the greenstone Terra Nostra Formation (amphibolites, lavas, and schists), and the Dennilton Formation (felsites) (Hartzer, 2000). Since the amphibolites of the Terra Nostra Formation are metasediments none of these formations represent a likely source for the chromites from this study, although older lithologies may exist at depth.

Magma mixing as the preferred mechanism

In light of the current lack of evidence for pre-Bushveld mafic lithologies, particularly those that contain chromite with characteristics consistent with forming in a layered cumulate; a magma mixing scenario is preferred. Many details of the mixing event are beyond the scope of this study, such as the nature of the mechanism that initiated the mixing, what type of ferromagnesian silicates were the chains of chrome spinel initially interstitial to (olivine or pyroxene), and why ferromagnesian are not

present in the Basal Rhyolite now. The fact that the chrome spinels maintained their configuration in clusters and chains may suggest that either the energies associated with mixing and eruption were not sufficient to break them apart, or that they may have been shielded by ferromagnesian silicates they were interstitial to during transport. The high Fe and Mg contents of the Basal Rhyolite in samples from this study, (2.6 - 5.9 wt % and 1.6 - 3.6 wt %) respectively, (excluding the remelted Basal Rhyolite from Loskop Dam), may suggest that ferromagnesian silicates were also entrained but were subsequently resorbed into the Basal Rhyolite. To conclude that ferromagnesian silicates were entrained and quickly resorbed with any confidence, a better understanding of how stable olivine and pyroxene are in a high silica melt is needed.

POSSIBLE IMPLICATIONS OF THE PETROLOGIC DIFFERENCES BETWEEN THE BASAL RHYOLITE FROM DIFFERENT LOCALITIES

The Basal Rhyolite near Loskop Dam and the Basal Rhyolite in the Stavoren Inlier

When the possibility that the Basal Rhyolite mixed with a mafic melt prior to eruption is considered, there are three characteristics of the remelted and recrystallized Basal Rhyolite near Loskop Dam which suggest that the entrained mafic component it contains originated from a more evolved melt than that which mixed with the Basal Rhyolite occurring at the Stavoren Inlier. These three characteristics are: 1) it has far less Cr (23 vs 173-837 ppm), 2) baddeleyites are larger, often exhibit twinning, and contain lower TiO_2 content and 3) the MgO content is much lower (0.65 wt % vs 1.182-2.467 wt %). The presence of baddeleyite indicates that at some point, contamination by a mafic source may have occurred. However, the Cr concentration of 33 ppm as well as the presence of ilmenite and magnetite as the main spinel population suggests that chrome

spinel was never present in these rocks, even prior to remelting and recrystalizing as granophyre. The low MgO content of the Basal Rhyolite at Loskop Dam compared to the Basal Rhyolite in the Stavoren Inlier could possibly be related to the absence of Cr. This would be true in if the Mg enrichment in the Stavoren Inlier is due to Fe-Mg silicates, once surrounding chromites, were resorbed. The lower TiO_2 content of baddeleyite near Loskop Dam suggests that if the baddeleyites were entrained from units of the RLS, they may have been derived from a more evolved mafic component than the baddeleyites found in the Stavoren Inlier. The absence of zircon crystals other than those present as partial replacement of baddeleyite is intriguing, and may provide clues to the Zr saturation history of the Basal Rhyolite near Loskop Dam.

The Basal Rhyolite in the Messchunfontein section and the Stavoren Inlier

The Basal Rhyolite in the type-Dullstroom section has received very little attention in this study. At this point, it is not known whether or not baddeleyite is present at all, since only one 5 x 7 µm zircon grain has been found to date after a very limited search. The average Cr concentration of the Basal Rhyolite in this locality is ~130 ppm and so far, Cr has only been found in very small concentrations within 20-50 µm magnetite grains. Larger magnetite grains, 200-400 µm in size, lack Cr altogether. The MgO content of the bulk rock is also higher, which may be due to abundant amphibole in the groundmass. If the Basal Rhyolite of the Messchunfontein section is correlated with the Basal Rhyolite at the Stavoren Inlier, the differences in spinel composition indicate that the Basal Rhyolite occurring in the Messchunfontein section mixed with a more evolved mafic melt.

IS THE BASAL RHYOLITE A DIFFERENTIATE OF RLS MAGMA OR A CRUSTAL MELT?

When considering the fractionation model of Turner and Rushmer (2009), the values of SiO_2/Al_2O_3 and K_2O/Na_2O for the Basal Rhyolite suggest efficient fractionation of a mafic melt. However, the presence of entrained quartz clasts and metasomatism throughout the Basal Rhyolite, means that none of these ratios are likely to be primary. The effects of secondary alteration will also impede geochemical analyses similar to those conducted by Buchanan et al. (1999; 2002; 2004; 2006).

The entrained quartz grains in Basal Rhyolite likely represent a population of quartz that was incorporated into the Basal Rhyolite from pre-existing sediments. If a population of quartz was entrained, it is expected that zircon grains from pre-existing sediments were entrained as well. Zoned zircon grains, 150-200 μm in size, have been documented in the upper Pretoria Group immediately underlying the Basal Rhyolite (Fig. 29) but no such grains have been found in the Basal Rhyolite to date.

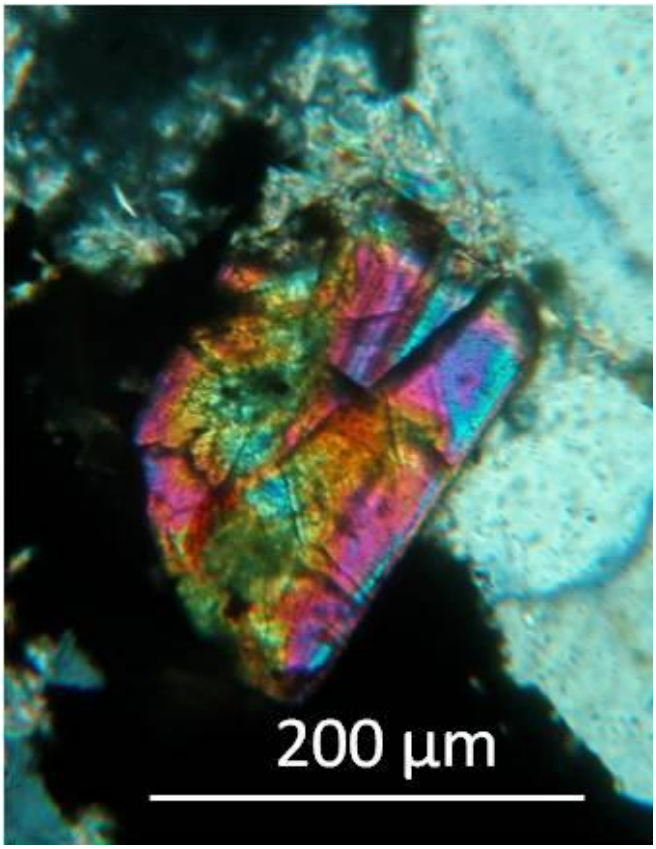

Figure 29. Photomicrograph of a ~200 µm zoned zircon, from an outcrop of the Mackekaan Subgroup directly beneath the Basal Rhyolite in the Stavoren Inlier. The zircon is situated between two large quartz grains. Cross-polarized light.

CHAPTER 11: FUTURE WORK

EXTENSION OF THE PRESENT STUDY

The present study is limited to a few samples of the Basal Rhyolite from three localities. This study could be extended to determine whether the apparent correlation between texture and Cr concentration are a general rule for the Basal Rhyolite in the Stavoren Inlier. The possibility that the presence of baddeleyite in Basal Rhyolite from the Stavoren Inlier corresponds to increased bulk Zr concentration could also be investigated. The Zr and Cr study also needs to be carried out extensively in other localities of Basal Rhyolite, such as the Type-Dullstroom Formation.

Additional chemical analyses of baddeleyite could also be carried out to see if their TiO2 content varies from locality to locality as shown in this study. This may support mixing between siliceous melts and mafic melts in differing stages of evolution based on locality.

Future work should also be extended within the stratigraphic Rooiberg column over a wide area to see how widespread baddeleyite and chromite really are. Of all the siliceous rocks in the Rooiberg Group, only the high-Mg felsite of the upper Dullstroom Formation has some samples with Cr concentrations in excess of 100 ppm (up to 268 ppm) (Schweitzer, 1998). Zirconium concentration increases systematically with stratigraphic height in the Rooiberg Group. Zircon is known to be present in the higher units, but there has been no search for baddeleyite to date.

ISOTOPIC ANALYSES

Using a new nanoSIMS technique, it may be possible to obtain U-Pb dates for the baddeleyite grains located in the Basal Rhyolite. The current limit of resolution for this technique is ~ 2 μm (Wang et al., 2012) which makes the baddeleyites from this study great candidates for these analyses. Obtaining an accurate date would be very important because currently the only U-Pb of the Rooiberg Group is from a zircon in the Kwaggasnek Formation (Walraven, 1997; Harmer and Armstrong, 2000). If a Bushveld age is obtained for a baddeleyite grain in the Basal Rhyolite, it could be viewed as evidence for the baddeleyite crystallizing in-situ as the impact scenario proposes, or the baddeleyite representing a contaminant that originally crystallized in a mafic magma of the early Bushveld Complex. However, if the baddeleyite is found to be older than the Bushveld Complex, the baddeleyite must have been entrained from a pre-Bushveld mafic lithology.

If a Bushveld age is obtained for the baddeleyite, oxygen isotopes could be used to determine if the baddeleyite originated from the chill sequence by comparing the O^{18}/O^{16} ratio of baddeleyites from both localities. If they are similar, a shared parent melt could be supported.

EXPERIMENTAL WORK

It is suggested that experiments be carried out with the intent of reproducing the conditions proposed by the impact hypothesis for crystallizing ZrO_2. To do this, it would be necessary to reproduce the conditions of the bulk chemistry, temperature at the time of ZrO_2 crystallization, and to consider the effects of additional contaminants and

hydrothermal alteration. These experiments could also be applied to chromite to determine if it is stable while the Zr-bearing phases are not, which is implied by the impact scenario.

PLATINUM-GROUP ELEMENTS (PGEs) IN CHROMITE

Numerous studies have shown that chrome spinel controls the behavior of PGEs during igneous differentiation (Park and Campbell, 2012, Brenan et al., 2011). In particular, the PGEs Ru, Os, and Ir as well as Rh are the most compatible in chrome spinel and increase with fO_2 and the corresponding enrichment in ferric iron (Brenan et al., 2011). It is recommended that analyses of PGEs be conducted on the high-Mg cores of this study as well as chrome spinels from the new chill sequence. The results of a PGE study have the potential to be useful for two reasons: 1) the fact that PGE concentrations are highly sensitive to secondary alteration (Stephen Barnes, personal communication) would suggest that if they are not present in the high-Mg cores, that the cores themselves have, contrary to the current interpretation, been thoroughly affected by secondary alteration and 2) Any correlation between the high-Mg cores and those of the chill sequence may provide evidence that they are indeed related. Since the high-Mg cores of this study and many of the chromites from the chill sequence are high in ferric iron, an abnormally high concentration of Ru, Os, Ir, and Rh in chromites from both the Basal Rhyolite and the chill sequence could provide strong evidence that the chromites formed in similar conditions, and are therefore related to the same mafic body.

CHAPTER 12: CONCLUSIONS

THE UNIQUE NATURE OF THE BASAL RHYOLITE

The presence of chromite and composite zircon-baddeleyite grains in the Basal Rhyolite in the Stavoren Inlier, baddeleyite in granophyrized Basal Rhyolite near Loskop Dam, and Cr-magnetite in the Basal Rhyolite of the Messchunfontein section, are important additions to a growing list of characteristics that distinguish the Basal Rhyolite from typical rhyolites. In addition, the presence of extremely numerous, unzoned, <10 µm zircon crystals, many of which exhibit irregular morphologies, is unlike any zircon population documented in a highly silicic rock. The absence of Hf in these zircons, as well as those rimming baddeleyite, is also unique in the geologic record. Future studies are needed to understand if secondary alteration or chemical conditions during zircon crystallization are the cause for this lack of Hf.

JUSTIFICATION FOR THE PREFERENCE OF THE IGNEOUS SCENARIO

Given the current limited, data, an igneous origin for the baddeleyite and chrome spinel is preferred over an impact origin. There are two reasons for this preference:

1. In both localities where it occurs, baddeleyite has compositions similar to, and occasionally preserves morphologies consistent with, baddeleyite that crystallizes in terrestrial mafic lithologies.
2. Chromites are configured in clusters and chains typical of chromites interstitial to olivine and pyroxene in ultramafic rocks, which is difficult to reconcile with the impact scenario which proposes that the chromites were rapidly excavated from a previously undiscovered mafic lithology.

To further differentiate between the igneous and impact scenarios, isotopic analyses of baddeleyite, aimed at obtaining a U/Pb date and O isotope ratios should be carried out. For these analyses to be meaningful they will have to include baddeleyite from the Basal Rhyolite and baddeleyite in the recently discovered chill sequence. Given the small size of baddeleyites in the Basal Rhyolite, a new nanoSIMS technique will be required for these analyses unless larger baddeleyites can be found.

CHROME SPINELS: A POSSIBLE LINK WITH THE NEWLY DISCOVERED CHILL SEQUENCE

The composition and euhedral morphology of the high-Mg cores of the chrome spinels are consistent with formation in a chromitite, or a chromite-rich orthopyroxene-olivine cumulate, as found in continental mafic intrusions, including the Bushveld Complex. The compositional zonation of the high-Mg cores may represent primary igneous zoning or the effects of subsolidous re-equilibration. The fact the fact that the high-Mg cores plot over, or very close to, plots of continental mafic intrusions in the spinel database, suggests that their chemistry has not been altered. At this point, the most intriguing source is a new chill sequence discovered by Wilson (2012) and related by him to the Bushveld Complex. The presence of both baddeleyite and chromites with low Ti and Fe^{3+} in the chill sequence makes it a potential source for both the chromite and baddeleyite. In terms of relative age, it is also a good candidate because it represents the oldest intrusive melt found in the Bushveld Complex to date, while the Basal Rhyolite represents one of the oldest extrusions of the Rooiberg Group. However, the absolute ages of the Basal Rhyolite or the chill sequence have not been determined to date. If the chromite and baddeleyite from the Basal Rhyolite are similar to those of the chill

sequence it follows that the chill sequence is more widespread than has been shown by the single drill core.

MAFIC AND SILICEOUS MAGMAS OF THE BUSHVELD COMPLEX

The magma mixing scenario implies the presence of a tectonically controlled magma chamber as a source of the Bushveld Complex, whereas a random impact would have no such implications. Shallow magma chambers have been invoked by Buchanan et al. (2002) and Vantongeren et al. (2010), among recent authors. Buchanan et al. (2004) suggested that siliceous melts of the Rooiberg Group may have existed in magma chambers considered an intermediate residence of the RLS. The primitive chemistry of the new chill sequence suggests that it may be an early offshoot of a larger source of primary ultramafic melt associated with the Bushveld Complex. The chill sequence could be a source of the mafic component of the Basal Rhyolite if the relationship between the chromites and baddeleyites of the Basal Rhyolite and the chill sequence can be confirmed. This would imply that some cumulates of the chill sequence had already formed prior to extrusion emplacement of the Basal Rhyolite, and that the Basal Rhyolite likely occurred in the same magma chamber(s) as the earliest RLS magmas.

REFERENCES

Ayalew, D., Gibson, S.A., 2009. Head-to-tail transition of the Afar mantle plume: geochemical evidence from a Miocene bimodal basalt-rhyolite succession in the Ethiopian Large Igneous Province. Lithos 112, 461–476.

Babayeju, O., 1999. Geophysical Investigation of the Marble Hall Fragment of the Bushveld Complex. Unpublished Master's Thesis, The University of Pretoria 1999.

Barnes, S. J., 1998. Chromite in komatiites, I. Magmatic controls on crystallization and composition. Journal of Petrology v. 39, p. 1689–1720.

Barnes, S. J., 2000. Chromite in Komatiites, II. Modification during greenschist to mid-amphibolite facies metamorphism. Journal of Petrology v. 41, p. 387–409.

Bindeman, I. N. and Valley, J. W., 2001. Low-O18 Rhyolites from Yellowstone: Magmatic evolution based on analyses of zircons and individual phenocrysts. J. Petrol. 42, 1491–1517.

Bryan, S.E., Ernst, R.E., 2008. Revised definition of large igneous provinces (LIPs). Earth Science Reviews 86, 175–202.

Bryan, S.E., Riley, T.R., Jerram, D.A., Stephens, C.J., Leat, P.T., 2002. Silicic volcanism; an undervalued component of large igneous provinces and volcanic rifted margins. Special Paper-Geological Society of America 362, 97–118.

Buchanan, P.C., 2006. The Rooiberg group. In: Johnson, M.R., Anhaeusser, C.R., Thomas, R.J. (Eds.), The Geology of South Africa. Geological Society of South Africa/Council for Geoscience, Johannesburg/Pretoria, pp. 283–289.

Buchanan, P.C., Reimold, W.U., Koeberl, C., Kruger, F.J., 2004. Rb–Sr and Sm–Nd isotopic compositions of the Rooiberg Group, South Africa: early Bushveld-related volcanism. Lithos 29, 373–388.

Buchanan, P.C., Reimold, W.U., Koeberl, C., 1999. Petrogenesis of the Dullstroom Formation, Bushveld Magmatic Province, South Africa. Contrib. Miner. Petrol. 137, 133–146.

Buchanan, P.C., Reimold, W.U., Koeberl, C., Kruger, F.J., 2002. Geochemistry of intermediate to siliceous volcanic rocks of the Rooiberg Group, Bushveld Magmatic Province, South Africa. Contrib. Miner. Petrol. 144, 131–143.

Bumby, A.J., Eriksson, P.G., Van der Merwe, R. 1998. Compressive deformation in the floor rocks to the Bushveld Complex (South Africa): evidence from the Rustenburg Fault Zone. J. Afr. Earth Sci. 27, 307–330.

Butterman, W.C., and Foster, W.R., 1967. Zircon stability and the ZrO2-SiO2 phase diagram. American Mineralogist, v. 52, p. 880-885.

Cameron, E.N., 1977. Chromite in the central sector of the Eastern Bushveld Complex, South Africa. American Mineralogist, v.62, p. 1082-1096.

Caress M. E., Elston, W.E., 1997. Sedimentary interbeds of the Rooiberg Group at the Loskop Dam section, Bushveld Complex, South Africa. Large Meteorite Impacts and Planetary Evolution 2, proceedings, abstract 6059.

Clarke, B., Uken, R., & Reinhardt, J., 2009. Structural and compositional constraints on the emplacement of the Bushveld Complex, South Africa. Lithos, v. 111, p. 21-36.

Collins, G., Melosh, H.J., Morgan H.V., Warner, M.R., 2002. Hydrocode simulations of Crater Collapse and Peak Ring Formation. Icarus v. 157 p. 24-33.

Droop, G.T.R., 1987. A general equation for estimating Fe3+ concentration in ferromagnesian silicates and oxides from microprobe analyses, using stoichiometric criteria. Mineralogical Magazine, v. 51, p. 431-435.

Duke, J.M., 1983.Ore Deposit Models 7. Magmatic Segregation Deposits of Chromite. Geoscience Canada, v. 10, p. 15-24.

Elkins-Tanton, L. T., 2005.Continental magmatism caused by lithospheric delamination. Special Papers Geological Society America v. 388, p. 449-461.

Elston, W.E., 2008. Proposed Bushveld Scenario: Impact, mantle upwelling, meltdown, collapse Large Meteorite impacts and Planetary Evolution IV. Abstract 3015.

Eriksson, P. G., Hattingh, P. J. & Altermann, W., 1995. An overview of the geology of the Transvaal Sequence and Bushveld Complex, South Africa. Mineralium Deposita, v. 30, p. 98-111.

Eriksson, P.G., Schreiber, U.M., Reczko, B.F. F., Snyman, C.P., 1994. Petogrophy and geochemistry of sandstone interbedded with the Rooiberg Felsite Group (Transvaal sequence, South Africa): Implications for provenance and tectonic setting. Journal of Sedimentary Research, v. A64 pp. 836-846.

Ernst, R.E., Bell, K., 2010. Large Igneous Provinces (LIPs) and carbonatites. Mineralogy and Petrology, v. 98, p. 55–76.

Ewart, A., Milner, S.C., Armstrong, R.A., Duncan, A.R., 1998b. Etendeka volcanism of the Goboboseb Mountains and Messum igneous complex, Namibia: Part II. Voluminous quartz latite volcanismof theAwahabmagma system. Journal of Petrology, v. 39, p. 227-253.

French B.M., Koeberl C., 2010. The convincing identification of terrestrial meteorite impact structures; What works, what doesn't, and why: Earth-Science Reviews, v. 98, p. 123-170.

French, B.M., 1990, Absence of shock-metamorphic effects in the Bushveld Complex, South Africa: results of an intensive search: Tectonophysics, v. 171, p. 287-301.

Garland, F., Hawkesworth, C.J., Mantovani, M.S.M., 1995. Description and petrogenesis of the Parana rhyolites, southern Brazil. Journal of Petrology 36, 1193–1227.

Hanchar, J. M., Watson B. E., 2003. Zircon saturation thermometry. Reviews in Mineralogy & Geochemistry v. 53, p. 89-112.

Harmer, R.E., Armstrong, R. A., 2000. Duration of Bushveld Complex (sensu lato) magmatism: Constraints from new SHRIMP zircon chronology. National Research Foundation, Bushveld Complex Workshop, Gethlane Lodge, South Africa, p. 11-12.

Hartzer, F.J., 2000. Geology of the Transvaal Inliers in the Bushveld Complex. Geological Survey of South Africa Memoir 88, 222 p. maps.

Hatton, C.J., Schweitzer, J.K., 1995. Evidence for synchronous extrusive and intrusive Bushveld magmatism. Journal African Earth Sciences, v. 21, p. 579–594.

Hatton, C.J., von Gruenewaldt, G., 1985, Chromite from the Swankop chrome mine - an estimate of the effects of subsolidus reequilibration. Economic Geology v. 80, p. 911-924.

Heaman, L.M., and LeCheminant, A.N., 1993. Paragenesis and U-Pb systematics of baddeleyite (ZrO_2): Chemical Geology, v. 110, p. 95-126.

Hulbert, L.J., Von Gruenewaldt G., 1985. Textural and Compositional Features of Chromite in the Lower and Critical Zones of the Bushveld Complex South of Potgietersrus. Economic Geology, v. 80, p. 872-895.

Irvine, T.N., 1965. Chromian spinel as a petrogenetic indicator. Part 1. Theory. Canadian Journal of Earth Sciences. v. 2, p. 648-672.

Irvine, T.N., 1967. Chromian spinel as a petrogenetic indicator. Part 2. Petrologic applications. Canadian Journal of Earth Sciences, v. 4, p. 71-103.

Ivanov, B.A., and Melosh, H.J., 2003. Impacts do not initiate volcanic eruptions: Eruptions close to the crater: Geology, v. 31, p. 869–872.

Jones, A.P., Price, G.D., DeCarli, P., Price, N., and Hayhurst, C., 2001. Modeling impact decompression melting: A possible trigger for impact induced volcanism and mantle hotspots. http://www.mantleplumes.org/WebDocuments/JonesSpringer2003.pdf

Kamenetsky, V. S., Crawford, A. J., Meffre, S., 2001. Factors controlling chemistry of magmatic spinel: an empirical study of associated olivine, Cr-spinel and melt inclusions from primitive rocks. Journal of Petrology v. 42, p. 655–671.

Kinnaird, J.A., 2005. The Bushveld Large Igneous Province. www.largeigneousprovinces.org/LOM.html [May 2005].

Kinny, P.D., Maas, R., 2003. Lu-Hf and Sm-Nd isotope systems in zircon. Reviews in Mineralogy and Geochemistry, v. 53, p. 327-341.

Maier, W.D., Arndt, N.T., Curl, E.A., 2000. Progressive crustal contamination of the Bushveld Complex: evidence from Nd isotopic analyses of the cumulate rocks. Contributions to Mineral Petrology, v. 140, p. 316–327.

Miller, J.A., Harris, C., 2007. Petrogenesis of the Swaziland and northern Natal rhyolites of the Lebombo rifted volcanic margin, South East Africa. Journal of Petrology v. 48, p. 185–218.

Naldrett, A.J., Kinnaird, J.A., Wilson, A.H., Chunnet, G.C., Yudovskaya, M., McQuade, S., 2010. Concentration of PGE and Chromite in the Bushveld Complex. 11th International Platinum Symposium. 2010.

(NAVDAT) The Western North American Volcanic and Intrusive Rock Database. www.Navdat.org

Olsson, J. R., Söderlund, U., Hamilton, M. A., Klausen, M. B., and Helffrich, G. R., 2011. A late Archean radiating dike swarm as possible clue to the origin of the Bushveld Complex. Nature Geoscience Letters, v. 4, p. 865-869.

Pankhurst, M.J., Schaefer, B.F., Betts, P.G., 2011. Geodynamics of rapid voluminous felsic magmatism through time. Lithos v. 123, p. 92–101.

Patchett, P.J., Kouvo, O., Hedge, C.E., Tatsumoto M., 1981. Evolution of continental crust and mantle heterogeneity: evidence from Hf isotopes. Contributions in Mineral Petrology, v.78, p. 279-297.

Peate, D.W., Hawkesworth, C.J., Mantovani, M.S.M., 1992. Chemical stratigraphy of the Parana lavas (South America): classification of magma types and their spatial distribution. Bulletin of Volcanology, v. 55, p. 119–139.

Rhodes, R.C., 1975. New evidence for impact origin of the Bushveld Complex, South Africa. Geology, v. 3, p. 549–554.

Roeder, P. L., 1994. Chromite: from the fiery rain of chondrules to the Kilauea Iki lava lake. Canadian Mineralogist v. 32, p. 729–746.

Schweitzer, J.K., 1998. The transition from the Dullstroom Basalt Formation to the Rooiberg Felsite Group, Transvaal Supergroup: a volcanological, geochemical and petrological investigation. Ph.D. thesis, University of Pretoria.

Schweitzer, J.K., Hatton, C.J., 1995. Chemical alteration within the volcanic roof rocks of the Bushveld Complex. Economic Geology, v. 90, p. 2218-2231.

Schweitzer, J.K., Hatton, C.J., de Waal, S.A., 1995. Regional lithochemical stratigraphy of the Rooiberg Group, upper Transvaal Supergroup: a proposed new subdivision. S. African Journal of Geology, v. 98, p. 245–255.

Sharpe, M.R., Evensen, N.M., Naldrett, A.J., 1986. Sm/Nd and Rb/Sr evidence for liquid mixing, magma generation and contamination in the Eastern Bushveld Complex. Geocongress Conf. Abstr. University of Witwatersrand, Johannesburg, p. 621–624.

Sheth, H.C., 2007. 'Large Igneous Provinces (LIPs)': definition, recommended terminology, and a hierarchical classification. Earth Science Reviews, v. 85, p. 117–124.

Stowe, C.W., 1994. Compositions and Tectonic Settings of Chromite Deposits through Time. Economic Geology, v. 89, p. 528-546.

Turner, S.P., Rushmer, T., 2009. Similarities between mantle-derived A-type granites and voluminous rhyolites in continental flood basalts provinces. Earth Environ. Sci. T. R. Soc. v. 100, p. 1–10.

Twist, D. & French, B. M., 1983. Voluminous acid volcanism in the Bushveld Complex: A review of the Rooiberg Felsite. Bulletin of Volcanology v. 46, p. 225-242.
Twist, D., 1985, Geochemical evolution of the Rooiberg silicic lavas in the Loskop Dam area, southeastern Bushveld. Economic Geology. v. 80, p. 1153–1165.

Vantongeren, J.A., Mathez, E.A., Kelemen, P.B., 2010. A felsic end to Bushveld differentiation. Journal of Petrology, v. 51, p. 1891–1912.

Von Gruenewaldt, G., 1972, The origin of the roof-rocks of the Bushveld Complex between Taugeshoogte and Paardekop in the eastern Transvaal: Geological Society of South Africa Transactions, v. 75, p.121-134.

Wager, L.R. and Brown, G.M., 1967. Layered Igneous Rocks, Edinburgh: Oliver and Boyd. 588 p.

Walraven, F., 1997, Geochronology of the Rooiberg Group, Transvaal Supergroup, South Africa. Economic Geology Research Unit, University of Witwatersrand, Information Circular 316.

Wilson A.H., 2012. A Chill Sequence to the Bushveld Complex: Insight into the First Stage of Emplacement and Implications for the Parental Magmas. Journal of Petrology. v. 53, p. 1123-1168.

Yang, W., Lin, Y., Zhang, J., Hao, J., Shen, W. Hu, S., 2012. Precise micrometer-sized Pb-Pb and U-Pb dating with NanoSIMS. Journal of Analytical Atomic Spectrometry, v. 3, p. 479-487.

Yudovskaya M.A., Kinnaird, J.A., 2010. Chromite in the Platreef (Bushveld Complex, South Africa): occurrence and evolution of its chemical composition. Mineralium Deposita, v. 45, p. 369-391.